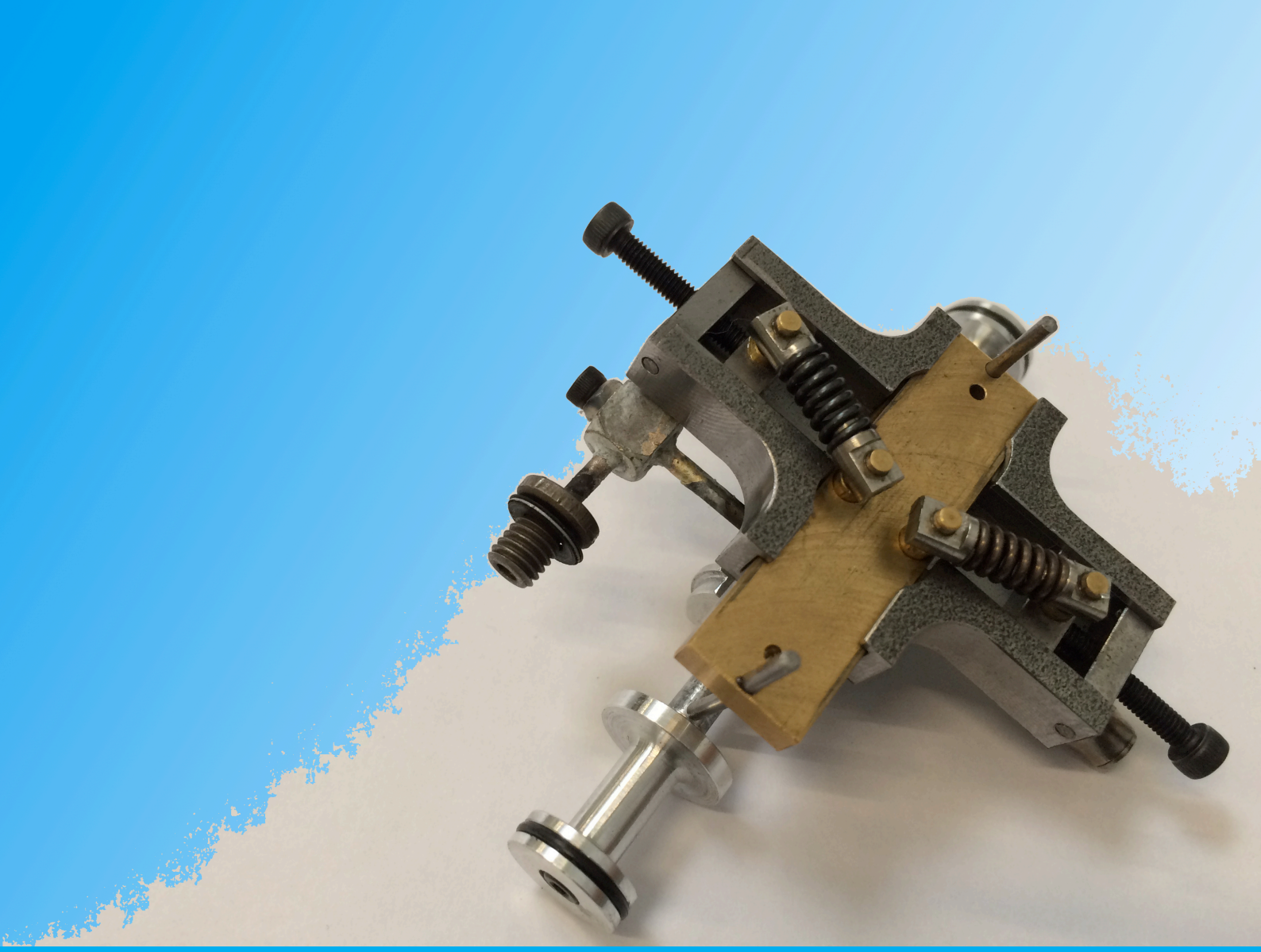

# Exergy saving pneumatically actuated autonomous systems

## Improving the efficiency of $CO_2$-powered pneumatic systems.

F.G.E. Verga

Technische Universiteit Delft

TU Delft

# Exergy saving pneumatically actuated autonomous systems

## Improving the efficiency of $CO_2$-powered pneumatic systems.

by

F.G.E. Verga

to obtain the degree of Master of Science
at the Delft University of Technology,
to be defended publicly in December 13 2016.

Student number: 4330080
Project duration: May 1 , 2016 – November 29, 2016
Thesis committee: Dr. ir. D. H. Plettenburg, TU Delft, supervisor
Prof. Dr. F. L. Van der Helm, TU Delft
Dr. ir. C. A. Infante Ferreira, TU Delft



TU Delft

# Preface

A new adventure is beginning with the end of another. Indeed the other was this master that prepared me to challenge the future, as the TU Delft motto says! All this would not have been possible without my family, my mom Ellade, my father Guido various sisters and last but not least Michelle. A special thank to Zio Mario that supported me till the end. Coming back to the academic staff and TU Delft related, I would like to thank Dick Plettenburg for the challenging project! Thanks to Jan van Frankenhuyzen, Krysten Oats and Monica Moreo to listen to me whining whenever something was not working! And finally, I would like to thank the workshop staff, Wim, Reinier and Nisse, for accepting me among their precious tooling machines letting me enjoy the pleasure of creation! If anyone is missing, well, I would like to thank you as well!

*F.G.E. Verga*
*Delft, November 2016*

# Abstract

Carbon dioxide pneumatically actuated autonomous systems suffer a major energy loss whenever the pressure is reduced from saturation pressure to the designed pressure. This loss account of approximately 60% of the total energy enclosed in the pressurized carbon dioxide canister, considering an isothermal expansion. To address this problem, this work propose a method to simulate and build a small free-piston expander-compressor. This machine is able to lower the pressure of the carbon dioxide at saturation condition to a required pressure level. As the free-piston expands the carbon dioxide, work is recovered compressing atmospheric air. The compressed air can be used in the pneumatic system. The free-piston does not need externally form of energy and it is a self-standing machine.

# Contents


**1 Introduction** **1**
1.1 Background . . . 1
1.2 Losses produced by a pressure regulator: theory . . . 2
1.2.1 The energy store . . . 2
1.2.2 Exergy and thermodynamic integrity . . . 3
1.2.3 Exergetic losses of a pressure regulator . . . 5
1.2.4 Quantitative mass specific energy loss . . . 6
1.3 concluding remarks . . . 7

**2 Requirements** **9**
2.1 Introduction . . . 9
2.2 Requirements . . . 9

**3 Choice of the machine** **11**
3.1 Introduction . . . 11
3.2 How to decrease exergetic losses . . . 12
3.3 Fluid machinery . . . 12

**4 Physical model** **15**
4.1 Introduction . . . 15
4.2 Limitations . . . 15
4.3 Structure of the model . . . 15
4.4 Expander . . . 16
4.5 Compressor . . . 17
4.6 System connection . . . 17
4.7 O-ring friction model . . . 18

**5 Design of the first prototype** **19**
5.1 Concept . . . 19
5.2 Geometry . . . 20
5.2.1 Wall thickness and shaft length . . . 22
5.2.2 Minimal shoulder thickness . . . 22
5.3 O-rings choice . . . 24
5.4 Lubrication . . . 24
5.5 Bering and gaps . . . 24
5.6 Functioning of the system . . . 25
5.6.1 Spool valve . . . 26
5.6.2 Inlet valve . . . 26
5.7 Test . . . 28

**6 Design of the second prototype** **29**
6.1 Introduction . . . 29
6.2 Concept . . . 29
6.3 Spool valve . . . 30
6.4 Test . . . 30
6.5 Valve timing and expander dead volume . . . 31
6.6 Possible caused . . . 31

**7 Design of the third prototype** **33**
7.1 Introduction . . . 33
7.2 Energy storage . . . 33
7.3 Bi-stable mechanism . . . 34
7.4 Design prototype number 3 . . . 35
7.5 Compressor valves . . . 36
7.6 Functioning sequence . . . 37
7.7 Test . . . 38

**8 Test setups** **41**
8.1 Introduction . . . 41
8.2 Alternating motion test and self-starting . . . 41
8.3 Pressure regulation test . . . 41
8.4 Energy recovery test . . . 42

**9 Possible improvements and future works** **45**
9.1 Introduction . . . 45
9.2 O-ring stretching . . . 45
9.3 New spool valve . . . 45
9.4 Dead volume in the expander . . . 46
9.5 Under expansion effect on the center spool O-ring. . . . 47
9.6 Compressor head . . . 47
9.7 Externally controlled free-piston expander compressor . . . 47
9.8 Simulation. . . . 47

**10 Discussions** **49**

**11 Conclusion** **51**

**A Expansion work** **53**

**B Example of positive displacement compressors** **55**
B.1 Scroll compressor-expander . . . 55
B.2 Rotary vanes compressor-expander. . . . 56
B.3 Screw compressor-expander . . . 57

**C Physical model** **59**
C.1 The model . . . 59
C.1.1 Simplifying assumptions . . . 59
C.1.2 Laws governing the expander . . . 59
C.1.3 Composition of the three phases . . . 61
C.1.4 Equation of state Soave-Redlich-Kwong . . . 61
C.1.5 Laws governing the compressor . . . 62
C.1.6 Governing equation for the flow . . . 62
C.2 Simulink model in detail . . . 64
C.2.1 Expander . . . 64
C.2.2 Flow model IN . . . 66
C.2.3 Flow model OUT . . . 68
C.2.4 Inlet/Outlet cross-section area . . . 69
C.2.5 Compressor. . . . 72
C.2.6 Compressor inlet and outlet flow. . . . 72
C.3 Constants used for the simulation . . . 73

**D Mechanical resistance** **75**
D.1 Aluminum 7075 properties . . . 75
D.2 hoop stress and diametrical expansion . . . 75
D.3 Shaft buckling. . . . 76
D.4 Shoulder thickness . . . 77

**E Bi-stable mechanism calculation** **79**
E.1 Spool estimated friction forces . . . 79

**F Manufacturing drawings of prototype number 3** **83**

**Bibliography** **95**

# Nomenclature

**Greek symbols**

| | | |
|---|---|---|
| $\eta$ | Viscous friction coefficient | $[Ns/m]$ |
| $\kappa$ | Heat capacity ratio | $[-]$ |
| $\omega$ | Acentric factor | $[-]$ |
| $\rho$ | Friction coefficient | $[-]$ |
| $\sigma$ | Normal stress | $[Pa]$ |
| $\tau$ | Shear stress | $[Pa]$ |

**Symbol**

| | | |
|---|---|---|
| $A$ | cross section area | $[m^2]$ |
| $a$ | Mass specific work in a closed system | $[J/kg]$ |
| $c$ | Flow average velocity | $[m/s]$ |
| $C_f$ | discharge coefficient | $[-]$ |
| $c_p$ | Specific isobaric heat capacity | $[J/kgK]$ |
| $c_v$ | Specific isochoric heat capacity | $[J/kgK]$ |
| $d$ | diameter | $[m]$ |
| $E$ | Young modulus | $[Pa]$ |
| $e$ | Mass specific energy in an open system | $[J/kg]$ |
| $g$ | Gravitational acceleration | $[m/s^2]$ |
| $I$ | Second moment of area | $[m^4]$ |
| $l$ | Mass specific exergy losses | $[J/kg]$ |
| $m$ | mass | $[kg]$ |
| $P$ | Pressure | $[Pa]$ |
| $q$ | Mass specific heat flow | $[J/kg]$ |
| $r$ | Mass specific dissipative energy | $[J/kg]$ |
| $r$ | Mass specific enthalpy | $[J/kg]$ |
| $r$ | Mass specific gas constant | $[kg]$ |
| $s$ | Mass specific entropy | $[J/kgK]$ |
| $T$ | Temperature | $[K]$ |
| $t$ | Time | $[s]$ |
| $U$ | Internal energy | $[J]$ |

| | | |
|---|---|---|
| $u$ | Mass specific internal energy | $[J/kg]$ |
| $v$ | Mass specific density | $\left[m^3/kg\right]$ |
| $W$ | Work | $[J]$ |
| $z$ | Piston position | $[mm]$ |
| $z$ | Vertical axis | $[m]$ |

**Subscript**

| | |
|---|---|
| $air$ | Related to air |
| $atm$ | Related to atmospheric conditions |
| $b$ | Related to pressurized bottle |
| $c$ | Related to the compressor |
| $CO_2$ | Related to carbon dioxide |
| $d$ | Related to the downstream conditions |
| $e$ | Related to the expander |
| $f$ | Related to inlet or outlet |
| $s$ | Related to the sink conditions |
| $u$ | Related to the upstream conditions |

# 1 Introduction

## 1.1. Background

Autonomous mechatronic system development will be just partially achieved if we are not able to provide them with sufficient power independence. The fact that untethered machines need to have an efficient power source is self-explanatory. Despite this logical conclusion, power sources used in autonomous systems seem to lack of this major requirement. Additionally, it seems evident that efforts towards an improved power supply rely on batteries and hardly towards any other method more exploitable for self-supporting mechatronic systems. Known machines for the transformation of energy are miniaturized and fitted on-board of robots, or new methods to produce energy are evaluated. Apparently, this is done while always leaving the inefficient use of the store as an inevitable side effect, e.g. [1].
Due to their characteristics, pneumatic systems appear to be the backbone for a perfect recipe in autonomous system design.

Controlling a pneumatic system may be challenging because of compressibility and sonic choke [2, 3] , yet the study of Goldfarb et al [4] shows that excellent results can be achieved on that matter of control. Moreover, Plettenburg says [5] a pneumatic system is fast, silent, reliable and can be built small. Granosik and Borenstein [6] add that a great advantage, as compared to electromechanical conventional methods, is that joint stiffness can be easily controlled varying the pressure in the cylinders. Again, Fite et al [7] add that pneumatics do not require extra energy for isometric contraction and natural passive limb bio-mechanics can be easily achieved.

Fresh interest in soft robotics and pneumatic muscles brings fluidic actuators back to the scene because of their advantages. There are many published works in this field [2, 8, 9]. Many efforts focus on improving fuel efficiency [5, 6, 10–13].

Carbon dioxide is one of the gas employed in pneumatically actuated autonomous system. It has advantages compared to others. For instance compared to monopropellants, $CO_2$ is substantially safer. Monopropellants are substances that decompose once in contact with a catalyst. Hydrogen peroxide, the most employed monopropellant in this field, produces an highly exothermic decomposition and gasses can easily reach a temperature of 300 $°C$ and more [14]. Microcompressors have an higher energy to mass ratio than $CO_2$, yet the flow rate of these machines and pressure levels are extremely limited [1]. $CO_2$ is stored as a fluid at saturation pressure. This helps to increase the energy density of the storage system. In order to use the fluid, a throttling process is necessary. The pressure drop is strongly dissipative and significantly impacts the efficiency of the supply.

**The aim of this work is to design, build and test a machine capable of recovering energy while reducing the pressure supplied to the pneumatic system.**

## 1.2. Losses produced by a pressure regulator: theory

Carbon dioxide pneumatically actuated autonomous systems suffer from low energetic efficiency. This is partially due by the low actuation pressure, that span a range between $P = [50; 500]kPa$ [1, 15–17]. In fact, Plettenburg [5] shows that at a pressure of 1,3 $Mpa$, the gas consumption meets its minimal value. In addition to that, an even greater loss of potential is caused by the pressure regulator. The pressure regulator is needed to reach the optimal pressure supply of 1,3 $Mpa$ or lower pressures. In fact, $CO_2$ is typically stored at saturation conditions in specific vessels ($P_{sat} = 5.729MPa, T = 293K$). This is beneficial because the pressure supplied by the vessel is isobaric for a large extent.

### 1.2.1. The energy store

An elementary system propelled by carbon dioxide can be composed by a rigid canister, containing $CO_2$ at saturation conditions ($P_{sat} = 5.729MPa, T = 293K$), a pressure regulator, and a pneumatic motor, as shown in Figure 1.1. For $CO_2$ an optimal pressure supply providing a minimal fuel consumption is found at $P \approx 1.3MPa$[5, 18].

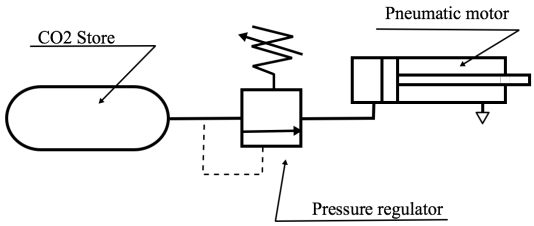


Figure 1.1: Principle scheme of a $CO_2$ actuation system. The system is composed by a pressure source a pressure regulator and a pneumatic motor

In other systems a lower operating pressure than the optimal pressure supply is imposed by design ($P = [50; 500]kPa$) [1, 15–17]. To cite an example, fluidic elastomer actuators (FEA), Figure 1.2, are a thin layer of low durometer rubber, and they operate within a range of 20 to 55 $KPa$ [2]. We can imagine that, if the wall thickness would grow or reinforcement materials were added, the capability of this motor may be impaired. We cannot yet exclude, however, that such a redesign would not function.

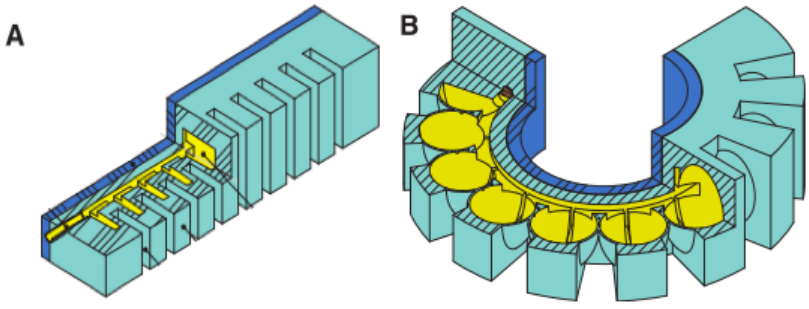


Figure 1.2: Example of unactuated FEA in (A) and actuated FEA in (B) from Marchese et al[2]. The yellow surface characterizes the interior chamber of the motor, where the pressurized air flows. Notice, in B, how the deformation of the material enables the motor to take a certain configuration.

Whether the designer chooses a well-defined operating pressure by necessity or otherwise, this working point is found to be inferior to the saturation condition imposed by the two-phase mixture of carbon dioxide, and therefore a pressure regulator is necessary.
A thermodynamic analysis of a pressure regulator leads to the conclusion that the transformation is isenthalpic, see Section 1.2.3. The pressure drop is due to an irreversible process.

This irreversible process leads to an increase of internal entropy.
The growth of internal entropy is proportional to the amount of exergy destruction (see Section 1.2.2). The pressure regulation produces a considerable amount of energy degradation or anergy.

That being said, it is clear that this process is incompatible with a good management of energy in an untethered device.

### 1.2.2. Exergy and thermodynamic integrity

The definition of exergy from the "Dictionary of Energy" [19] reads as follows:

**exergy:** *Thermodynamics, the maximum amount of useful work (ordered motion) that a system can perform when it is brought into thermodynamic equilibrium with its surrounding by reversible processes*

The efficiency and the coefficient of performance (COP) based on the first law of thermodynamics, are both figures of merit generally used to assess the energetic performance of systems. These methods, however, are not fully coherent and so different technologies are impossible to compare with each other. For example, the efficiency of a thermal pump expressed as COP is bigger than unit, which would corroborate the idea of a *perpetuum mobile*. Or in another example, a monothermal process done by an electrical space heater gives an efficiency of $\approx 100\%$! In the first example the energy balance does not take in account the energy extracted from the cold source, taking into account just the work introduced in the system and the amount of heat shed to the environment. In addition, the heat energy is assumed to have equal quality as the mechanical work. In the space heater example, a high-quality electrical energy was degraded to heat energy trough a fully dissipative process. As mentioned earlier, dissipation produces a considerable amount of internal entropy leading to the consequent increase of exergetic losses.
For the first law of thermodynamics, energies are all the same, and they just change form (i.e. mechanical, electrical, heat). Inversely, exergy accounts for the irreversible processes using the second law of thermodynamics (entropy balance). Doing so, energies have different quality levels defined by their capability to produce work. A conventional analysis of a system using the first principle of thermodynamics (enthalpy-based) is incapable of describing notions such as quality and energy level along with losses and thermodynamic efficiency [20, 21]. The introduction of the exergy balance using the first and second laws, allow the so-called energy degradation to be analyzed.

In their article Rosen and Bulucea [21] compare the efficiency of different processes using the first law approach and the second law approach (exergetic approach). The more significant examples are reported in Table 1.1. Note how the exergetic approach penalizes the degradation of energy in the electric space heater. The efficiency of the heat pump is now smaller than unit for an exergetic approach. These two examples show how well exergy analysis attributes a quality to different forms of energy and the processes used for the transformation.
Also, notice that the second law approach gives unit efficiency for an ideal thermal cycle. This is because in an ideal cycle the energy is entirely dedicated to the production of mechanical work, without any dissipation. The process was able to optimally convert all forms of energy (heat) into mechanical energy. Due to the fact that the heat energy is assessed differently in a first law approach (overestimated), the energy efficiency of an ideal cycle is lower than the second law approach (exergetic approach). The heat energy is greater than the mechanical energy produced. In fact, the transformation of heat into mechanical work is limited by the Carnot factor $1 - \frac{T_c}{T_h}$, where $T_c$ it the temperature of the cold source while $T_h$ is that of the warm source.
In Table 1.1, it can be seen that the efficiency of a hydraulic power plant gives identical results for both approaches. Heat flows in a hydroelectric power plant are really small. The transformation can be modeled basically through an enthalpic exchange of high quality en-

ergy and this is the reason why the two methods give identical results.

Systems similar to our $CO_2$ storage were analyzed by scholars. The study of Luo et al. [22] compares the first law and second law approaches to calculate the efficiency of a switching expansion reduction (SER). SER is employed on air powered systems to reduce the pressure of the power source without using throttling processes. The conclusion of Luo et al was that the first law approach was producing higher efficiency than the second law (exergy) approach. Luo et al found the reason for that discrepancy in the fact that the energetic approach (1st principle) relies more on the initial pressure supply, while the exergetic one is primarily related to the reduced pressure ratio. It is therefore possible to assume that a first principle efficiency would overestimate the efficiency of a carbon dioxide pneumatic system.

To show how important the use of exergy is, we can cite the following example: In the Swiss Confederation laws, exergy became mandatory in the analysis of large building projects [23]. The use of exergy instead of a first law approach is important for the future rational and clever use of resources. This means that engineers must be pushed into this direction in order to correctly analyze their systems' capabilities. This enables engineers to more easily compare technologies and to be consistent while speaking about efficiency. The concept of consistently defining efficiency will be clear later on when we report different performance values based on different thermodynamic paths. It is important to realize that efficiencies based on different thermodynamic paths are impossible to compare.

To clarify this concept I would like to introduce the following example. Assume that we want to assess the performance of a trip. We define, as a reference, the distance of a car trip from Rotterdam to Delft driving on the highway, 15 Km. As a second reference distance, we assume a crow flight between both cities, 10 Km. These two references represent particular thermodynamic paths as it could be an isothermal transformation or whatever state we want to maintain constant. Now using the following formula we would like to assess the performance of the trip based on these two paths.

$$\eta = \frac{reference \quad path}{real \quad trip}$$

The performance of the trip we would like to assess is a car trip following secondary roads, from Rotterdam to Delft. The distance of this travel is 18 Km. Using our performance formula we calculate the corresponding value for $\eta$ based on the two reference paths. The result of these calculations is: $\eta_{highway} = 0.83$ and $\eta_{crow.flight} = 0.55$.
Despite the fact that these efficiencies give an indicative performance of a car travel trough secondary roads as compared to one of the two paths, these results are difficult to compare because they are not coherent with each other. The reference paths are completely different from each other, even though they have the same initial and final states. Similarly, in thermodynamics, we can assess the efficiency based on different paths to express the performance of a transformation that begins and ends at well-defined thermodynamic conditions. Therefore, comparing the isothermal or isenthalpic efficiency of different systems would be meaningless. The problem becomes further complicated if the reference path is not even specified.
Using exergy, this inconvenience is no longer there because an exergetic efficiency is solely assessed accounting for the amount of internal entropy production.

Table 1.1: Some comparative value of first law and second law efficiency [21].

| Process | Efficiency % | |
|---|---|---|
| | 1st law | 2nd law |
| Hydroelectric power plant | 90 | 90 |
| Heat pump | 380 | 19 |
| Resistance space heater | 99 | 6 |
| Ideal thermal power plant | 64 | 100 |

### 1.2.3. Exergetic losses of a pressure regulator

Exergy was chosen to analyze the system because it is a much more coherent way to define performances. More information related to energetics can be found on "*Thermodynamics and Energy Systems Analysis: From Energy to Exergy*" [20]

Assume a pressure regulator with an inlet and an outlet mass flow of $\dot{m}$, as shown in Figure 1.3. The border of the system is represented by the red square around the pressure regulator.

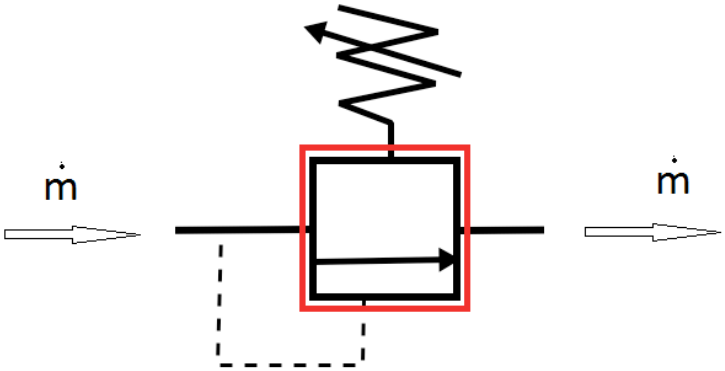


Figure 1.3: Schematics of a pressure regulator with considered border in red

Applying the fundamental equation of thermodynamics for open systems in its mass specific form we have:

$$\delta e^{-} + \frac{dc^2}{2} + gdz + \delta r = -vdP = -dh + \delta q^{+} + \delta r = -dh + Tds \tag{1.1}$$

The sign $+$ and $-$ in superscript indicate the direction of the flow. The positive sign indicates flows entering the system, while the negative sign indicates flows leaving the system.

Furthermore, the following hypotheses are applied to the system:

- Difference of velocity between inlet and outlet $dc \approx 0$.
- Difference of potential energy equal to zero $dz = 0$.
- Phenomenon sufficiently fast to assume adiabatic conditions $\delta q = 0$
- No exchange of work is done through the system $\delta e^{-} = 0$

Applying the aforementioned hypotheses leads to:

$$\delta r = -vdP = -dh + \delta r = -dh + Tds$$

The transformation is isenthalpic $dh = 0$.

We can conclude that the drop in pressure is due to a fully dissipative process which leads to an increase in entropy.

$$-vdP = \delta r = Tds$$

The exergetic losses in mass-specific form are expressed as:

$$l = T_a s^i$$

Entropy is composed of internal and external contributions. External contributions of entropy result in an exchange of entropy, while internal contributions of entropy define the amount of disordered motion.

Within internal entropy, contributions are found dissipative processes. In the case of a pressure regulator the increase of entropy leads to an increase of internal entropy, directly affecting exergetic losses. We can, therefore, rewrite the exergetic mass specific losses for a pressure regulator as:

$$dl = -T_a v dP$$

It is trivial now to see that exergetic losses are proportional to the amount of pressure drop.

### 1.2.4. Quantitative mass specific energy loss

It is possible to estimate the isothermal energy produced by the expansion of carbon dioxide. In this Section, the mass specific energy is calculated assuming an expansion of the $CO_2$ from saturation condition to two regulated pressure levels (0.6 $MPa$ and 1.3 $MPa$). Also, the same calculations are made from the two regulated pressure to atmospheric condition.
This analysis will lead to a conclusion on how much energy is lost due to pressure reduction, thus motivating the importance of the present work.

If we assume a store of $CO_2$ expanding isothermally at $T = 20°C$ from saturated liquid form to a pressure of 0.6 $MPa$, we can estimate the potential work that such a store can produce. Applying the Soave Redlich Kwong equation of state [24] we can define a specific isothermal expansion work. The details can be found in Appendix A.

After integration from the saturated state with vapor quality of $x = 0$ to a pressure of 0.6 $MPa$, the resulting potential work is equal to 150 kJ/kg. Now let's assume that we expand further the gas on the same isotherm from 0.6 $Mpa$ to atmospheric pressure at 0.1 $MPa$. Following the same procedure, an estimate of the potential between these pressures is calculated. Integrating from $P = 0.6Mpa$ to $P = 0.1MPa$, the resulting potential work is 100 kJ/kg. The potential is generally recovered from the regulated pressure level to atmospheric conditions. Yet 50% more potential is available from the saturated state to the regulated pressure.

Following the same procedure described before, but assuming a regulated pressure of $1.3MPa$, there is more recoverable potential from regulated pressure to atmospheric pressure (145 kJ/kg) than from saturation condition (107 kJ/kg) to regulated pressure. This is an important aspect to point out, because it may be more favorable to regulate the pressure at a lower level, affecting gas consumption, but improving the energy recovery. Yet we can not exclude that a pressure recovery along with the optimal pressure will not lead to excellent results.

The values found in this analysis are reported on Figure 1.4 where images explain the considered integral well. The energy from the saturation condition to the regulated pressure is represented in blue, while the work between regulated pressure and atmospheric conditions is represented in orange. The reader should keep in mind that the $x$ axis of the graph is in logarithmic scale for sake of compactness. Therefore, the areas are not visually directly comparable.

This is a first estimation that shows the pertinence of recovering energy while reducing pressure. It is now clear how a pressure regulator strongly affects the energetic performance of a $CO_2$ autonomous system. It is important to realize that this analysis can be applied to any type of gas leading always to the conclusion that a pressure regulator dissipates energy as it was exposed in Section 1.2.3

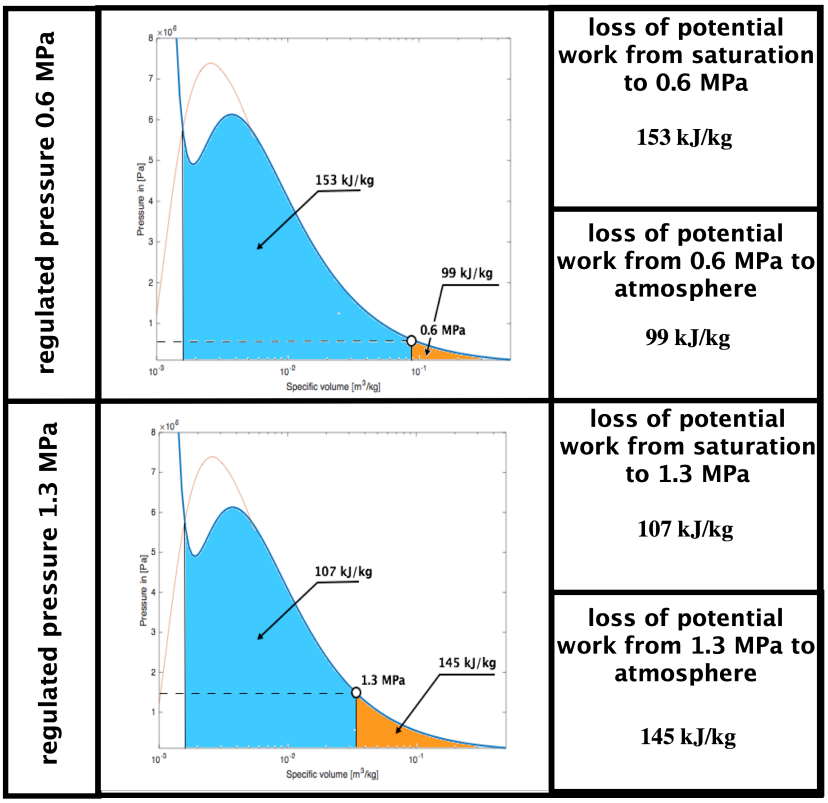


Figure 1.4: Comparative value of mass specific potential energy between two regulation pressure levels, 0.6 $MPa$ and 1.3 $MPa$, on a P-v diagram. The v axis, specific volume, is in a logarithmic scale. The Blue area represents the mass specific isothermal work from saturation condition to the regulated pressure. The orange area represents the mass specific isothermal work from the regulated pressure to the atmospheric condition.

## 1.3. concluding remarks

In this Chapter, the flaws regarding carbon dioxide pneumatically actuated autonomous systems are exposed. It was seen in Section 1.2.3 that due to the absence of work, the pressure regulation produces a fully dissipative process. This leads to the conclusion that work should be extracted by the system (pressure regulator) in order to decrease the exergetic losses, see Section 3.2. Also, the magnitude of a hypothetical isothermal expansion of the gas was considered, Section 1.2.4. It was shown that, for pressure regulated at 0.6 $MPa$, 60% of the available potential energy is lost due to pressure regulation. It should be clear by now the motivation that drives this work as well as the magnitude of the energy that can be recovered.

# 2

# Requirements

## 2.1. Introduction

It is crucial, before beginning to design anything, that the requirements are well defined and motivated. In this Chapter, the requirements the machine should ultimately meet are identified and explained. Requirements are not divided into *must* and *wish*. The requirements are all considered equally important. During the design and the test phase some of these prerequisites will be dropped to put more emphasis on the essence of the machine. For instance, the mass can be further lowered, or dimensions slightly decreased, working upon a functioning concept. A retrospective analysis will be therefore necessary to define how to ameliorate the device.

## 2.2. Requirements

### Recovered energy form

This requirement is meant to restrict the form of energy recovered by the machine. In a pneumatically actuated autonomous systems, the energy needs to be used to increase operational time of the autonomous device; considering the fact that pneumatic autonomous systems may lack completely of electronics. Also, if any electronics is employed to control the autonomous system, the energy for the controller is very small compared to the energy used to actuate the system. The recovered energy must indeed be pressurized gas.

### Energy recovery

It was shown in Section 1.2.4 that a significant amount of energy is lost during pressure regulation. This loss depends on the pneumatic system working pressure. The lowest amount of theoretical energy loss was found for the expansion that goes from saturation pressure to 1.3 $MPa$, Section 1.2.4. For an isothermal expansion this value was 100 $KJ/kg$. This quantity is found using a reversible process, i.e. isothermal expansion. It is important to realize that a real expansion following an actual path would give an inferior value. Due to the fact that this work does not have precedents, it is hard to compare. We may assume a recovered energy equal to the 25% of the isothermal expansion. The energy recovered is therefore fixed at a value of 25 $KJ/kg$.

### Mass of the machine

Recovering energy increasing the mass of the autonomous system would not lead to an appreciable increase in performance. In autonomous systems, the energy to mass ratio is vital. The mass of a pressure regulator can reach up to 24 $g$ [25]. The machine designed to increase the energetic performance of a carbon dioxide storage should weight 24 $g$ or less.

### Independence of the machine
Untethered machines often lack other sources of energy other than the pressurized gas. It would be arguable to add an extra form of energy to control the recovery system. The recovery system should, therefore, be able to autonomously manage its operations as well as stopping at a well-defined output pressure. The only form of energy exploitable by the recovery system is the pressurized $CO_2$.

### Machine self-starting
The machine needs to start its functions autonomously. An eventual drop of pressure on the autonomous system will induce the recovery system to actuate itself.

### Size of the machine
Similarly to the mass, size is also an important aspect of pneumatically actuated autonomous systems. Generally, these machines are fairly small. A maximal volume, that the machine can occupy, is defined based on the size of an ultralight pressure regulator designed by Rob [25]. The recovery system should fit within a prism of 25x25x60 $mm$.

### Mass flow rate
The recovery machine needs to manage a certain flow rate to do not slow down operation of the untethered machine. The flow is therefore set at a minimum value of 1.5 $g/min$ equals to 25 $10^{-6} kg/s$.

Table 2.1: Table of requirements

| Requirement | Metric | Value |
|---|---|---|
| Mass specific energy recovery | $kJ/kg$ | 25 |
| Mass | $g$ | 24 |
| Mass flow rate | $g/min$ | 1.5 |
| Size of the machine | $mm$ | 25x25x60 |
| Recovered energy form | - | Compressed gas |
| Machine self starting | The machine maintains the system pressure | - |
| Independence | Number of external energies other than $CO_2$ | 0 |

# 3

# Choice of the machine

## 3.1. Introduction

In the literature, the losses produced by throttling or pressure regulation are well known. Despite this fact, in pneumatics, only one paper was found where a possible solution was investigated. Xu et al [26] propose to regulate the pressure of a high-pressure pneumatic system using a swash-plate motor-pump, Figure 3.1. The swash-plate motor-pump is used to expand the pressurized air in order to recovery work. It is a brilliant choice because in a swash-plate motor the expansion volume can be easily modified varying the angle of the swash plate. The swash plate directly affects the stroke length. This machine cannot probably be exploited in our case because of the evident difficulties in scaling down such complex motor.
The literature on this subject seems rare. More examples of similar works, related to recovery energy from a throttling process, can be found on thermodynamics cycles. These thermodynamics cycles are generally: Organic Rankine cycles and refrigerating cycles. Organic Rankine Cycle (ORC) is the well-known steam turbine cycle, with the difference that instead of using water, the fluid is a low boiling temperature fluid, as $CO_2$, for instance. In ORC and refrigerating cycle, many are the expander used in experimental setups, but none of them deal with such a small flow, energy and sizes. Furthermore, ORC and refrigerating cycles operates in closed loop. This means that the expander operates in steady state condition, and internal leakages are less of a concern, because indeed the fluid cannot be fully exploited, yet energies a greather that wat we are confronted in this work. Steady state conditions allow the machine to be perfectly designed.
The subject investigated in this work appears to be the first of its kind. Due to this fact, many choices will be based on sound judgment.

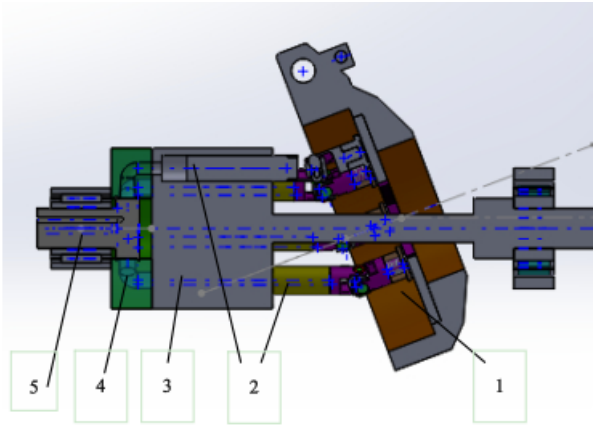


1.swash plate 2.piston-shoe assembly 3.cylinder-shaft assembly
4.valve plate 5.valve shaft

Figure 3.1: Model of a swash plate motor from Xu et al [26]. The main components are showed in the drawing. Note how the angle of the swash plate influences the volume of the machine varying the pistons' stroke.

## 3.2. How to decrease exergetic losses

It was shown using the fundamental equation of thermodynamics, Section 1.2.3 Equation 1.1, that a pressure regulator produces a dissipative process.
Recalling the same formula, Equation 1.1, reported hereafter, can be shown how to reduce these losses extracting work from the system.

$$\delta e^{-} + \frac{dc^2}{2} + gdz + \delta r = -vdP = -dh + \delta q^{+} + \delta r = -dh + Tds \tag{3.1}$$

Applying the assumptions below to Equation 1.1:

- Difference of velocity between inlet and outlet $dc \approx 0$.
- Difference of potential energy equal to zero $dz = 0$.
- Phenomenon sufficiently fast to assume adiabatic conditions $\delta q = 0$

we lead to:

$$\delta e^{-} + \delta r = -vdP = -dh + \delta r = -dh + Tds \tag{3.2}$$

If it is assumed that the work produced is equal to $\delta e^{-} = -vdP$ the dissipative energy $\delta r$ goes to a null value.

It is now clear that the machine used to reduce the pressure needs to produce work in order to decrease exergetic losses.
Fluid machines are systems capable of achieving this result.

## 3.3. Fluid machinery

To choose the most adequate fluid machine it is important to remind the following requirements:

- Compactness 25x25x60 $mm$
- Self starting
- Mass flow 25 $10^{-6} kg/s$

Due to the extremely low mass flow and the fact that we may aspect this flow to be particularly unsteady, turbo-machinery will be directly excluded.
The category of machines that best fit this minuscule mass flow is probably the positive displacement devices. Within this group we can find: scroll expander, rotary vanes, reciprocating (piston) machines, screw expander, etc. Some examples of the cited machines can be found in Appendix B, more information can be found on the literature [27–30].
Scroll expanders, rotary vanes and screw expanders, minimize internal leakage thank to really tight tolerances of moving parts or complex sealing systems. These tolerances to be achieved need an extremely high-quality machinery process. Internal leakage can be described as the gas escaping the expansion volume within the machine producing no work. Furthermore, these gaps, even if small enough, are an easy passage for the gas, especially at high pressure (5.7 $MPa$).
It is safe to assume that these expanders are not suited for the studied case because of internal leakage. In Figure 3.2 is shown a section of a rotary vane expander from Fukuta et al. [31]. Fukuta et al. describe internal leakages as one of the factors lowering the efficiency of a rotary vane expander. Similarly, this phenomenon affects turbo-machines, because they lack of seal methods the dynamic elements. The gas would just pass through the turbine blades without produce actuation.

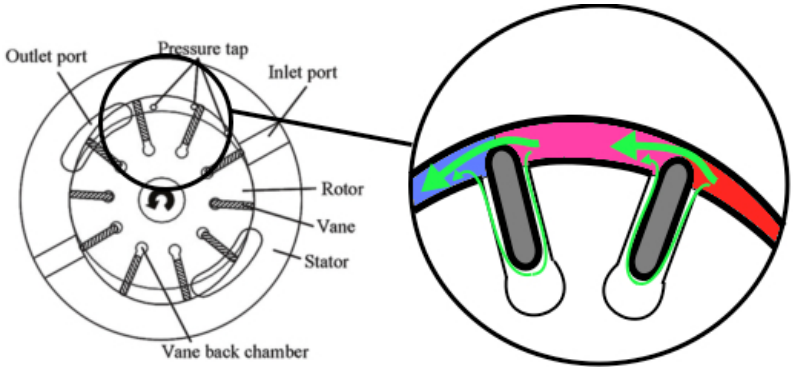


Figure 3.2: Modified section of a rotary vane expander from Fukuta et al [31]. In the drawing the arrows represent the two paths where leakage occurs. The gaps are accentuated on purpose to better understand where the gas could leak through.

Reciprocating machines are those machines that make use of pistons to convert a linear motion into a rotational movement. These devices are generally rigidly connected to a crankshaft.
Pneumatic cylinders are simple positive displacement machines. The piston can effectively be leaks free using adequate sealing [32].
Sealed pistons of a reciprocating machine may, therefore, avoid unwanted internal leakage. Being the piston rigidly attached to a crankshaft makes the auto-starting of these expanders difficult. Imagine if the piston would stop at the bottom dead center, even with an infinite pressure, the machine would not start. A crank mechanism is therefore needed. This may increase the complexity of the machine and may require considerable energy only to crank the system. Reciprocating machines of this type seem therefore not suited for this project.

The only viable option appears to be a simple device that closely looks like a pneumatic piston. These similarities can be found on a free-piston expander. A free-piston expander indeed looks like a pneumatic cylinder. It has minimal moving parts compared to other machines, and it can be built extremely compact.
In the literature related to autonomous systems is described the use of the free-piston engine to convert chemical energy into pressurized fluids [33, 34]. These authors choose free-piston engine because of its compactness, simplicity and the property to be self-starting. In Figure 3.3 a double acting free-piston machine is shown, note its simplicity. This free-piston was designed to work with hydrogen peroxide. Hydrogen peroxide is a substance that when in

contact with a catalyst decomposes into a large amount of gas and heat.

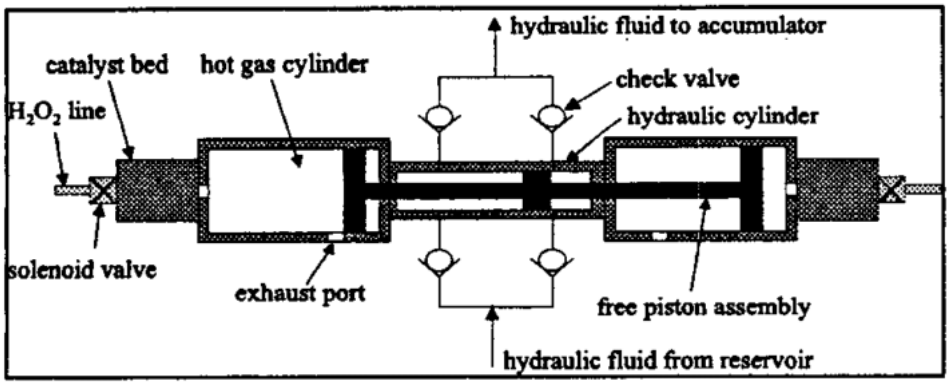


Figure 3.3: Double acting free-piston concept from Raade et al[34].

The free-piston expander, due to its simplicity, compactness, and self-starting properties appears to be the best option. In the following Chapter, this option will be further investigated.

# 4

# Physical model

## 4.1. Introduction

The physical model is the composition of mathematical interpretation of physical phenomena occurring in a free-piston expander-compressor. This model is proposed to understand the behavior and the effect of parameters change on the free-piston machine. Furthermore, the model was used to run an optimization trough genetic algorithms to find the best geometrical dimensions to achieve a maximal performance of the compressor-expander. The mathematical relations were implemented in Simulink® and optimized trough Matlab®.

## 4.2. Limitations

The model is limited to the amount of precision of the relationships describing a determined phenomenon. Increasing the accuracy and the complexity of the model will, of course, enhance the precision of the simulation. Sometimes the limitations come from the fact that many relations are empirical and defined for a particular case, yet still applicable. To cite an example, the flow through an orifice, the empirical relationship is based on a slightly different geometry of the orifice than what we may design for the free-piston. Other limitations come from the fact that the physical phenomena are still not completely understood as it is the case for the sonic choke for a biphasic $CO_2$.

## 4.3. Structure of the model

The structure of the model is essentially split into four subsystems. Two systems represent the expander, while the last two represents the compressors. The piston position $z$, by the use Newton's second law, connects the four system together, representing the whole machine. In Figure 4.1, a schematics of the model is shown. Two infinite vessels compose the model at a pressure of 5.7 $MPa$ and 1.3 $MPa$. The first vessel represent the pressure supply at saturation pressure (for $CO_2$ at room temperature), while the second represent is the Pneumatic autonomous system operation pressure. The pneumatic autonomous system pressure was chosen to be 1.3 $MPa$ because, following the study of Plettenburg [5] and the practical assessment of Doedens [18], this pressure assure a minimal consumption of gas per cycle.

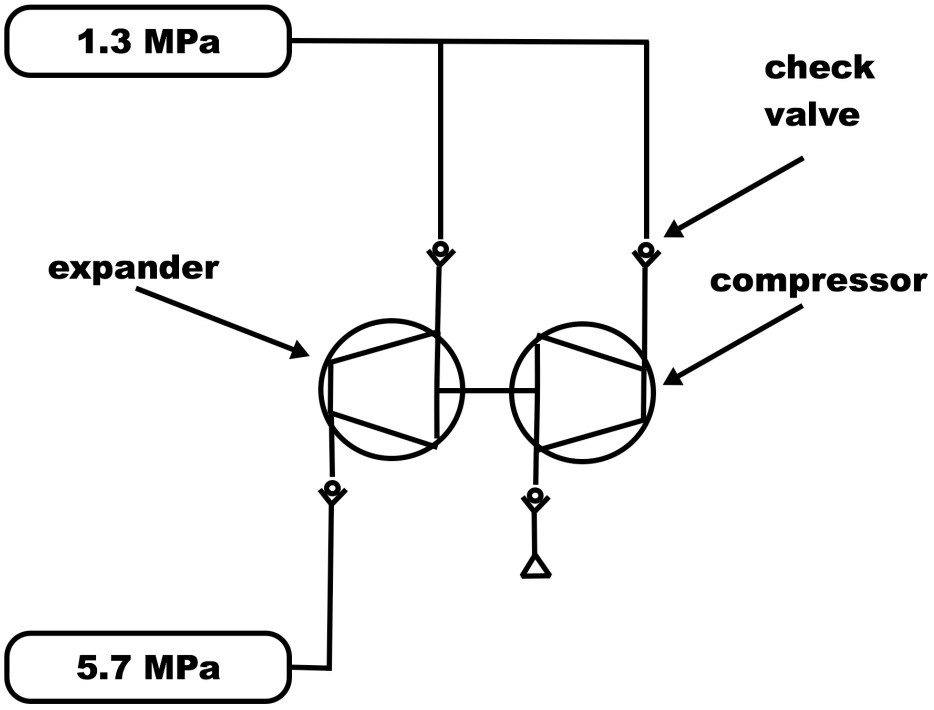


Figure 4.1: Visual representation of the mathematical model structure.

## 4.4. Expander

The expander was modeled using energy conservation, mass conservation and simplifying assumptions as that of an adiabatic transformation, meaning that the cylinder is thermally insulated. The first principle was applied to a control volume within the expander, see Figure 4.2. A detailed procedure is described in Appendix C.1.2.

The thermodynamic behavior of the $CO_2$ is describe using the Soave-Redlich-Kwong Equation (SRK) of state [24], see Appendix C.1.4. It is important to treat $CO_2$ as a real gas because at conditions so close to the saturation conditions the gas behavior is far from that of an ideal gas. The SRK can well describe the thermodynamic characteristics with a sensible increase in the difficulty of the equations. The governing equation for the expander during the three phases (suction, expansion, and discharge) can be found in Table 4.1. These differential equations describe the temperature behavior within the control volume, Figure 4.2. It would have been more intuitive to express the pressure variation in time, yet the temperature was chosen because it was easier to explicitly be defined after the introduction of the SRK equation of state.

The flow was treated as compressible and subjected to sonic choke. The mass flow is, therefore, linearly proportional to the pressure of the source, or upstream pressure when the sonic conditions are met. When the flow is subsonic, the mass flow will depend non-linearly on upstream and downstream pressures. Therefore it depends on the pressurized bottle and the pressure within the expander chamber. For more details see Appendix C.1.6.

Table 4.1: Formulas derived from the 1st principle of thermodynamics applied on the expander

| Formula reference | Formula |
|---|---|
| Suction | $\frac{dT}{dt} = -\left[\frac{P_e A_e}{c_v m_e}(\mathbb{X}+1)\right]\frac{dz}{dt} + \left(\frac{P_s v_s + u_s - u_c}{c_v m_c} + \frac{P_c v_c}{c_v m_c}\mathbb{X}\right)\frac{dm_e}{dt}$ |
| Expansion | $\frac{dT}{dt} = -\frac{P_e A_e}{c_v m_e}(1+\mathbb{X})\frac{dz}{dt}$ |
| Discharge | $\frac{dT}{dt} = -\left[\frac{P_e A_e}{c_v m_e}(\mathbb{X}+1)\right]\frac{dz}{dt} + \left[(\mathbb{X}+1)\frac{P_e v_e}{c_v m_e}\right]\frac{dm_s}{dt}$ |
| Common term $\mathbb{X}$ | $\mathbb{X} = \frac{T_e}{P_e}\left(\frac{r}{v_e - b} - \frac{\frac{\partial a}{\partial T_e}}{v_e^2 + v_e b}\right) - 1$ |

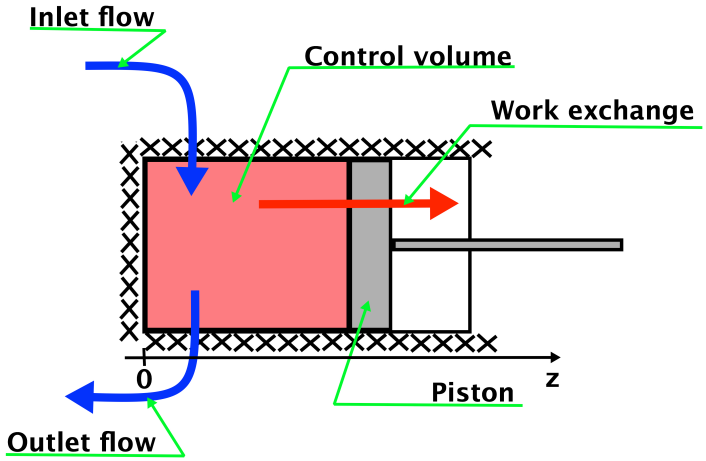


Figure 4.2: Schematics of the expander. It is well visible the control volume, the positive direction of the piston movement as well as the exchange of flow and work

## 4.5. Compressor

The compressor is analogically modeled as the expander. The first principle, mass conservation, flow equation ( sonic and subsonic), compose the set of equations describing the compressor.

The equation of state differs from the one used for the expander. The equation of state used is the ideal gas relationship, which well describes the air thermodynamics. A complete procedure can is found in Appendix C.1.5. The differential equation governing the three phases of the compressor are in Table 4.2. The ideal gas equation of state makes the differential equations simpler than that of the expander. This time the variation of the pressure in time is explicitly found.

## 4.6. System connection

A shaft physically connects the four systems. The displacement of the shaft affects the position of the three pistons of the machine (two system describing the expander and two de-

Table 4.2: Formulas derived from the 1st principle applied on the compressor

| Formula reference | Formula |
|---|---|
| Suction | $\frac{dT}{dt} = -\left[\frac{P_e A_e}{c_v m_e}(\mathbb{X}+1)\right]\frac{dz}{dt} + \left(\frac{P_s v_s + u_s - u_c}{c_v m_c} + \frac{P_c v_c}{c_v m_c}\mathbb{X}\right)\frac{dm_e}{dt}$ |
| Expansion | $\frac{dT}{dt} = -\frac{P_e A_e}{c_v m_e}(1+\mathbb{X})\frac{dz}{dt}$ |
| Discharge | $\frac{dT}{dt} = -\left[\frac{P_e A_e}{c_v m_e}(\mathbb{X}+1)\right]\frac{dz}{dt} + \left[(\mathbb{X}+1)\frac{P_e v_e}{c_v m_e}\right]\frac{dm_s}{dt}$ |
| Common term $\mathbb{X}$ | $\mathbb{X} = \frac{T_e}{P_e}\left(\frac{r}{v_e - b} - \frac{\frac{\partial a}{\partial T_e}}{v_e^2 + v_e b}\right) - 1$ |

scribing the compressor), see Figure 4.3. Note, that even though the expander shares the same cylinder, there are two distinct systems physically separated from each other by the expander piston.

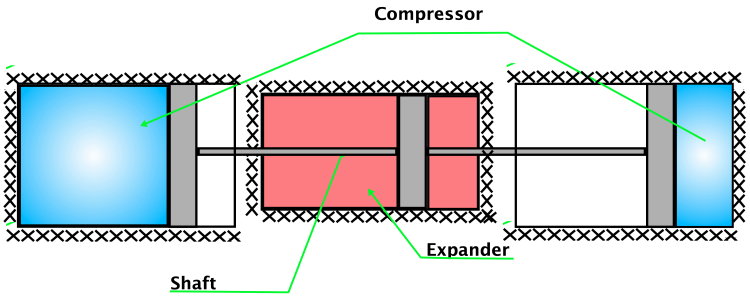


Figure 4.3: Schematics of the free-piston. The expander volume is represented in red, while the compressors volumes (left and right) are represented in blue. The shaft connects the expander's piston with the compressor's pistons

The formulas derived by dynamics governing the piston movement are in Equation 4.1.

$$\frac{d^2 z}{dt^2} = \frac{(P_{e1} - P_{e2})A_e + (P_{c1} - P_{c2})A_c - \eta\frac{dz}{dt}}{m_{shaft}} \tag{4.1}$$

The system, being frictionless, was unstable. To mitigate that, a little viscous friction ($\eta = 0.05 Ns/m$) was add to maintain the motion stable adding the term $-\eta\frac{dz}{dt}m_{shaft}$ in Equation 4.1.

## 4.7. O-ring friction model

Friction may be a great source of losses in performance. Friction greatly influences the actuation of the free-piston as all mechanical machines. Many are the models developed found in the literature [32, 35–37]. Even if these models well define the friction behavior, as its dependence on pressure difference, translation velocity, stick-slip, etc; it is really difficult, or almost impossible to be applied. In fact, these functions need parameters. These parameters are identified using real setups. Thus, without a physical free-piston compressor-expander from which we can determine the many parameters governing the friction behavior, these functions models are of little value. The Parker Corporation [38] propose a simple method to estimate resistance. It is a much more rudimentary way than the methods previously cited. Unfortunately, also this estimation, the one suggested by Parker, it appears to be too conservative giving friction forces difficult to imagine correct.
Due to this impossibility to give a good estimate to friction the models was made upon frictionless assumptions. It is important to notice that this is a critical assumption and strongly affects the results of the mathematical model.

# 5

# Design of the first prototype

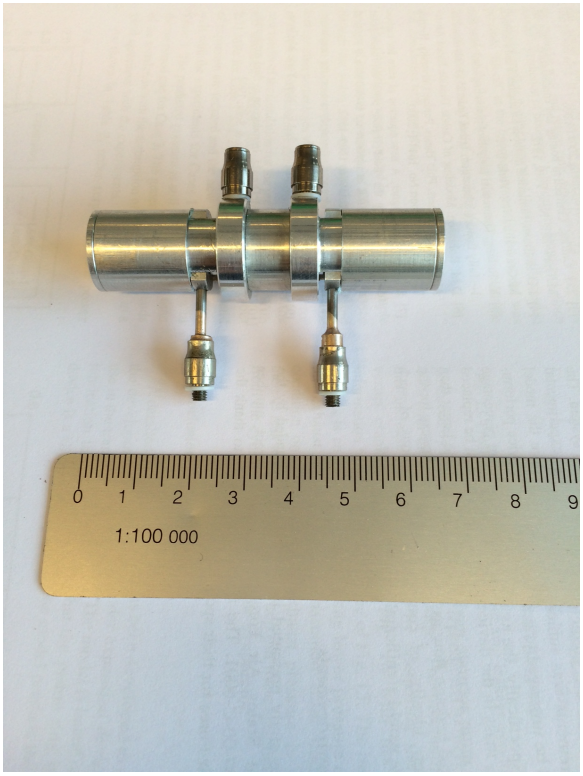


Figure 5.1: Picture of the first prototype assembled.

## 5.1. Concept

The choice of the machine felt on a double acting free-piston expander-compressor. The energy will be recovered in the form of compressed air. The expanded $CO_2$ will be merged with the compressed air to aliment the pneumatic system. In order to combine the flows, the compressed air needs to reach a slightly higher pressure than the carbon dioxide. Check valves will be placed on the compressor side to avoid a backflow of the fluids (air and or $CO_2$). The machine should stop when the sum of the forces acting on each surface of the three pistons is null. The inlet and outlet port of the motor will be open and closed using a spool valve controlled by the position of the pistons. In Figure 5.2 is represented a schematic of the concept.

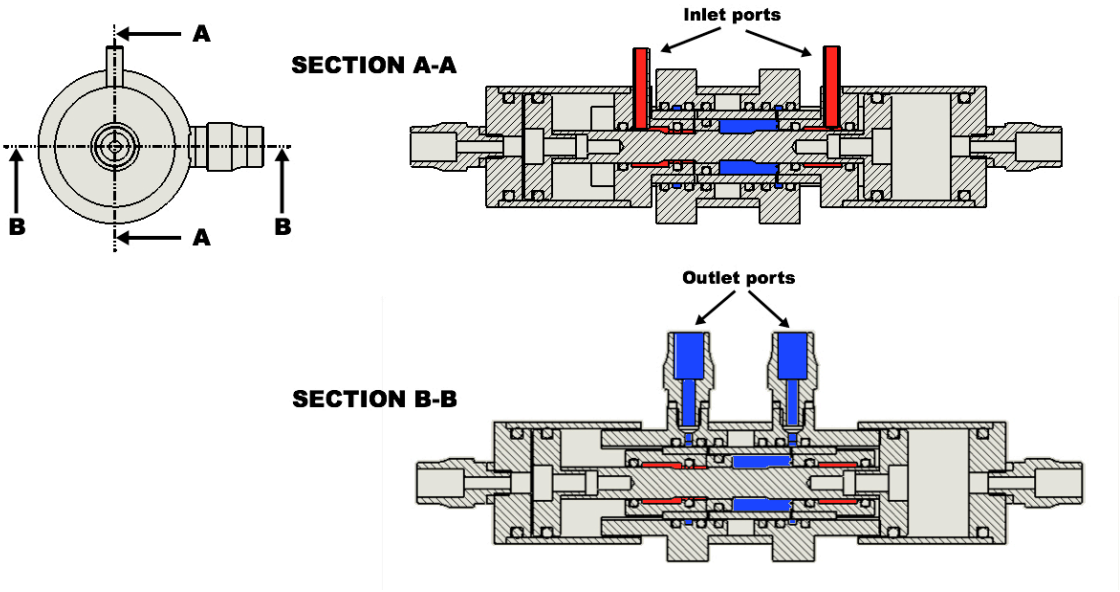


Figure 5.2: Axial cut of the first prototype. In red can be seen the passage of the high pressure gas while in blue is shown the exhaust port

## 5.2. Geometry

A double acting free-piston expander-compressor is composed of a shaft where, in this design, three pistons are rigidly connected to it. The pistons need to have specific dimensions to produce the necessary forces and the needed expansion. Another critical aspect is the stroke length. Together, cylinders diameter and stroke length, define the amount of gas that can be expanded either compressed.
Another important geometric parameter is the state of the inlet and outlet port of the expander (open or closed).
Also the timing of the spool valve, therefore its relative position with respect to the pistons is parameterized to be used in a simulation.
The model proposed in Chapter 4 was used to define these critical dimensions that would allow the free-piston to recovery a maximal amount of work.

The fact that the optimization was run on a frictionless model does not entirely lead to inconsistent results. It is safe to say that, at least, upper and lower geometrical boundaries are known, this would eventually facilitate an empirical search using a prototype.
To optimize the free-piston parameters, genetic algorithms were applied to the Simulink model. Table 5.1 shows the constraints applied on the parameter for the genetic algorithm optimization.

Table 5.1: Constrained parameters used in the genetic algorithm optimization.

| Parameter | $Symbol$ | Unit |
|---|---|---|
| Compressor piston diameter | $5 < d_c < 15$ | $mm$ |
| Expander piston diameter | $5 < d_e < 15$ | $mm$ |
| Stroke | $5 < z_s < 20$ | $mm$ |
| Inlet $CO_2$ open | $0 < z_{CO_2 open} < z_s$ | $mm$ |
| Outlet open distance | $0 < z_{open} < z_s$ | $mm$ |
| Outlet close distance | $0 < z_{close} < z_s$ | $mm$ |

The target function $f_{opt}$ that defines the fitness level of each generation was chose to be the outlet mass of compressed air $m_{air}$ over the inlet mass of $CO_2$ $m_{Co_2}$, Equation 5.1.

$$f_{opt} = -\frac{m_{air}}{m_{Co_2}} \tag{5.1}$$

The genetic algorithm to creates generations that are composed of the parameters to be varied. Each generation is evaluated trough the Simulink model and ranked using the proposed target function using Matlab. The generation with best fitness value, which is the group of parameters that minimize more efficiently the target function, has more opportunities to participate in the composition of the next generation of parameters. This process is repeated until the stopping criteria are meet.

Note that Equation 5.1 has a negative sign. The negative sign was add because by default Matlab's genetic algorithm has for objective to minimize the value of the target function. Adding a minus has the effect of maximize the ratio.

The initial population is listed in Table 5.2. The population size was set at 25 individuals and the fitness limit was set at negative 0.5. The other parameters were left as by default. The stopping criteria meet during optimization was the number of generation; $Generation = 100 * numberOfVariable = 600$. This maximum number of generations is a default value. The simulation reached relatively fast the neighboring of the final optimum, also for slightly different initial populations. Mutation factor and migration factor were left as a default. These two factors help the optimization to explore the function more effectively, due to the narrow constraints, Table 5.1,it is believed that there is no need of a broad exploration.
Among all the parameters the one with less effect on the fitness function result was the stroke.

Table 5.2: Values of the initial population for the genetic algorithm optimization.

| Parameter | $Symbol$ | Unit |
|---|---|---|
| Compressor piston diameter | $d_c = 8$ | $mm$ |
| Expander piston diameter | $5d_e = 10$ | $mm$ |
| Stroke | $z_s = 7$ | $mm$ |
| Inlet $CO_2$ open | $z_{CO_2open} = 1$ | $mm$ |
| Outlet open distance | $0 < z_{open} = 1$ | $mm$ |
| Outlet close distance | $0 < z_{close} = 1$ | $mm$ |

The optimization reached a fitness function of 0.25 with the parameters listed in Table 5.3. This means that per each 100 unit of mass of carbon dioxide can be compressed 25 unit mass of air at 1.3 $MPa$.

Table 5.3: Constrained parameters used in the genetic algorithm optimization.

| Parameter | $Symbol$ | Unit |
|---|---|---|
| Compressor piston diameter | $d_c = 13$ | $mm$ |
| Expander piston diameter | $d_e = 6$ | $mm$ |
| Stroke | $z_s = 7.5$ | $mm$ |
| Inlet $CO_2$ open | $z_{CO_2open} = 1$ | $mm$ |
| Outlet open distance | $z_{open} = 1.5$ | $mm$ |
| Outlet close distance | $z_{close} = 2.5$ | $mm$ |

These parameters are easily identifiable in Figure 5.3. Note that since the model assumed a dimensionless shaft, the diameters $d_c$ and $d_e$ have to be corrected. The correction simply implies that the piston needs to have an equivalent area as for the diameters listed in Table 5.3. The Parameters $z_{open}$ and $z_{close}$ are not equals, this simply means that the open port should close 1 $mm$ earlier than when the opposite port should open.A second simulation,

where both ports open and close simultaneously showed a decrease in mass of air compression of only 0.03 %. The simulation shows an imperceptible loss of performance, it was therefore decided to simultaneously close and open the ports controlled by the spool valve. This would not have significantly affected the efficiency.

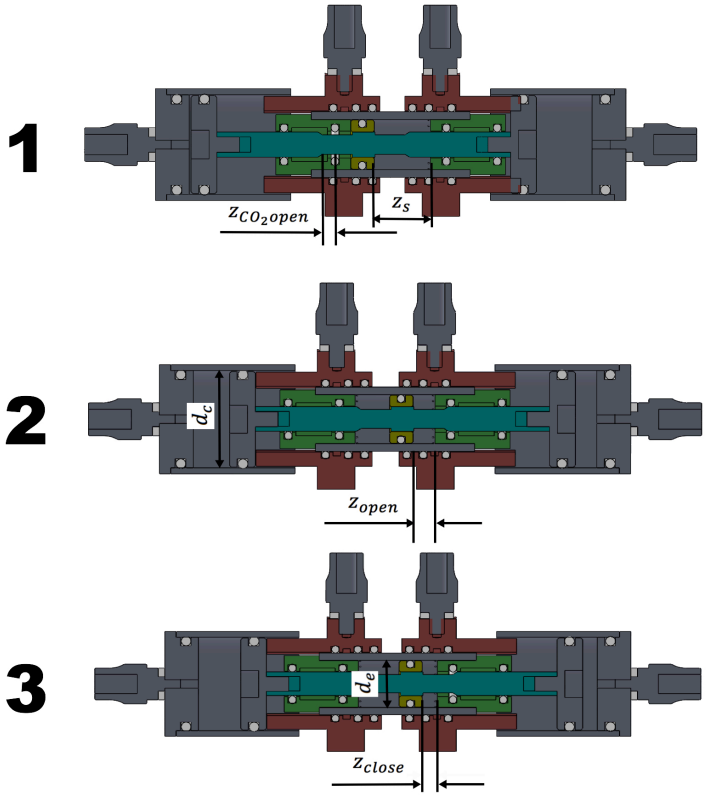


Figure 5.3: Graphical representation of the parameters used in the optimization.

### 5.2.1. Wall thickness and shaft length

Wall thickness of the cylinders may be a concern if incredibly thin. In fact, as detailed exposed in Appendix D.2, the wall thickness of an aluminum cylinder (alloy 7075) capable of withstanding a pressure of 5.7 $MPa$ for $5{\cdot}10^8$ cycles is approximately $0.2mm$. Yet, because the cylinders need to be handled and machined, a certain thickness is needed. Therefore the choice of the wall thickness is 1 $mm$ for practicality only and not related to resistance issues. The shaft was chosen to be 4 $mm$ in diameter. This will allow M 2 screws to secure the compressor piston on the shaft in addition to a little guidance, Figure 5.4a. The length of the shaft is 35 $mm$. As detailed shown in Appendix D.3 this length will not compromise the stability of the shaft.

### 5.2.2. Minimal shoulder thickness

O-rings are generally mounted on grooves on a shaft or a bore. A shoulder, Figure 5.4b, prevent the O-ring from moving. For the sake of compactness, it is important that these shoulders are as thin as possible without making them impractical to manufacture. The minimum shoulder thickness was chosen to be 0.5 $mm$. This allows an easy manufacturing process, compactness as well assuring resistance as shown in Appendix D.4.

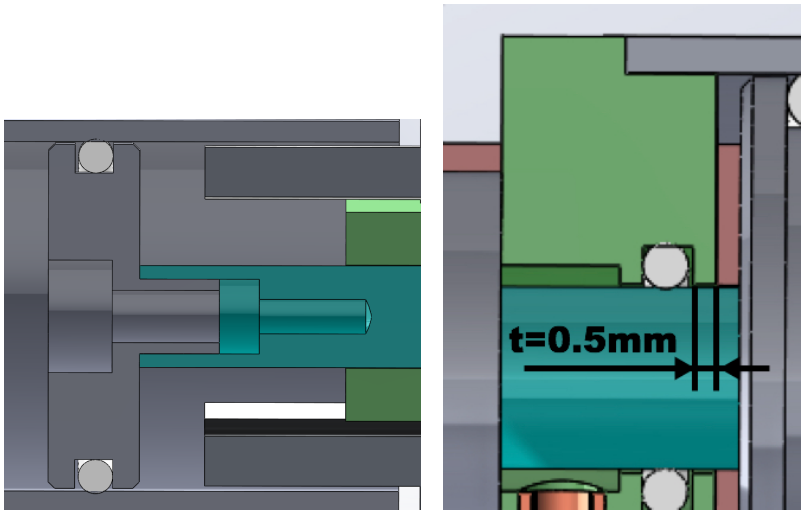


(a) Detail of the compressor piston and shaft fitting. A small circular boss center the piston on the shaft.

(b) Detail of the shoulder minimal thickness for the high pressure side.

Figure 5.4: Design details of the free-piston

## 5.3. O-rings choice

The O-rings choice is based on the dimension of the various designed parts and vice versa. Sometimes the O-rings would dictate specific dimension. In general, O-rings are provided at 1 $mm$ of incremental diameter. It was therefore not difficult to slightly modify the design to fit them into the system.
A more important aspect to consider is the friction effect of the O-ring. In fact, greater is the cross section of the O-ring and higher is the friction [5]. Hence to reduce friction forces, the smallest O-rings cross section available was chosen.
The material of the O-ring was acrylonitrile-butadiene-rubber (NBR). This material is a standard O-ring rubber, and it has the advantage that the O-rings are readily available, especially for small sizes.
The stability of this material to $CO_2$ was also a choice criteria as well as the temperature resistance. Indeed the temperature of a $CO_2$ flow can reach levels as low as -40°C [1]. Figure 5.5 shows the temperature range of elastomeric material used to produce O-rings. The hardness of the O-rings was generally $70sh$. Also, O-rings of $90sh$ were considered for parts of the system where wear could occur. It is preferable to use the softer O-rings though. In fact, O-rings hardness increases friction as well.

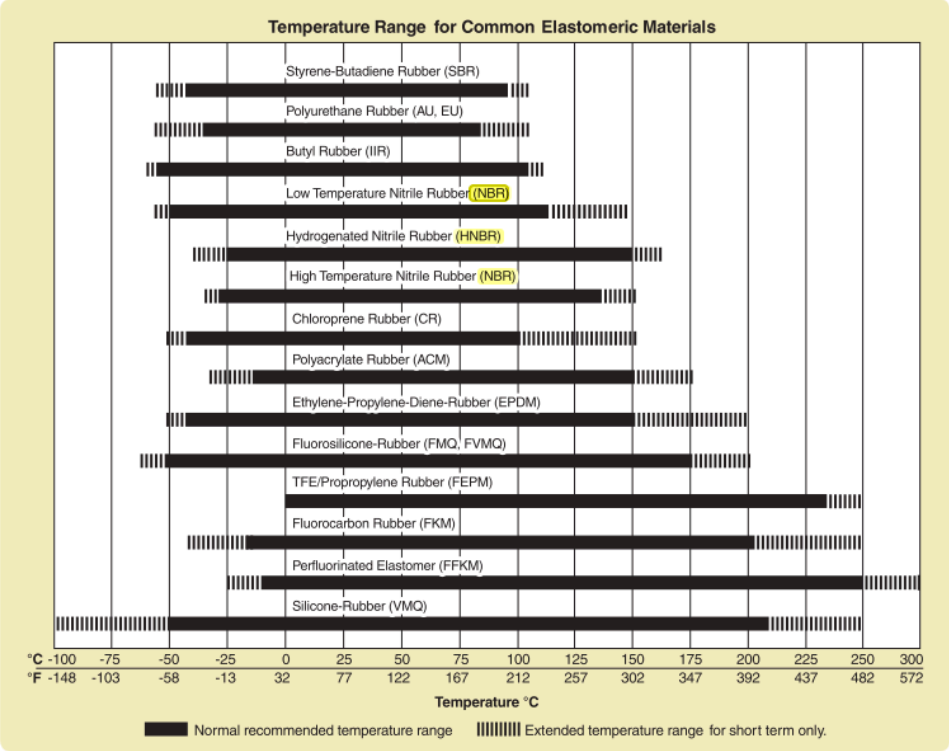


Figure 5.5: Temperature range for common elastomeric materials, from Parker Corporation [38]

## 5.4. Lubrication

Lubrication is important to reduce wear, increase sealing and decrease friction. The grease ROCOL kilopoise 0001 was chosen based on the experience in pneumatics of the DIPO (Delft Institute of Prosthetics and Orthotics) of the Delft University of Technology.

## 5.5. Bering and gaps

The design of the device does not expect the use or any bearing. The extremely light weight shaft pistons composition (3 $g$), will produce a minimal radial force on the O-rings, compared to the forces that O-rings produces over the shaft. The O-rings bear and center the shaft.
To avoid the contact of moving parts, a gap is necessary, Figure 5.6. The gap was arbitrarily

chosen to be around $0.02^{0}_{+0.01} mm$; this would prevent extrusion. Extrusion is an O-ring failure where the O-ring escape from its groove and get trapped between moving parts, Figure 5.7.

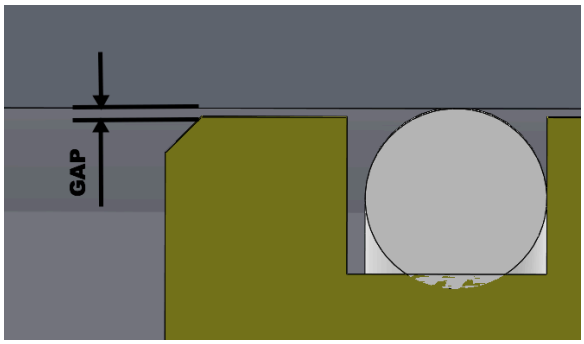


Figure 5.6: Gap between static and dynamic parts. The gap was arbitrarily chose to be around $0.02^{0}_{+0.01} mm$

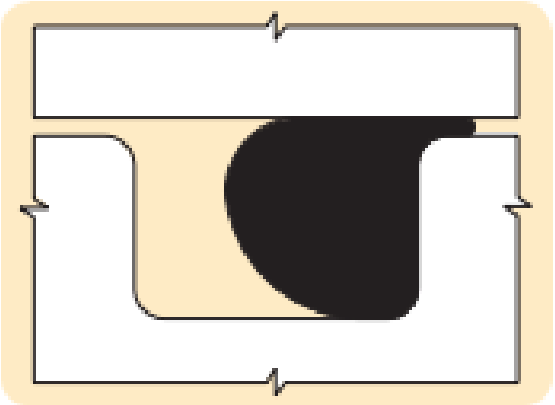

Figure 5.7: Schematic view of the O-ring extrusion from Parker Corporation [38]

## 5.6. Functioning of the system

The free-piston expander-compressor, Figure 5.2, is composed by a piston in the expansion chamber and 2 pistons for the compression of the air. A spool valve controls the opening and closing of the expansion chamber outlet. In order to obtain a compact design, the spool valve is composed of an outer shell, and it is mounted directly on the expansion cylinder. The valve is controlled by the position of the two compressor cylinders, Figure 5.8. The shaft, while moving, actuates at a particular position the spool valve. The spool valve simultaneously closes the outlet port on one side of the expander cylinder opening the outlet port on the opposite expander cylinder. The spool valve, through the compressor pistons, controls the alternating motion of the machine.

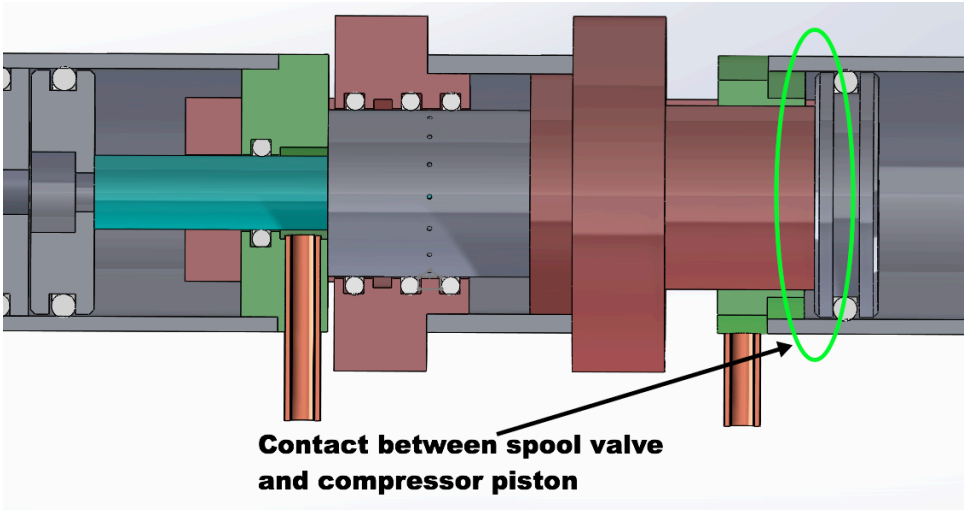


Figure 5.8: Detail of the contact between spool valve and compressor piston. The picture show a fully actuated spool spool valve.

### 5.6.1. Spool valve

The spool valve, Figure 5.9, is composed of an outer shell, six O-ring in NBR 11x1.3 70 sh and a spool. The spool is also the expander chamber. When the valve is open, the gas flows from the expander chamber to the pneumatic system after expansion. The flow is channeled trough little holes of 0.25 $mm$ in diameter. This solution was chosen because of the sensitivity of O-rings to travel over voids. In fact the O-ring, due to the pressure, have the tendency to fill gaps and consequently get caught between the two surfaces and shear off, strongly compromising sealing capabilities.

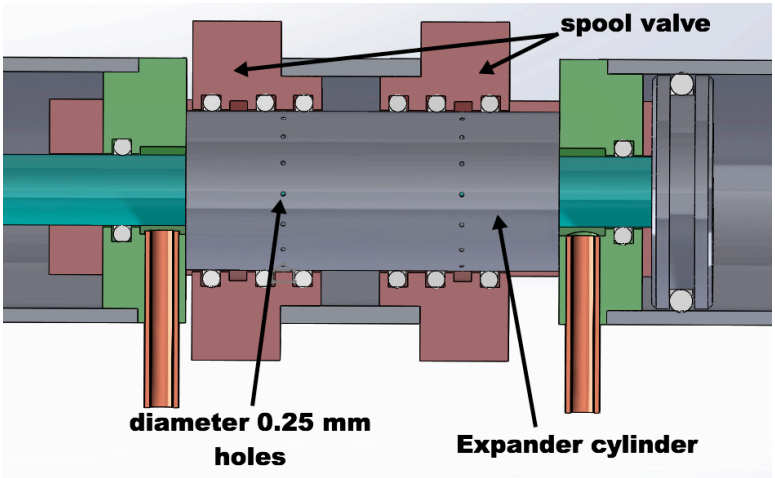


Figure 5.9: Detail of the spool valve. The expander cylinder is also the spool shaft. On the expander cylinder are present the ⌀ 0.25 mm holes for the gas passage.

### 5.6.2. Inlet valve

The inlet valve, Figure 5.10, is composed of the piston shaft and an outer shell. Groves in the shaft allow the bypass the sealing function of the O-ring enabling the gas to fill the expansion chamber. Once the piston has traveled a well-defined distance($z_{CO_2 open} = 1mm$), the sealing is restored because the shaft touches homogeneously the O-ring. Two were the designed options. One design has 0.30 $mm$ groove on the circumference of the shaft, left column of Figure 5.10. The second design has a groove connected trough a 30°chamfer to the major shaft diameter, right column Figure 5.10.

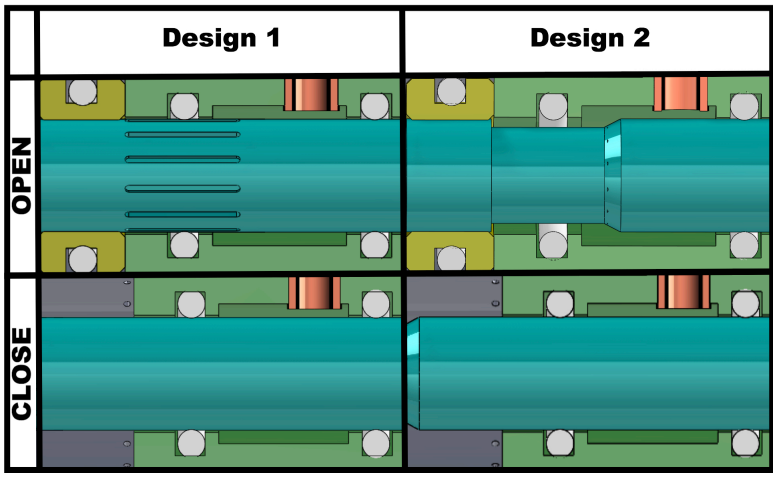


Figure 5.10: Detail of the inlet valves. On the left, the flow valve opens thanks to a 0.35 $mm$ grove manufactured of the pistons shaft. On the right, a grove with a 30°chamfer allows the gas passage. Both valves close when the piston rod touches the O-ring homogeneously.

## 5.7. Test

The free-piston expander-compressor was built and tested. Initially, the most important aspect to verify was the alternating motion of the machine.
The compressor's pistons were not able to actuate the spool valve. Therefore an autonomous oscillatory movement was not achieved.
One of the reason would lie in the fact that the filling of the expansion chamber was insufficient. This insufficient filling would lead to a lack of potential energy per stroke. Therefore the energy accumulated within the expander was not enough to overcome the friction forces of the spool valve and shaft sealings.
A second reason could have been the spool valve timing. The spool valve closes and opens the two expander chamber simultaneously. When the spool valve is actuated, the expanding chamber suddenly sees its pressure dropping because the gas escapes through the open outlet port. The chamber that is now in the discharge phase will see the outlet port closing and the pressure will build up creating resistance to the movement of the expander piston. In Figure 5.11 is shown the development of the pressure against the expander piston position. While the piston travels toward the positive displacement the pressure in one chamber decreases while in the opposite chamber increases. The phenomenon revers when the piston moves in the opposite direction.

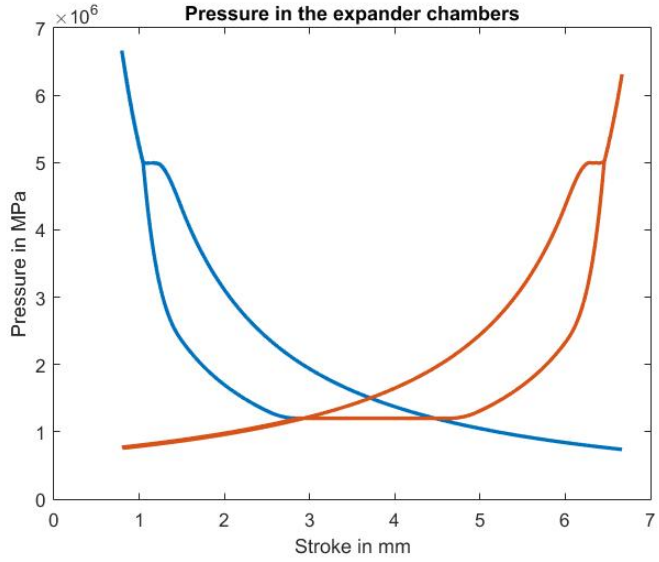


Figure 5.11: Graph of the pressure within the two expander chambers. While the pressure decreases in the left chamber the pressure increases on the right chamber.

Furthermore, while the O-rings or the spool valves were unaffected by traveling over the small size holes, the two designs of the inlet valve led to the failure of the O-rings. The failure resulted in a continuous flow within the expansion chamber. This flow had the effect to balance the force acting on both sides of the expander piston disabling the movement.
These malfunctions of the first prototype led to the design of the second prototype.

# 6

# Design of the second prototype

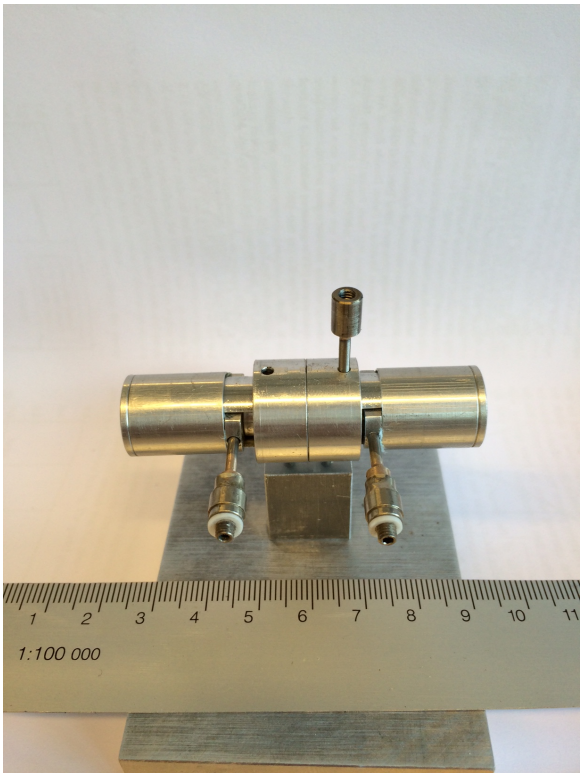


Figure 6.1: Picture of the second prototype assembled.

## 6.1. Introduction

The second prototype, Figure 6.1, was meant to solve some of the issues hypothesized in Section 5.7 that did not allow the first prototype to work, namely the under-filling of the expansion chamber.

## 6.2. Concept

The second prototype keeps the apparently well-functioning design of the first prototype. The second prototype in contrast to the first has inlet and outlet port position dependent from each other. Or better, when the spool is actuated the inlet port closes as the outlet port opens and vice versa. This would have the effect of maintaining the inlet port open for a longer period.

Keeping the inlet port open for a longer period affects the efficiency of the system because it influences the expansion. Indeed an under-expansion is expected in this case. Under-expansion means that the recoverable energy is not fully exploited because the pressure does not lower as aspected while the expander volume increases. Figure 6.2 shows the dynamic of one stroke. The high pressure is shown in red while the low-pressure side is shown in blue.

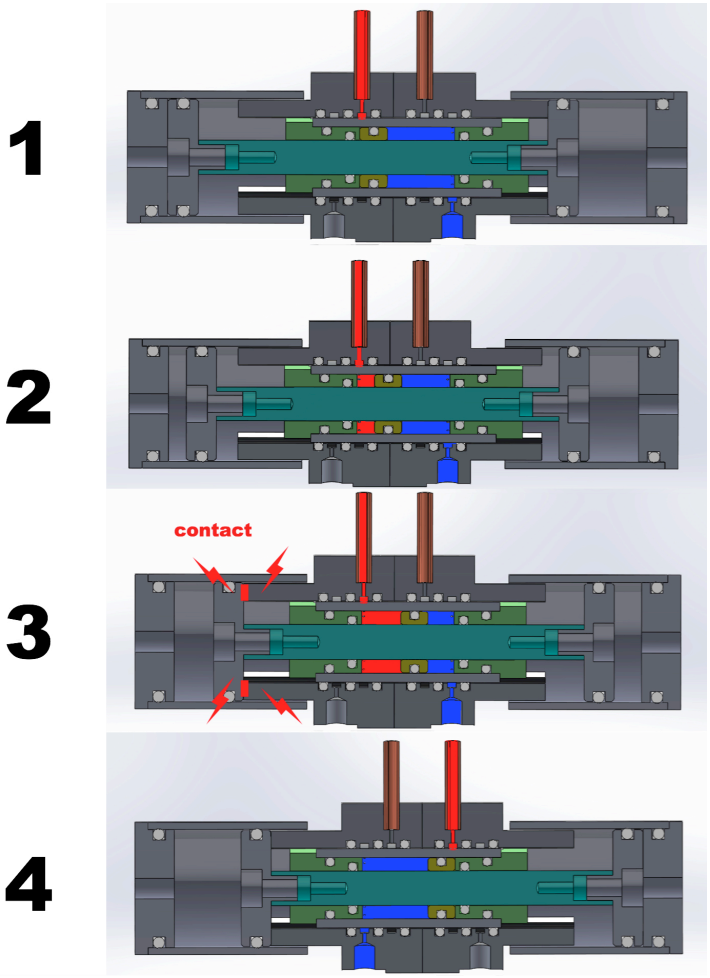


Figure 6.2: The four functioning phases of the free-piston expander-compressor. In 1 the high-pressure port is open. In 2 the shaft begins displace. In 3 the compressor piston is in contact with the spool valve. In 4 the cycle restarts and the shaft travels in opposite direction.

## 6.3. Spool valve

The spool valve is composed by an outer shell, six O-rings of 11x1.3 NBR 70 sh and a spool that is also the expansion cylinder. In this design, the inlet port is controlled by the spool valve. The spool valve channel the gas in and out from the expansion cylinder. The spool valve is controlled by the position of the compressor pistons.

## 6.4. Test

The second prototype, as the first prototype, does not start the autonomous alternating motion. The positive aspect is that the O-rings, even if under a pressure of 5.7 $MPa$, does not fail as in the previous prototype. The small 0.25 $mm$ hole are therefore able to support the O-ring sufficiently preventing the sealing to get cut when traveling over the ports.

## 6.5. Valve timing and expander dead volume

Looking at Figure 6.2 it is possible to notice, from picture number 1 and 4, how far the piston needs to travel to actuate the spool valve fully. Indeed it is much more physically correct if some dead volume remains in the expander and compressor chamber. In fact, as the dead volume tends to zero the pressure tends to infinity. To allow a larger dead volume at the end of the stroke, and actuate earlier the spool valve, shims were added on the compressor piston, Figure 6.3. The thickness of the shims was 0.5 *mm*. Several shims were put together, up to 3 *mm*, to increase the dead volume and anticipate the valve switch. Unfortunately, no improvement was recorded.

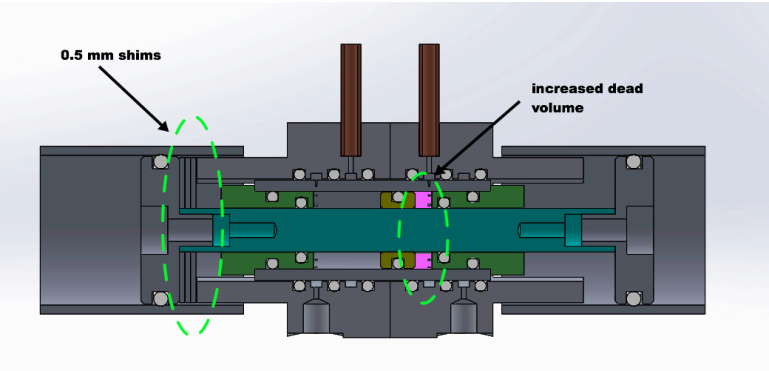


Figure 6.3: Shims are added to allow the spool valve to commute earlier in order to increase the dead volume at the end of the stroke.

## 6.6. Possible caused

The expansion chamber was indeed filling up with pressurized gas. Therefore the under-filling of the expansion chamber can be excluded.
The little inertia does not allow the shaft to store sufficient energy to displace the spool valve. This design presents again the same unwanted effect of the loss of pressure of the expansion side along with the increase in pressure of the discharging side, during spool valve actuation. Another interesting aspect that is worthy to notice is the, as we will call it in this work, the geometrical delay in *mm* between the open and closed position. The geometrical delay is distance that in this case is approximately 2 *mm*. It is measured between the center of the two position (open and closed). This is the length between the fully open position to fully closed position of the spool valve, The valve needs to travel this distance to effectively open and close the ports. If we compare the total expansion volume of the cylinder to the expansion volume corresponding to a distance of 2 *mm*, which is what is needed to actuate the spool valve fully, we lead with a value of 26%. Miniaturizing has the effect of accentuate these unwanted phenomena. A longer stroke may have improved the functioning because within these two millimeters the drop of pressure due to expansion could be lowered. This delay is complicated to reduce because of the cross section diameter of the O-ring already measures, in this particular case, 1.3 *mm*. In addition to that, the shoulder thickness of 0.5 *mm* needs to be add. It is possible that with a reduced delay, the energy accumulated within the expansion would be enough to commute the spool valve efficiently.
During the test, another problem relating to the sealing was noted. The actuation of the spool valve was only partial. This partial actuation had the effect of connecting high pressure to the low pressure, Figure 6.5. Clearly, the gas has the tendency to flow toward the path of less resistance, and this happened to be the outlet port of the system. Furthermore also the gas enclosed in the expander chamber was escaping. This would explain the partial actuation. The pressure within the expander suddenly drops, and the friction forces prevail over the pressure force on the piston.

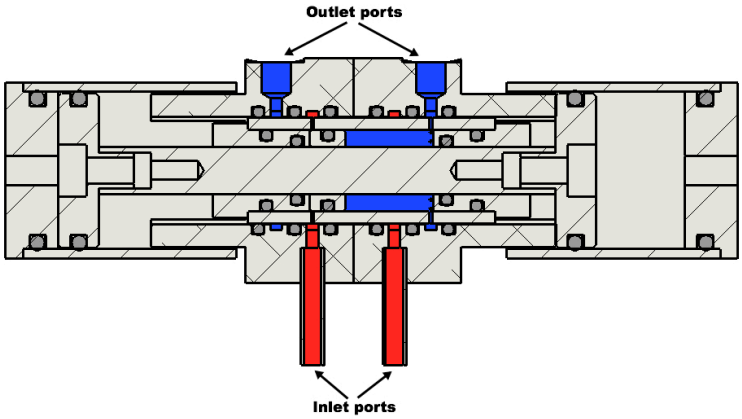


Figure 6.4: The drawing shows an axial cut of the second prototype. In Red is represented the path of the high pressure whereas in blue the path of the low pressure.

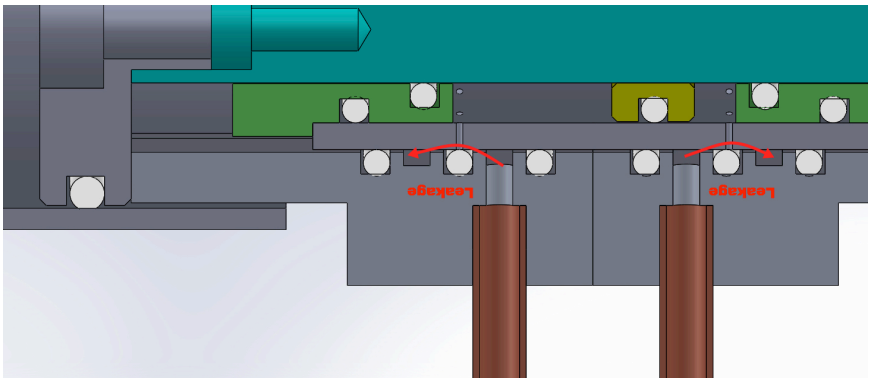


Figure 6.5: The drawing shows an axial cut of the second prototype. The red arrows represent the flow bypassing the O-rings while on top of the inlet/outlet holes of the expander.

# 7

# Design of the third prototype

## 7.1. Introduction

It was evident after the second prototype that the energy used to commute the spool valve needs to be stored somehow. The stored energy has to be taken when the expander can produce work more efficiently. This temporally stored energy will be given back to the system when it is more needed. That is when the spool valve shifts; this third attempt leads to the design of a 100 $g$ system occupying a volume of 120X45X25 $mm$. To improve the efficacy in limit leakages the expander casing is build of steel. This allowed tubing to be soldered on the valve. In addition the bi-stable mechanism is added as a prove of concept and it is heavily oversized and not weight-efficient.

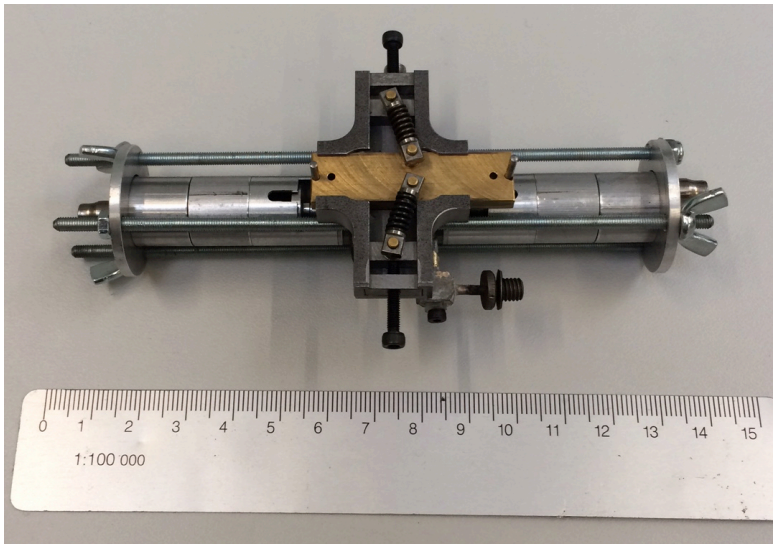


Figure 7.1: Picture of the third prototype assembled.

## 7.2. Energy storage

Energy can be stored in a rotating flywheel, within the inertia, as it is the case for reciprocating engine. Energy can also be stored in a mass, for linear translation. These two options rely on kinetic energy, therefore, both proportional to inertia and the square of the velocity. Furthermore increasing the inertia is equal to increase the mass of the overall system. These energy storage systems do not seem to be reliably applicable to our case. A linear inertia would lead an increase in mass. A rotational inertia will probably affect the mass but also the size of the machine.

Springs are capable of deforming under load and returning this power with minor losses.

Furthermore, springs can be extremely light. Due to their low weight and little volume springs may seem a secure and reliable solution to the problem.

## 7.3. Bi-stable mechanism

A bi-stable mechanism is a machine that is stable in two positions. Many different solutions exist. The chosen configuration is shown in Figure 7.2. This configuration is selected because the springs face each other. Thanks to these springs position the friction forces can be minimized. If the springs are perfect, perfectly placed and with equal pretension and length, the only friction would be caused by the own weight of the slider and the resistance within the pins.

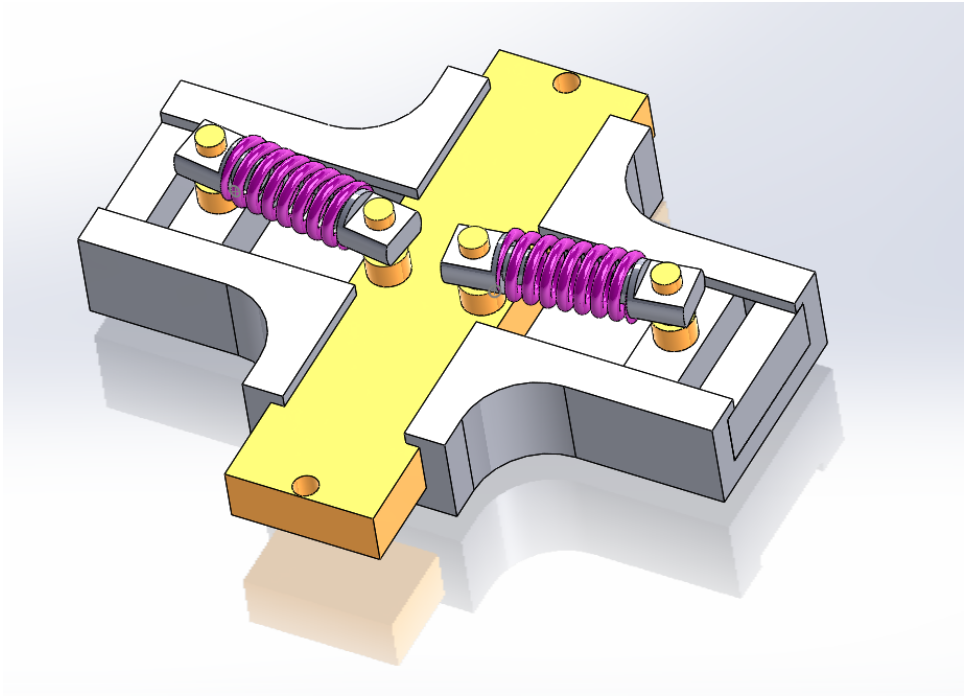

Figure 7.2: CAD model of the chosen bi-stable mechanism

The energy of the system is minimal in two positions as shown schematically by Figure 7.3. When the slider is in the central position the spring is compressed. This position represents the maximal potential energy of the bi-stable mechanism for a compressed spring. This state is unstable. A little displacement out of the equilibrium position will bring the system to reach the minimal potential. The other two positions of the slider show the system at is minimum energy. The spring is completely elongated to its initial length.
The spool valve needs to be stable in two positions per cycle, allowing a reciprocal opening and closing of the ports on both side of the expander.
A symmetrical bi-stable mechanism can, therefore, be employed to store energy and release it to switch the valve state.

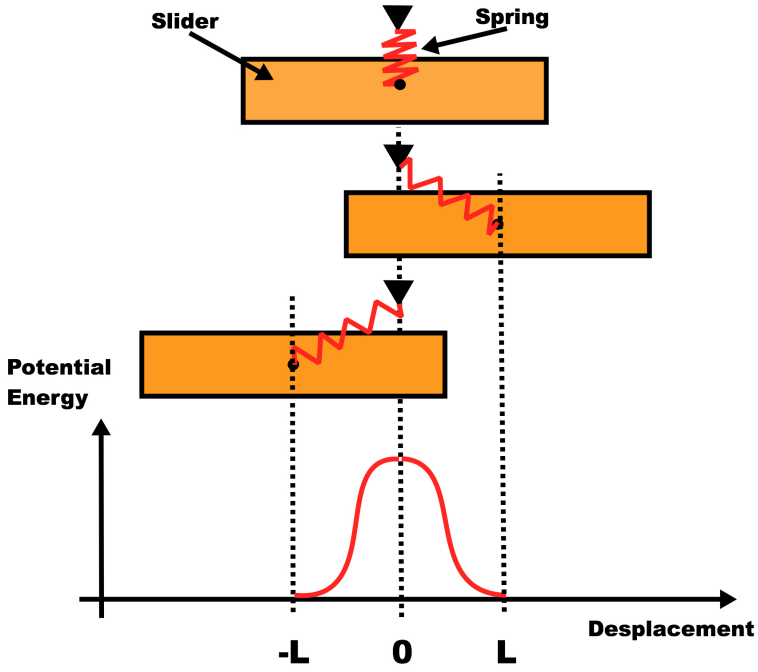


Figure 7.3: Schematics of the potential energy of a bi-stable mechanism against the displacement.

In Appendix E can be found an estimation for the minimal displacement necessary for the slider and valve to be actuated solely by the springs. This displacement is necessary because friction is present in the machine, therefore a minimal offset of the spring will allow elastic forces to be generated on the sliding direction.

## 7.4. Design prototype number 3

After learning from previous mistakes, the third prototype is developed slightly differently in the dimensions and the configuration. Indeed the compressor piston was smaller to take into account the losses produced by friction. This decision was taken after that the alternating motion was achieved. The compressor piston diameter was 13.5 *mm* in the previous prototypes while in the current is 11 *mm*. The size of the new compressor piston is not theoretically assessed. The ⌀ 13.5 *mm* was found with a frictionless model; indeed this dimension is the superior limit and a smaller dimension is more suited. The significant difference compared to the others is that it is provided with a bi-stable mechanism to store energy at the beginning of the stroke and release it to commute the control valve. The spool valve is this time not concentric with the expander cylinder. In Figure 7.4 is shown a cut of the expander and spool valve casing. The small ⌀ 0.25 *mm* holes are substituted with a ⌀ 0.8 *mm* hole with chamfer. Two little pins mediate the contact within the compressor piston and spool valve, Figure 7.5. This configuration was chosen because, due to the smaller O-rings, the friction forces are smaller. Also, it may be possible that the new hole size produces smaller pressure losses than ten ⌀ 0.25 *mm* holes having the same total cross-section area.

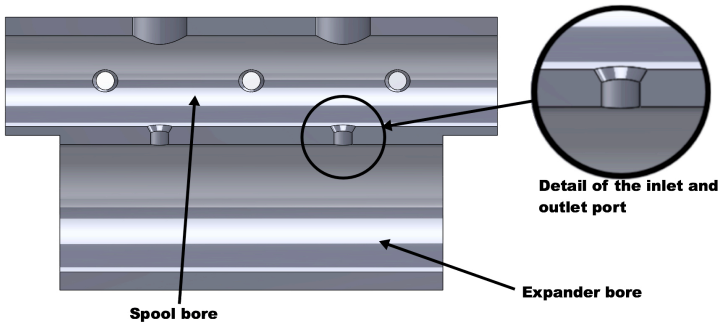


Figure 7.4: CAD model of the casing of prototype number 3. The inlet- and outlet-port is detailed

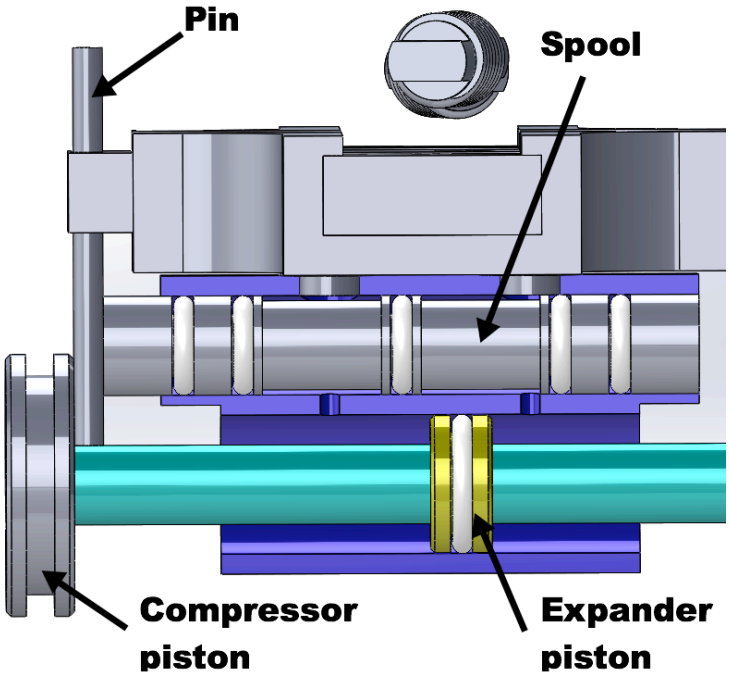


Figure 7.5: Horizontal cut of prototype number 3. The compressor and expansion pistons are visible and mounted on their shaft. The compressor piston actuates the bi-stable mechanism through the pin and the pin actuates the spool.

## 7.5. Compressor valves

The compressor valves are embedded in the compressor head. The sealings are taken from bicycle valves and positioned inside a custom made head. The bicycle valve were the Presta valve type, Figure 7.6, and it was chosen because of its small dimensions. The valve was disassembled, and the sealing element was modified to fit within the compressor head.

Figure 7.6: On the picture are represented the Presta valve type assembled, left. On the center the unmodified sealing element of the valve and on the right the modified sealing element use for the compressor head.

A longitudinal cut of the compressor head is shown in Figure 7.7. The valves were positioned as close as possible to the compressor side to decrease the dead volume. A spring of 0.15 $N/mm$ was used to maintain a light pressure on the valve. The spring preload was 0.15 $N$ therefore the spring was initially compressed one millimeter, maintaining the seal in contact with its seating.
This design appears bulky compared to the overall size of the machine, yet the space within the cylinder head was well managed.

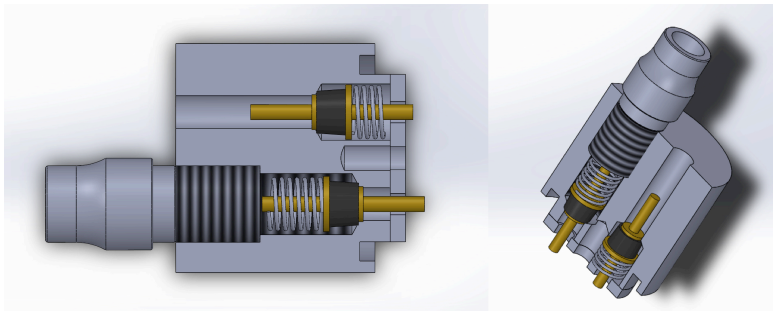

Figure 7.7: CAD model of the compressor head. The image shows a longitudinal cut of the head. It can be seen the sealing element taken from the Presta valve as well as the preload springs.

## 7.6. Functioning sequence

Prototype number 3 work as illustrated in Figure 7.8, where a section of the free-piston in different phases is represented. In position number 1 the shaft is completely retracted to the right. The gas flows from the inlet into the expander chamber. The shaft begins to move to the left. In position 2 the shaft is traveling to the left and the piston compressor

gets in contact with the slider pin of the bi-stable mechanism. The bi-stable mechanism is displaced to the point where it can autonomously actuate the spool. In position three the bi-stable mechanism actuates the spool fully and the movement reverses.

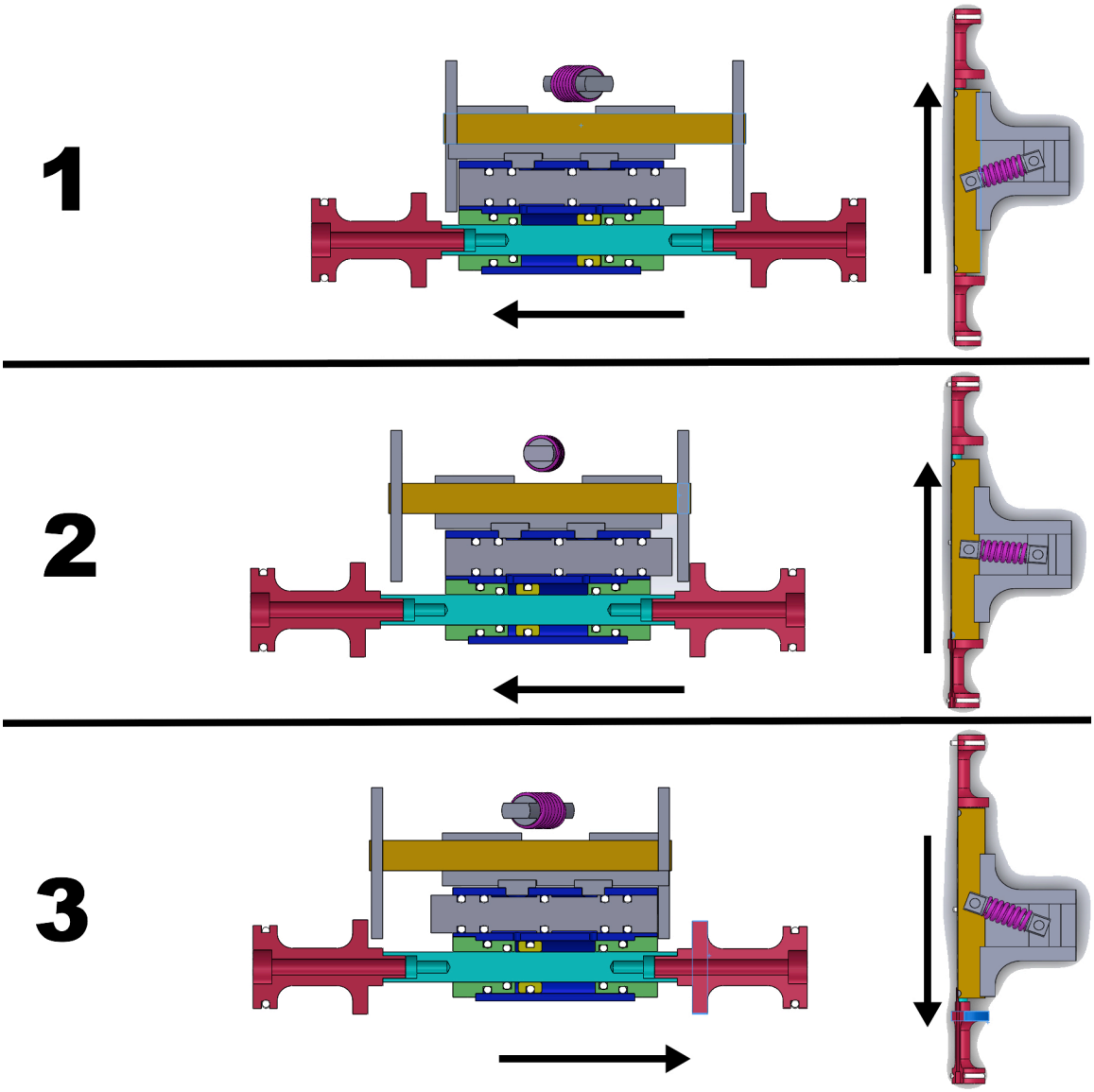


Figure 7.8: Section view of prototype number 3. The rows shown the free-piston in a specific position. The free-piston is also represented from the top to highlight the spring position.

## 7.7. Test

Prototype number 3 was tested and the alternating motion was achieved. The first major problem encountered in this work was solved using the bi-stable mechanism. Now, that the free-piston was moving, other problems related to premature wear were directly observed. In fact, the centered O-ring of the spool was failing. The O-ring was made of NBR 70 $Sh$. A new O-ring NBR 90 $Sh$ was used to substituting the softer O-ring. An increase in functioning time was observed, yet the failure was not solved. Due to this fact, the tests were inconclusive.
For the limited test carried on with the limited functioning time of the machine, a major issue was noticed. The machine, in the actual state, is not able to sufficiently lower the pressure of the $CO_2$ within the expander. This phenomenon is called underexpansion. The reason is intuitive and simple. The inlet port stays open too long. Doing so the gas is continuously flowing into the expander while the expander volume increase, maintaining a quasi-isobaric

condition.
This phenomenon was easily identified using the energy recovery test setup, Section 8.4. In this trial, a weight was used to produce isobaric conditions at 1.3 $Mpa$. The $CO_2$ delivered after only 1 stroke was sufficient to bring the piston to its end position. This is not an extensive examination but sufficient to understand that the gas delivered was at a much higher pressure level than desired.
The Cylinder head with embedded check valve was assessed within the limited functioning time of the free-piston machine. The pressure measured at the output of the compressor rose after 3-4 strokes to 4 $bar$ without apparent drops due to leakages.

# 8

# Test setups

## 8.1. Introduction

In this Chapter, the test setup is explained. Due to the malfunctioning of the prototypes, these tests were just partially carried out. Therefore the tests need still to be properly validated. Despite this fact, they can be used as a base guideline for future works.

## 8.2. Alternating motion test and self-starting

This test consists of applying pressure, using a bottle of $CO_2$ at saturation condition, through the inlet port of the free-piston.
The bottle contains 500 $g$ of $CO_2$. A relatively large bottle with a valve was chosen. If a leak was spotted, the valve allows an easy cut-off of the gas supply. Furthermore, a large bottle gives the opportunity to tune the free-piston finely, giving longer operational time. The bottle is shown in Figure 8.1.
The test visually assesses the alternating motion of the free-piston, leaving the outlet port at atmospheric conditions. The test is fulfilled if the machine autonomously starts its motion and it maintains it. Prototype number 3 is able to autonomously start and achieve an oscillatory motion.

## 8.3. Pressure regulation test

This test has the aim to assess at what pressure the machine stops its movement, therefore the supply of gas to the pneumatic system.
In Figure 8.1 is shown the test setup. The test setup is composed by a bottle of $CO_2$ of 500$g$ on which a valve is mounted. There is a the free-piston expander-compressor a barometer and a rigid canister that has the function to create a constant volume.
Once the valve is open, the free-piston begins its operations filling up the constant volume bottle. By loading the constant volume with gas, the pressure increases. Once a certain pressure is reached, the free-piston expander stops. Note that all the pneumatic line connects to the constant volume vessel. With the use of the barometer, an easy reading of the constant volume vessel is performed.
This test was conducted on prototype number 3. Unfortunately, due to the failure of the central O-ring of the spool valve no functional data could have been recorded.

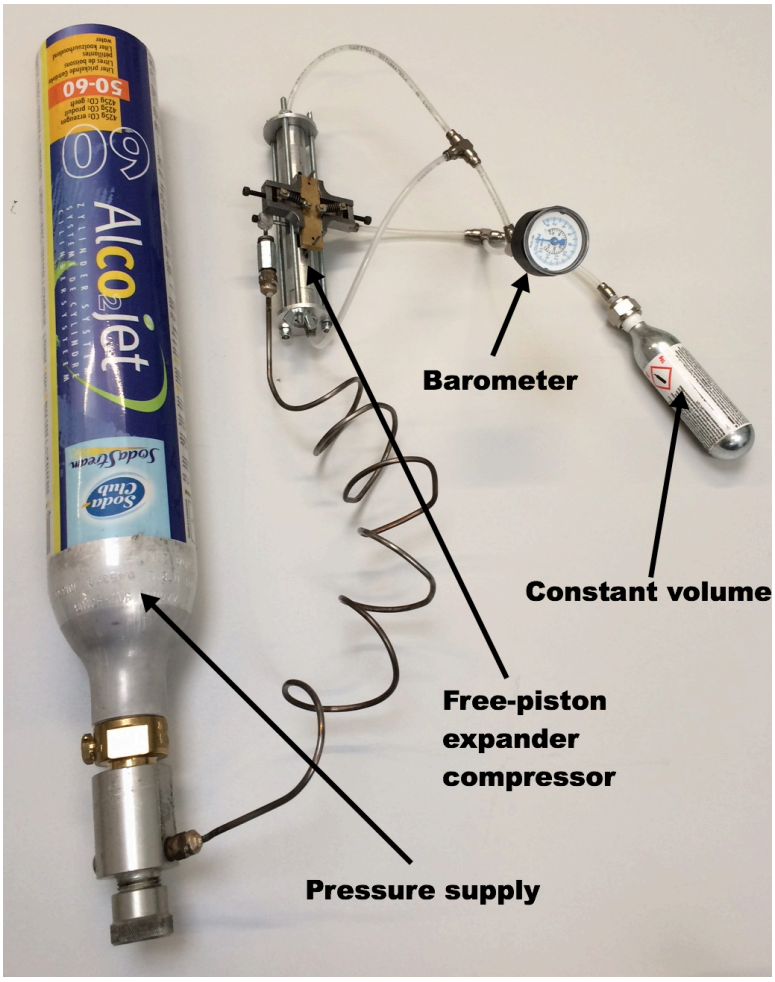


Figure 8.1: Pressure regulation set up. The setup is composed by a pressure supply, the machine to be tested, a barometer and a constant volume vessel.

## 8.4. Energy recovery test

This test allows an easy assessment of the amount of energy recovered. The peculiarity of the trial is the double chamber piston, Figure 8.2. A double chamber piston is composed of two identical cylinders and a double piston rod. The gas discharged by the expander flows in one cylinder while the air discharged from the compressor flows into the opposite cylinder, see Figure 8.2. A weight, for instance, can be used to produce isobaric conditions in the two chamber. After actuation of the free-piston expander-compressor, the stroke on both cylinders can be measured. The energy can be assessed calculating the work generated by the two cylinders. The energy of the expander gas is defined as $E_{expander} = MgL_1$ while the energy produced by the compressor is: $E_{compressor} = MgL_2$, as shown in Figure 8.3. $M$ is the mass of the weight. Due to the failure of the central O-ring no data were gathered.

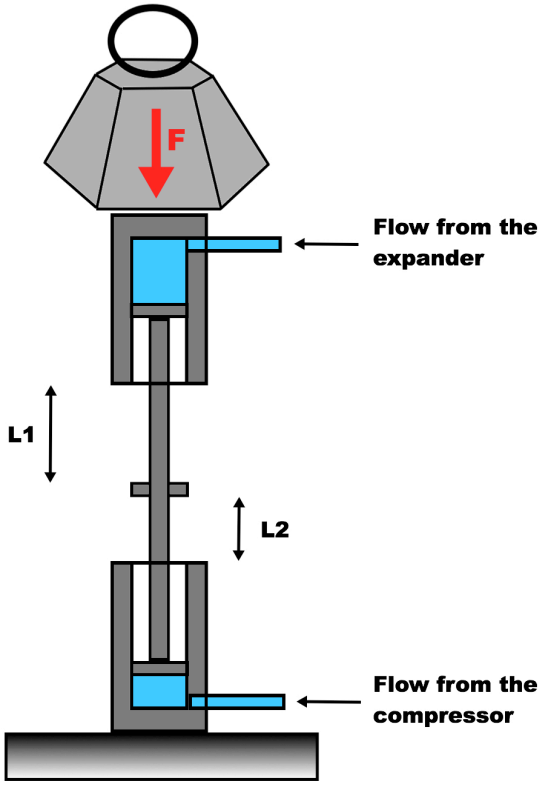


Figure 8.2: Sketch of the double piston for the energy test.

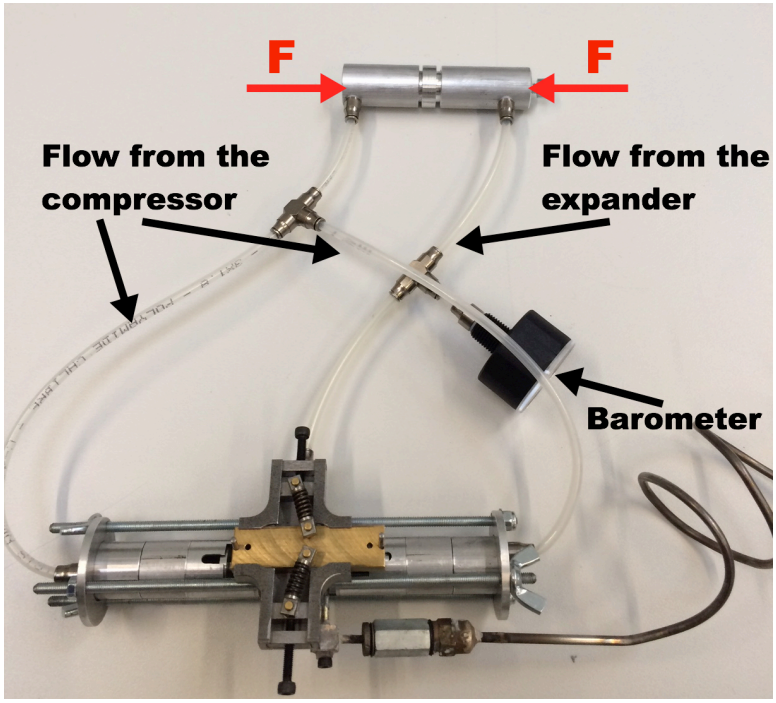


Figure 8.3: Particular of the free-piston connections to the energy test setup.

# 9

# Possible improvements and future works

## 9.1. Introduction

From the limited testings that were carried out, two main problems were noticed. The failure of the center O-ring and the under expansion of the $CO_2$. Other improvements can be suggested based on the experience matured during this work. This mean to give some pieces of advice for future works and improvements.

## 9.2. O-ring stretching

When nonstandard bore diameters are necessary, O-rings can be stretched on their groves. This stretching reduces the O-ring cross-section. Stretching is, therefore, a practice that can be applied on O-rings to match the wanted dimensions.
It may be possible that stretching can by applied for other reasons. The failure of the center O-ring it is probably due to nonperfect machining and more probably due to the significant deformation of the O-ring due to pressure. In fact, the pressure difference was constantly, probably, close to 5.6 $MPa$. This large pressure difference strongly deforms the sealing into the bore, facilitating its rupture.
If the O-ring is stretched onto its grove on the shaft, this may limit the radial deformation of the O-ring preventing failure.

## 9.3. New spool valve

It was shown on prototype number 2 that small holes, namely of ⌀ 0.25 $mm$ could be compatible with O-rings. Indeed, the spool valve was pressurized at 5.7 $MPa$ and the spool outer shell was manually actuated several times without causing any damages to the sealing.
Differently to prototype 1 and 2 the holes touches the minor diameter of the O-ring, the internal periphery. Assuming that these holes can avoid damages to the O-ring even when positioned on the outside diameter a new design is proposed, Figure 9.1. This new design would eventually prevent the O-ring failure.

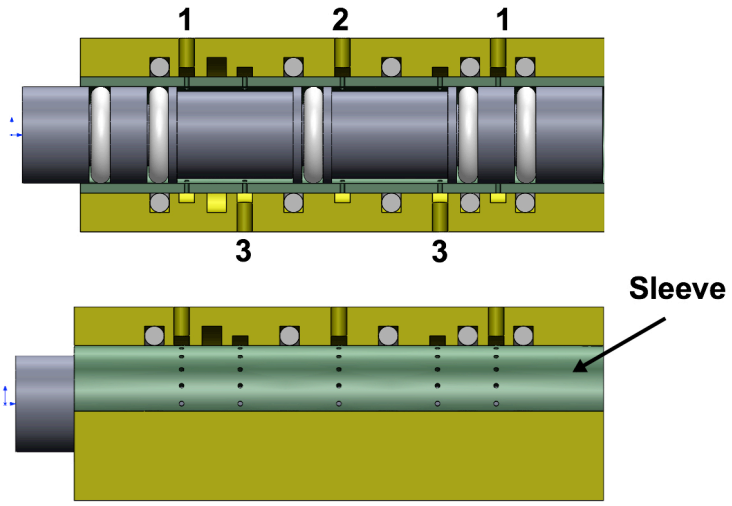


Figure 9.1: Section of the new spool. In 1 there is the high-pressure inlet, in 2 the outlet low pressure and in 3 the inlet and outlet of the expansion chamber. Note the sleeve with the tiny holes.

## 9.4. Dead volume in the expander

Small dead volume has the effect of reducing gas consumption. It also promotes the increase in pressure in the expander at stroke end. By the use of the simulation, it is shown that the increase in dead volume indeed lowers the pressure at stroke end. The counter pressure decreases along with a decrease of the performances.
In Figure 9.2, is shown the evolution of the pressure within the two opposite expander chamber against the stroke length. In Figure 9.2a, the pressure evolution for a dead volume of 5 $mm^3$ can be seen. Note the pressure reaches theoretical values of 11 $Mpa$. For this configuration, the recovered air mass ratio was 0.25. In Figure 9.2b, is shown the evolution of the pressure within the expander for a dead volume of 40 $mm^3$. The maximal pressure is dramatically decreased to 7 $Mpa$. Furthermore, note that the real stroke is slightly increased. This time the mass recovery ratio was 0.23.
An increase in dead volume lower the efficiency, yet the counter pressure decrease. This may allow to efficiently, and easier achieve the alternating motion without employing a bistable mechanism.

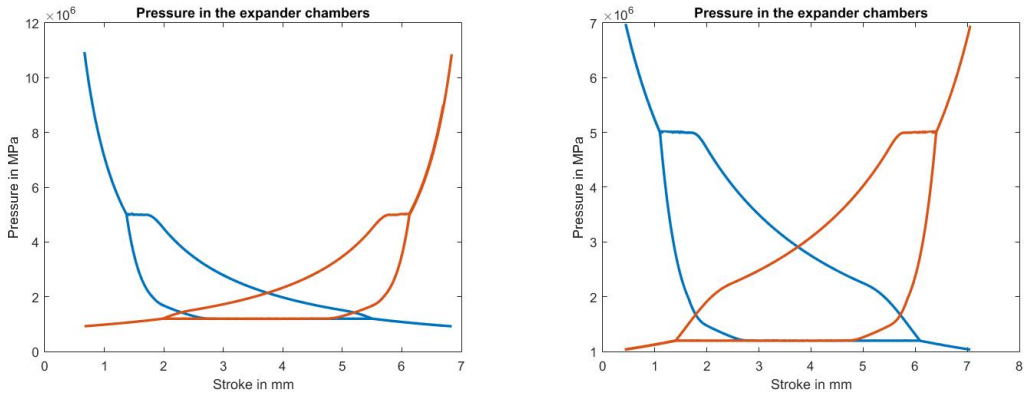


(a) Pressure within the expander chamber for a dead volume of 5 $mm^3$.

(b) Pressure within the expander chamber for a dead volume of 40 $mm^3$.

Figure 9.2: Pressure of the expander for two different dead volumes.

## 9.5. Under expansion effect on the center spool O-ring.

Under expansion was without doubt produced by the prototype. This affects the capability of the machine to lower the pressure as well as its properties to recovery efficiently work.
Additionally, this limited expansion may contribute to the O-ring failure. It was proposed that the failure of the center O-ring was caused by shearing of a small portion of the seal surface. This rupture is due to the O-ring being trapped between the outlet port and the spool. The O-ring deforms under the pressure forces acting on both sides of the sealing. Higher is the difference of pressure and larger is deformation of the O-ring. The under expansion, hence, increase the difference of pressure between the outlet port and the expander cylinder chamber, contributing to the O-ring failure. The reduction of underexpansion increases the machine performance and may avoid O-ring failures.
In order to improve this problem the inlet and outlet port should be controlled independently. The inlet port should close, allowing the gas to expand producing work and discharging the gas at the end of the stroke.

## 9.6. Compressor head

It was seen during testing that, for the limit amount of time that machine was working properly, a pressure of 4 *bar* was measured at the output of the compressor. This is a good indication that the bicycle valves were working correctly. Yet a problem was observed. The guidance of the modified bicycle valve is limited and a slight distortion of the spring or non-parallel spring ends rotates the valve. This rotation affects the sealing function and the valve leaks. It is therefore important to better guide the valve in order to maintain its concentricity with the bore.

## 9.7. Externally controlled free-piston expander compressor

It was proven that a small self-controlling motor can be manufactured and that it does work. The energy recovery, as well as the proper expansion, was not fully achieved for reasons already described. It would be interesting to maintain the free piston setup and controlling its motion with electronic components. By measuring the piston position, chamber pressure, valve state, etc., the free-piston expander-compressor can be easily controlled. The purpose of this is to well define the optimal working conditions. The gathered data will then successively used to build the autonomous auto-controlled free-piston expander-compressor.

## 9.8. Simulation

The simulation as it was presented and used did not bring the aspected results. The main reason was the absence of friction. It would be of primary importance to define a viable friction model to be implemented in the model. This would eventually decrease the design time, and it can be used, ultimately, to control an electrically controlled free-piston expander-compressor.

# 10 Discussions

The requirements are compared with the actual results achieved in this work. In Table 10.1 the requirements expressed in Section 2 are reported.

Table 10.1: Table of requirements

| Requirement | Metric | Value |
|---|---|---|
| Mass specific energy recovery | $kJ/kg$ | 25 |
| Mass | $g$ | 24 |
| Mass flow rate | $g/min$ | 1.5 |
| Size of the machine | $mm$ | 25x25x60 |
| Recovered energy form | - | Compressed gas |
| Machine self starting | The machine maintains the system pressure | - |
| Independence | Number of external energies other than $CO_2$ | 0 |

### Energy recovery

Due to the failure of the center O-ring of the spool, no data regarding the actual energy recovery was collected or assessed. Regardless, compression of the air takes place. As a consequence of the limited working time of the machine, the capability of the free-piston expander-compressor within a realistic scenario was not measured.

### Mass of the machine

The mass of prototype number 3 was 100 $g$; this is 76 $g$ greater than the required mass. Prototype number 3 was built with heavy materials to facilitate the assembly and machining. Also, the bi-stable mechanism was made of brass and steel. Clearly these materials do not fit within lightweight categories. Brass and steel were chosen to reduce friction. Prototype number 3 was intended to solve the problems related to the first two prototypes, while leaving the mass as a consequence of the materials choice. The CAD model shows that if the parts would have been made completely of aluminum, the overall mass would decrease to 60 $g$. A last redesign of the parts could further lower the mass of the machine.

### Mass flow rate

The mass flow rate could not be effectively measured because a stable function of the machine was not achieved.

### Size of the machine

The machine size is 120x45x25, which is greater than the requirements defined. This size can be reduced. In fact, the bi-stable mechanism was oversized in order to allow different spring lengths to be mounted and the spring pretension to be regulated. The length of the

machine can be reduced as well. Prototype number 3 appears to be long (120 $mm$), yet this was a consequence of the redesign. In fact, the parts composing prototype number 3 were reused from the previous attempt.

### Recovered energy form

The free-piston expander-compressor recovers energy in the form of compressed air. The compressed air flow can be merged into the main $CO_2$ circuit and be used by the autonomous system. The requirement is fulfilled.

### Machine self-starting

The machine is capable of autonomously establishing its movement when a difference of pressure at the inlet and outlet port is produced.

### Independence of the machine

The free-piston expander-compressor can control its operations autonomously. This control is not as refined as it should be. Therefore, due to an erroneous timing of the opening and closing of the ports the free-piston is not capable of fully expanding the gas as required.

# 11

# Conclusion

The goal of this work was to design and test a machine capable of efficiently lowering the pressure of $CO_2$ stored at saturation pressure in a canister to be used in a pneumatically actuated autonomous system.
It is well known that a pressure regulator produces energy losses, but despite this, solutions are virtually inexistent in pneumatics. Due to this, there was no work to build upon.

A free-piston expander-compressor was chosen as a starting point, because of its simplicity and compactness. Indeed one of the challenges that this work brought up was due to the small size of the machine and its weight limit ($25g$).

A mathematical model of a free-piston expander-compressor was developed. The simulated model appears to be far removed from the real behavior of a free-piston expander-compressor. Yet, it seems to be a good starting point for future improvements. The inconsistency of the model lies in the fact that no friction model was implemented. Frictional models are very difficult to be applied *a priori* because they rely on identification of parameters using test setups. Without a free-piston expander-compressor or smaller subsystem test setup from which the parameters can be identified, this machine appears very challenging to simulate.
An optimization was run to assess specific parameters of the free-piston machine. Using these parameters, three prototypes were built. The first two prototypes evidently showed difficulty in achieving a steady alternating motion. The motion was not possible due to the difficulty in switching the spool valve, which relies on the energy stored solely in the inertia of the shaft.
The third prototype stores energy in the springs when work from the expansion can be well exploited. The energy stored in the springs is then released to actuate the spool. A bi-stable mechanism ensures a well-defined state of the spool (open or closed). The actuation of the spool was the major issue in achieving a steady alternating movement. In fact, a partial spool actuation results in a stall of the free-piston expander. This problem occurred due to the small kinetic energy of the shaft-pistons system.
The bi-stable mechanism enabled the alternating motion of the machine. Issues related to the wear of the O-ring were noted. One of the five O-rings mounted in the spool regularly failed in this configuration. The O-ring was initially a NBR $70Sh$; it was replaced with a NBR 90 $Sh$. The change of O-ring hardness slightly improved its lifetime. More in-depth research on the best O-ring to use is needed to solve this significant failure. Another solution could be to design a spool valve differently.
Due to the O-ring rupture, the tests on the machine were limited. An evident underexpansion was noted, but detailed data were not available.
The underexpansion strongly affects the recovery capability of the machine as well as its ability to lower the $CO_2$ pressure at designed levels.

An alternative self-starting movement was successfully achieved. The free-piston autonomously controls its movement without the use of an external controller or valve. The associated elements were successfully embedded in a small system.
Though this work does not meet the original requirements, this little machine shows potential. The compactness and low weight were secondary aspects of this work. Despite this fact, the device appears to be well predisposed to meet the predefined requirements of mass and dimensions. Furthermore, if a successful valve control is implemented and friction is reduced, the underexpansion problem would be solved, leading to a successful increase of the specific mass energy of the pneumatically actuated autonomous system.

# A

# Expansion work

In an isothermal expansion, the pressure decreases following an isotherm. The Soave Redlich Kwong equation [24] is implemented to account for the real behavior of the carbon dioxide within the saturation dome and in its gaseous state. The mass specific work can be determined calculating the integral between an initial pressure and a final pressure. The work is defined as:

$$\delta a^{-} = -P_{(v,T)}dv$$

The Soave Redlich Kwong equation reads as:

$$P_{(v,T)} = \frac{rT}{v-b} - \frac{c_{(T)}}{v^2+bv}$$

$$c_{(T)} = 0.42748\frac{(rT_c)^2}{Pc}\left[1 + f_{(\omega)}\left(1 - \sqrt{\frac{T}{T_c}}\right)\right]^2 ;$$

$$f_{(\omega)} = 0.48 + 1.574\omega - 0.176\omega^2$$

Integrating from the initial pressure to the final pressure, the following equation:

$$\delta a^{-} = \frac{rT}{v-b} - \frac{a_{(T)}}{v^2+bv}dv$$

leads to the amount of mass specific work done by the expansion of carbon dioxide at a constant temperature.

# B

# Example of positive displacement compressors

## B.1. Scroll compressor-expander

A scroll compressor is composed by two involutes. One of the two involutes is generally fixed while the second orbits within a well-defined path. The second involute orbiting produces a series of chambers where the gas can expand either be compressed. In Figure B.1 is shown the functioning principle divided by small orbiting movement, from 1 to 5. The picture represents an expander. The pressurized gas enters at the center, 1, and expand within the chambers produced by a scroll involute orbiting around the other until the gas discharge in 5.

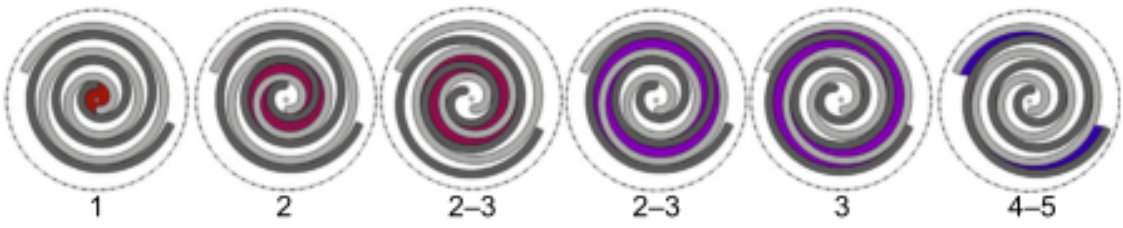


Figure B.1: Schematic of a scroll expander functioning from Lemort and Legros [27]. In 1 the compressed gas enters in the expander. The gas is confined within the chambers produced by the orbiting motion of the involute. The chambers' volume increase while the involute makes is orbiting motion until the gas is discharged in 5.

This machine is subjected to internal leakages. In Figure B.2 are shown possible leakage paths for this compressor-expander. In this figure the chambers created between the two involutes are well visible. It is intuitive how difficult would be to limit the leakages.


Figure B.2: Leakage path in a scroll expander. Lemort and Legros [27].

## B.2. Rotary vanes compressor-expander

In Figure B.3 is shown a rotary vane expander. It is composed by a cylindrical housing in which is mounted a rotor. The rotor is eccentric to the cylindrical housing. Vanes are mounted on the rotor, and thanks to springs or similar mechanisms, are always in contact with the housing. The vanes in contact with the housing define the expansion chambers. In Figure B.3 the leakage path are highlighted. As for the scroll compressor these are difficult to limit.

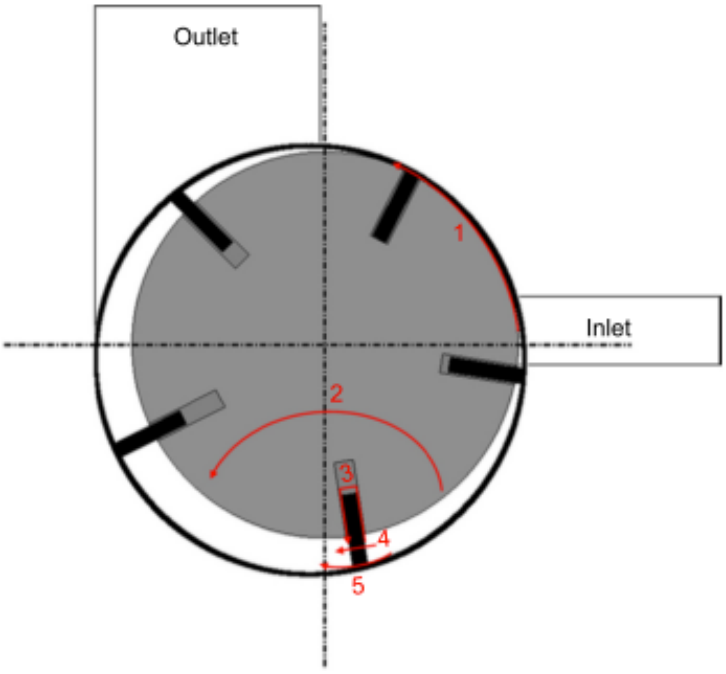


Figure B.3: Leakage path of a rotary vane expander from Lemort and Legros[27]. In addition to the path represented with the red arrows, The different chamber delimited by the vanes a well visible.

## B.3. Screw compressor-expander

Screw expander, are generally twin screw expander configuration, Figure B.4. Chambers are formed within the helix of the two screws and the casing. Rotating, the two screws, increase the chamber volume allowing expansion. Clearly, if used in the opposite direction, the gas can be compressed. Once again the complex surface that compose the expansion chamber are difficult to seal.

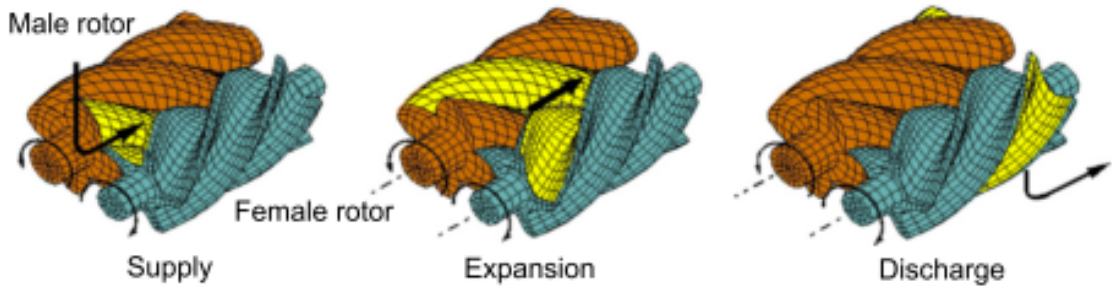


Figure B.4: Functioning principle of the screw expander from Lemort and Legros[27]. The gas enters in the little volume enclosed by the screw and the casing. The gas, expanding, exchange energy to the screws that rotate. The rotations allow the gas to expand until the chamber meet the outlet port where discharge take place.

# C

# Physical model

## C.1. The model

In this Section, the model is divided into subsystems. To each subsystem is attributed a well-defined equation that was then implemented in Simulink® to form the complete system.

### C.1.1. Simplifying assumptions

To decrease the complexity of the model, simplifying assumptions are needed. This is an important aspect in order to reach a good approximation in a relatively short time, maintaining an appreciable similarity with the real word. Starting from the proposed model the difficulty can be build up to reach a more accurate simulation, reducing the number of assumption.

- Potential and kinetic energy are neglected.
- The free-piston compressor-expander is adiabatic.
- The air is assumed to behave as an ideal gas.
- The $CO_2$ is assumed to behave following the Soave-Redlich-Kwong equation of state.
- The isochoric heat capacity of $CO_2$ is considered constant.
- The check valves on the compressor simply prevent the gas from flowing back into the chamber.

### C.1.2. Laws governing the expander

The expander model was essentially divided into three parts. A first part, the suction phase, describe the expander piston at the most retracted position. The inlet port is open allowing a $CO_2$ flow to enter the piston chamber. The second phase describes the expansion of the cylinder chamber. In this phase inlet and outlet port a closed. The expansion is done solely thanks to the temporally accumulated pressure within the chamber. The third phase represents the discharge of the gas from the expander chamber.

Suction phase, phase 1

The suction phase is characterized by and expansion of the control volume along with an enthalpic flow entering the system.

Applying the first principle to the expander chamber along with the simplifying assumption of Section C.1.1 we have:

$$U = \sum^{k} W_k^{+} + \sum^{i} h_i m_i \tag{C.1}$$

Equation C.1 can be rewrite using the mass specific internal energy $u$ as:

$$m_e u = W^{-} + h_b m_e \tag{C.2}$$

taking the derivative with respect to time of C.2 we lead to:

$$\frac{dm_e}{dt}u_e + m_e\frac{du_e}{dt} = \frac{dW^-}{dt} + h_b\frac{dm_e}{dt} \tag{C.3}$$

Using the definition of enthalpy: $h = u + pv$ and relating the work $W$ to the variation of the expander piston position as: $dW = P_e A_e dz$ we can rewrite C.3.

$$\frac{dm_e}{dt}u_e + m_e\frac{du_e}{dt} = -P_e A_e\frac{dz}{dt} + (P_b v_b + u_b)\frac{dm_e}{dt} \tag{C.4}$$

The variation of mass specific internal energy can be expressed as a function of the variation of volume and temperature as:

$$du = \left[\frac{T}{P}\left(\frac{\partial P}{\partial T}\right)_v - 1\right]Pdv + c_v dT \tag{C.5}$$

At this point, it is necessary to introduce the equation of state in order to describe one state variable in function of other two. The state equation chosen is the Soave-Redlich-Kwong (SRK) equation of state [24]. More information regarding this equation of state can be found in Section C.1.4. The SRK reads as:

$$P = \frac{rT}{v-b} - \frac{a_T}{v^2 + bv} \tag{C.6}$$

In order to be introduced in Equation C.5 the SRK need to be differentiate. Taking the partial derivative of Equation C.6 with respect to the temperature at constant volume we lead to:

$$\frac{\partial P}{\partial T} = \frac{r}{v-b} - \frac{\frac{\partial a_T}{\partial T}}{v^2 + bv} \tag{C.7}$$

It is now possible, combining Equations: C.4, C.5 and C.7, to explicitly define the temperature variation in time of the expander chamber solely function of the variation of the mass within the expander chamber and the velocity of the expander's piston as:

$$\frac{dT}{dt} = -\left[\frac{P_e A_e}{c_v m_e}(\mathbb{X}+1)\right]\frac{dz}{dt} + \left(\frac{P_b v_b + u_b - u_e}{c_v m_e} + \frac{P_e v_e}{c_v m_e}\mathbb{X}\right)\frac{dm_e}{dt} \tag{C.8}$$

Where:

$$\mathbb{X} = \frac{T_e}{P_e}\left(\frac{r}{v_e - b} - \frac{\frac{\partial a}{\partial T_e}}{v_e^2 + v_e b}\right) - 1 \tag{C.9}$$

Taking the integral with respect to time of Equation C.8 we can find the temperature of the volume enclose in the expander. With temperature and the mass-specific volume (Equation C.10), the pressure at time $t$ within the expander can be calculated using the SRK equation of state C.6

$$v_e = \frac{v_{0e} + z_t A_e}{m_{0e} + \int \frac{dm_e}{dt}} \tag{C.10}$$

It may seem unpractical and counter-intuitive to express the pressure of the considered volume passing through the temperature, yet it was the only straightforward way to explicitly express the differential equation once the SRK equation of state is introduced.

Expansion phase, phase 2

The expansion phase is characterized by a change in volume maintaining the mass of the control volume constant, therefore the enthalpic flow exchange to and from the system is null.

Starting from Equation C.1 and setting the term $\sum h_i m_i$ equal to zero we have:

$$m_e \frac{du_e}{dt} = -P_e A_e \frac{dz}{dt} \tag{C.11}$$

Using the variation of internal energy in function of volume and temperature expressed by Equation C.5 and expressing the temperature variation in time we lead to:

$$\frac{dT}{dt} = -\frac{P_e A_e}{c_v m_e} (1 + \mathbb{X}) \frac{dz}{dt} \tag{C.12}$$

Where the pressure can be found following the method exposed in Section C.1.2.

Discharge, phase 3

In this phase, the outlet port opens allowing the gas to escape the expander chamber. This phenomenon can be describe similarly to the one describe in Section C.1.2. The essential difference lies in the fact that this time the enthalpic flow is leaving the control volume. Equation C.13 can therefore is found to be:

$$\frac{dT}{dt} = -\left[\frac{P_e A_e}{c_v m_e} (\mathbb{X} + 1)\right] \frac{dz}{dt} + \left[(\mathbb{X} + 1) \frac{P_e v_e}{c_v m_e}\right] \frac{dm_s}{dt} \tag{C.13}$$

## C.1.3. Composition of the three phases

The three phases can be now coupled in an only equation. Looking at Equations C.8, C.12 and C.13 can be easily seen that are composed of a common term, independent of the mass flow, and two different terms proportional to inlet and outlet mass flow. We can therefore assembly the behavior of the control volume of the expander as follow:

$$\frac{dT}{dt} = -\left[\frac{P_e A_e}{c_v m_e} (\mathbb{X} + 1)\right] \frac{dz}{dt} + \left(\frac{P_b v_b + u_b - u_e}{c_v m_e} + \frac{P_e v_e}{c_v m_e} \mathbb{X}\right) \frac{dm_e}{dt} + \left((\mathbb{X} + 1) \frac{P_e v_e}{c_v m_e}\right) \frac{dm_s}{dt} \tag{C.14}$$

From Equation C.14 we can see that during suction phase ($\frac{dm_e}{dt} \neq 0$ and $\frac{dm_s}{dt} = 0$ we found Equation C.8, similarly we can found the equation representing solely the expansion, Equation C.12, and the equation representing the discharge phase, Equation C.13. Note that a composition of the suction and discharge phase is also described if ($\frac{dm_e}{dt} \neq 0$ and $\frac{dm_s}{dt} \neq 0$ simultaneously.

## C.1.4. Equation of state Soave-Redlich-Kwong

It is important to realize that the $CO_2$ cannot be considered as an ideal gas for the modeled free-piston. At pressures closed to the saturation conditions, the size of $CO_2$ molecules is no longer negligible. The molecules' size impact the behavior of the gas to be compressed. Therefore, the Soave-Redlich-Kwong (SRK) equation of state [24] was used to describe the states of the $CO_2$. The SRK equation of state reads as:

$$P = \frac{r}{v - b} - \frac{a_T}{v^2 + vb} \tag{C.15}$$

Where the two constants are found as:

$$a = \frac{0.42748 r^2 T_{critical}^2}{P_{critical}} \left[1 + f_{(\omega)} \left(1 - T_r^{1/2}\right)\right]^2 \tag{C.16}$$

$$f_{(\omega)} = 0.48 + 1.574\omega - 0.176\omega^2 \tag{C.17}$$

$$b = \frac{0.08664 r T_{critical}}{P_{critical}} \tag{C.18}$$

The symbol $\omega$ is the acentric factor. It is used to take into account the nonspherical shape of the molecules. For $CO_2$ and an acentric factor of 0.288 is used. The other constant can be found in Table C.1. $T_r$ is the reduced temperature that is a ratio of the real temperature over the critical temperature $T_r = \frac{T}{T_{critical}}$.

Table C.1: Parameters for $CO_2$

| Constant | value | Unit |
|---|---|---|
| $r$ | 188 | $J/(kgK)$ |
| $T_{critical}$ | 304.19 | $K$ |
| $P_{critical}$ | 7.381 | $MPa$ |

### C.1.5. Laws governing the compressor

Also the compressor, as for the expander, was divided into three phases (suction compression and discharge). Equation C.19 show the first principle applied on the compressor boundary for the suction phase.

$$\frac{dm_c}{dt}u_c + m_c\frac{du_c}{dt} = -P_c A_c \frac{dz}{dt} + h_{atm}\frac{dm_c}{dt} \tag{C.19}$$

During suction phase the enthalpy $h_{atm}$ is that of the atmospheric conditions. The enthalpy can be rewritten as $h_{atm} = u_{atm} + P_{atm}v_{atm}$. Rearranging the terms we leads to Equation C.20.

$$\frac{dm_c}{dt}(u_c - u_a) + m_c\frac{du_c}{dt} = -P_c A_c \frac{dz}{dt} + P_{atm}v_{atm}\frac{dm_c}{dt} \tag{C.20}$$

The internal energy can be written as $du = \frac{c_v}{r}(vdP + Pdv)$ and using the thermodynamics properties: $c_p = c_v + r$ and $\frac{c_p}{c_v} = \kappa$. Rearranging the terms we lead to Equation C.21

$$\frac{dP_c}{dt} = -\frac{(\kappa-1)P_c A_c}{zA_c}\frac{dz}{dt} + \left(P_{atm}v_{atm} - \frac{P_c v_c}{\kappa-1} + \frac{P_{atm}v_{atm}}{\kappa-1}\right)\frac{\kappa-1}{m_c v_C}\frac{dm_c}{dt} - \frac{P_c}{v_c}\left(\frac{m_c A_c}{m_c^2}\frac{dz}{dt} - \frac{zA_c}{m^2}\frac{dm}{dt}\right) \tag{C.21}$$

Knowing that $v = \frac{V}{m}$ or $dv = \frac{mdV - Vdm}{m^2}$ and that $V = A_c z_c$ everything reduces to:

$$\frac{dP_c}{dt} = -\frac{\kappa P_c}{z}\frac{dz}{dt} + \frac{\kappa P_{atm}v_{atm}}{zA_c}\frac{dm_c}{dt} \tag{C.22}$$

Similarly the equations governing compression and discharge phase can be found. Equation C.23 describes compression and Equation C.24 describes discharge.

$$\frac{dP_c}{dt} = -\frac{\kappa P_c}{z}\frac{dz}{dt} \tag{C.23}$$

$$\frac{dP_c}{dt} = -\frac{\kappa P_c}{z}\frac{dz}{dt} + \frac{\kappa P_c v_c}{zA_c}\frac{dm_c}{dt} \tag{C.24}$$

### C.1.6. Governing equation for the flow

The flow through an orifice produces a large pressure drop and turbulence. The flow was modeled as compressible and subjected to sonic choke. This means that for a specific pressure ratio the pressure has two well defined states (sonic and subsonic). The choked flow is established when the gas velocity hit the speed of sound. From that point on the velocity of the flow cannot increase further.

The equation governing the flow mass through an orifice for subsonic condition is:

$$\dot{m} = C_f A_v C_2 \frac{P_u}{\sqrt{T}} \left[\frac{P_d}{P_u}\right]^{1/\kappa} \sqrt{1 - \left(\frac{P_d}{P_u}\right)^{\frac{\kappa-1}{\kappa}}} \qquad \forall \frac{P_d}{P_u} > P_{critical} \tag{C.25}$$

In Equation C.26 we can find the flow equation for sonic conditions.

$$\dot{m} = C_f A_v C_1 \frac{P_u}{\sqrt{T}} \qquad \forall \frac{P_d}{P_u} \leq P_{critical} \tag{C.26}$$

$C_f$ is the discharge coefficient. Kim J. and Kim H. [39] give the values of discharge coefficients for miniature nozzles. For the studied case a discharge coefficient of 0.98 was chosen for the expander and the compressor, inlet, and outlet.

The other two terms found in the flow equation,$C1$ and $C2$ are found in Equation C.27 and Equation C.28.

$$C1 = \sqrt{\frac{\kappa}{r}\left(\frac{2}{\kappa+1}\right)^{\frac{\kappa+1}{\kappa-1}}} \tag{C.27}$$

$$C2 = \sqrt{\frac{2\kappa}{r(\kappa-1)}} \tag{C.28}$$

## C.2. Simulink model in detail

In this Section, the Simulink model is detailed explained. All the formulas and connections will be exposed. Following the explanations, a functioning model can be build. The blocks are shown from inside-out. Therefore, the more fundamental equation will be introduced a earlier while the equation necessary to define a particular value needed for these fundamental equations will follow in the text.

### C.2.1. Expander

The expander block is shown in Figure C.1. The input signals are found in Table C.2. The functions $f_u$ used to compute $dT/dt$ are in Table C.3

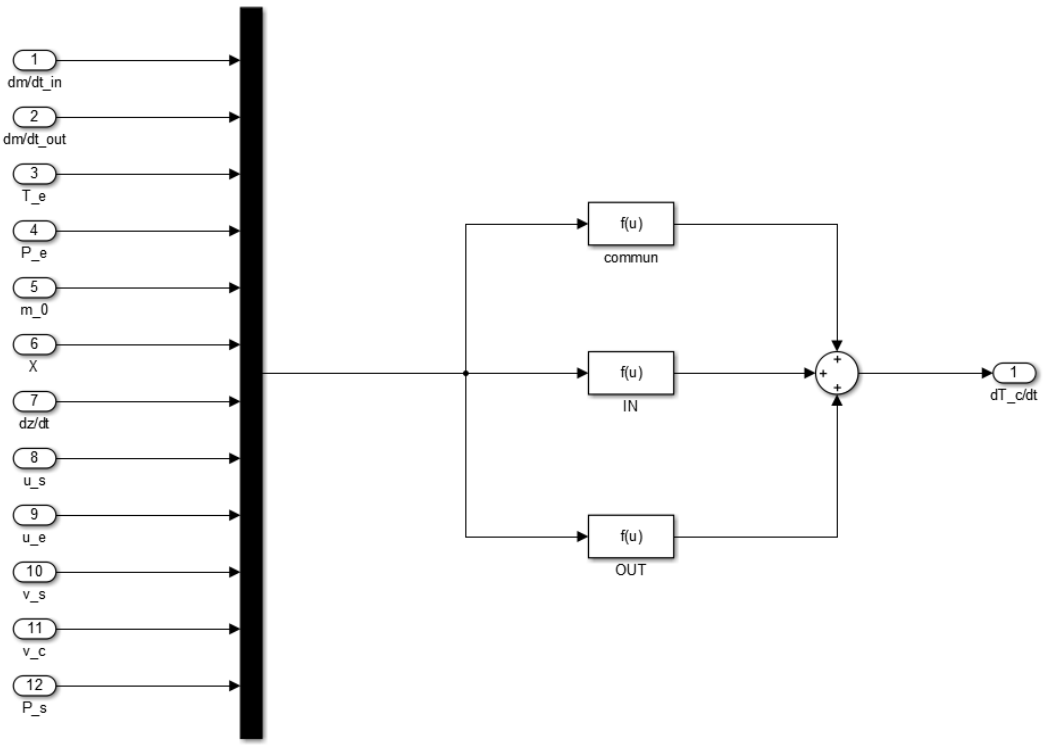


Figure C.1: Expander block 1 with input in on the left and the output on the right.

In Figure C.2 is represented how the signals found with the formulas in Table C.2 are connected with the Expander block 1.

Table C.2: input signals for expander block number 1

| Formula reference | Formula |
|---|---|
| $\frac{dm}{dt}_{in}$ | see Section C.2.2 |
| $\frac{dm}{dt}_{out}$ | see Section C.2.3 |
| $T_e$ | $\int_{t_i}^{t_{i+1}} \frac{dT}{dt} dt$ with the initial condition $T_{init} = 293.15K$ |
| $P_e$ | $\frac{T_e r}{v_c - b} - \frac{a}{v_c^2 + b v_c}$ |
| $m_0$ | $\int_{t_i}^{t_{i+1}} \sum \frac{dm}{dt} dt$ with the initial condition $m_{init} = \frac{V_{init}}{v_{init}}$ |
| $\mathbb{X}$ | $\frac{T_e}{P_e}\left(\frac{r}{v_e - b} - \frac{\frac{\partial a}{\partial T_e}}{v_e^2 + v_e b}\right) - 1$ |
| $\frac{dz}{dt}$ | $\int_{t_i}^{t_{i+1}} \frac{\Delta P_e A_e + \Delta P_c A_c - \eta \frac{dz}{dt}_i}{m_{shaft}} dt$ |
| $u_e$ | $\mathbb{X} P_e v_e + T_e c_v$ |
| $v_e$ | $\frac{V_0 + z A_e}{m_0}$ |
| $u_s$ | Mass specific internal energy of the vessel considered constant |
| $v_s$ | Specific mass volume of the source considered constant |
| $P_s$ | Pressure of the source considered constant |

Table C.3: Formulas applied on Expander block number 1

| Formula reference | Formula |
|---|---|
| $f_u$ IN | $\left(\frac{P_s v_s + u_s - u_c}{c_v m_c} + \frac{P_c v_c}{c_v m_c}\mathbb{X}\right)\frac{dm_e}{dt}$ |
| $f_u$ commun | $-\frac{P_e A_e}{c_v m_e}(1 + \mathbb{X})\frac{dz}{dt}$ |
| $f_u$ OUT | $\left((\mathbb{X} + 1)\frac{P_e v_e}{c_v m_e}\right)\frac{dm_s}{dt}$ |
| $\mathbb{X}$ | $\mathbb{X} = \frac{T_e}{P_e}\left(\frac{r}{v_e - b} - \frac{\frac{\partial a}{\partial T_e}}{v_e^2 + v_e b}\right) - 1$ |

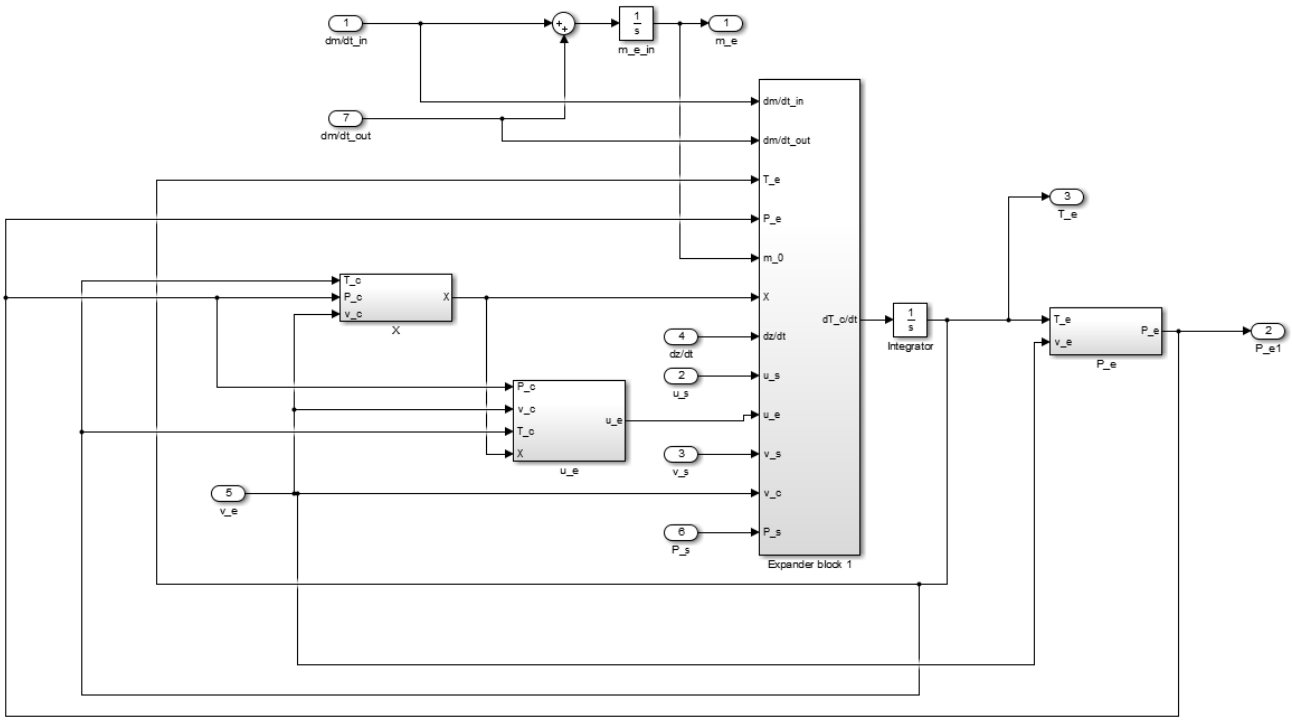


Figure C.2: Expander block 2 with input in on the left and the output on the right.

This procedure is for one expander chamber. The second expander chamber is modeled similarly, taking care that the stroke will have the value of the difference between the actual position and the total stroke length. This means that assuming a stroke of 10 $mm$ if $z$ in the left chamber is $3mm$ the opposite chamber it will have a value of $z = 7mm$.

## C.2.2. Flow model IN

The block scheme of the input flow is shown in Figure C.3. The block has logical components to compare the flow state (sonic or subsonic conditions). In addition to that, an opening and closing law is implemented. This opening-closing law is a function of the expander piston position. In Table C.4 the formulas and constant are explained. The instantaneous pressure of the expander is compared with the critical pressure. In function of which condition is satisfied the flow equation is chosen accordingly.

Table C.4: input signals for input expander flow

| Formula reference | Formula |
|---|---|
| $P_e$ | Instantaneous expander chamber pressure, see Table C.2 |
| $P_c$ | Constant source pressure |
| surface | see Section C.2.4 |
| $\frac{dm}{dt}sonic$ | Equation C.26 |
| $\frac{dm}{dt}subsonic$ | Equation C.25 |

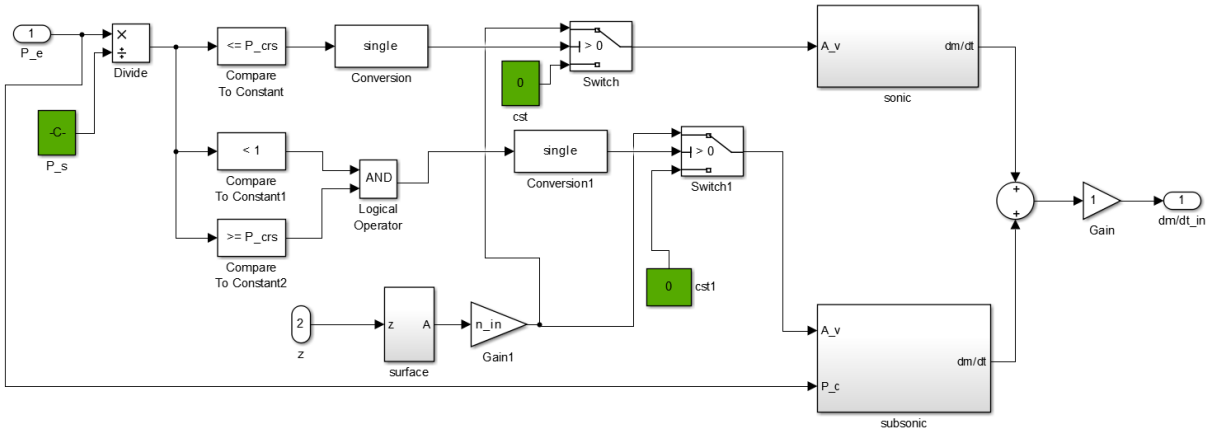


Figure C.3: Block scheme of the input flow.

### C.2.3. Flow model OUT

The output flow is modeled identically to the input flow. Of course, we have to take care of using the correct upstream pressure and temperature. These, pressure and temperature, are the instantaneous condition within the expander chamber. The block scheme is shown in Figure C.8. Table C.5 explains the parameters and address the reader to the needed formulas.

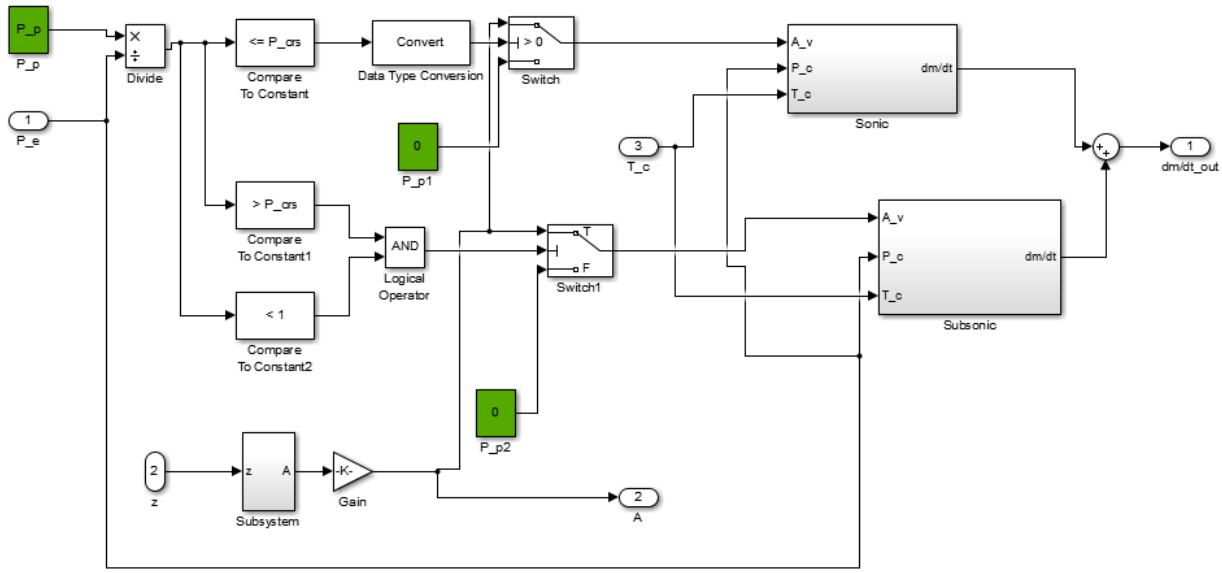


Figure C.4: Block scheme of the output flow.

Table C.5: Output signals for input expander flow

| Formula reference | Formula |
|---|---|
| $P_e$ | Instantaneous expander chamber pressure, see Table C.2 |
| $P_p$ | Constant sink of pressure |
| surface | see Section C.2.4 |
| $\frac{dm}{dt}sonic$ | Equation C.26 |
| $\frac{dm}{dt}subsonic$ | Equation C.25 |

### C.2.4. Inlet/Outlet cross-section area

Flow cross-section area formulation is found in Equation C.29. This is a geometrical relation that defines the area of the port effectively open. More detailed information can be found in the paper of Richer et al [40]. The considered are is shown in Figure C.5

$$A_z = \frac{d_f^2}{2} arctan\left(\sqrt{\frac{z}{d_f - z}}\right) - \left(\frac{d_f}{2} - z\right)\sqrt{z(d_f - z)} \tag{C.29}$$

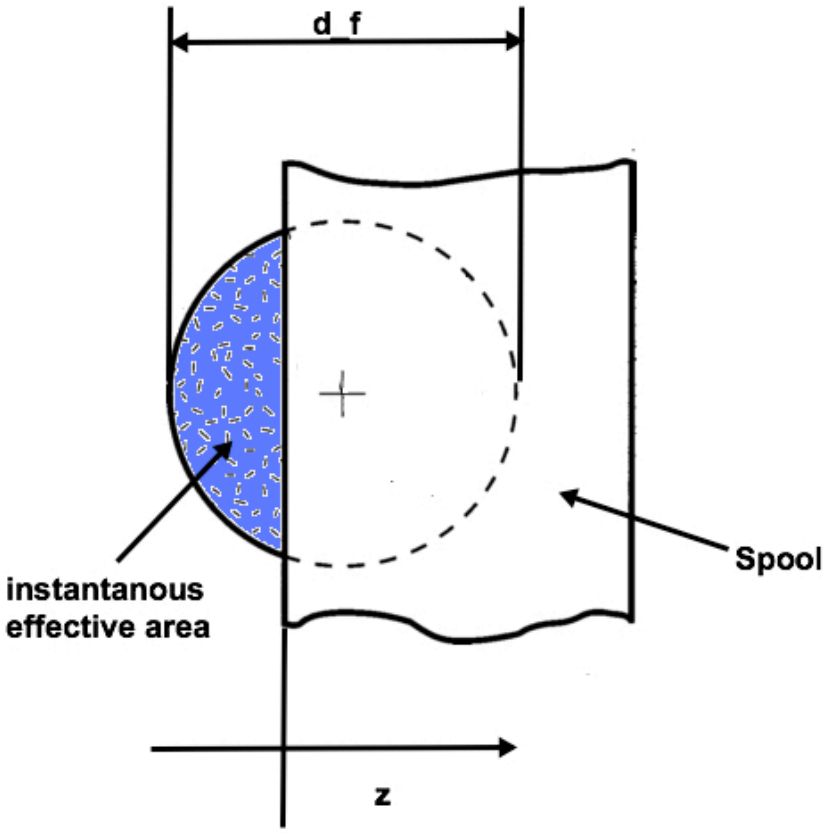


Figure C.5: Block scheme of the input flow.

This function is active only in a specific position of the piston position, I.E. when $z_d < z < z_d + d_f$. Otherwise, when $0 < z < z_d$ the valve is fully open the area is equal to $A = d_f^2\pi/4$. If the piston is not found within these range the cross-section area is null, indicating that the port is closed.

The outlet port has the same opening/closing law regarding the effective area, yet the function is not only in relation to the piston position but also the direction of the piston movement. In Figure C.6 is shown a sequence of the functioning process of the free-piston. An arrow indicate the direction of the velocity with its associated sign (+ or -). Figure C.6 can be associated with Figure C.7. The graph in Figure C.7 shows the valve of the left expander chamber for a stroke of the piston from the most left position to the right dead point and back. The number in the graphs corresponds to the number of associated configuration shown in Figure C.6. The inlet port is initially open, blue line, traveling the piston actuate the outlet port at 5 $mm$ stroke, orange line. The outlet port remains open and closes at a stroke length of $3mm$, when the velocity is negative. Eventually, the inlet valve opens again following the

blue line.

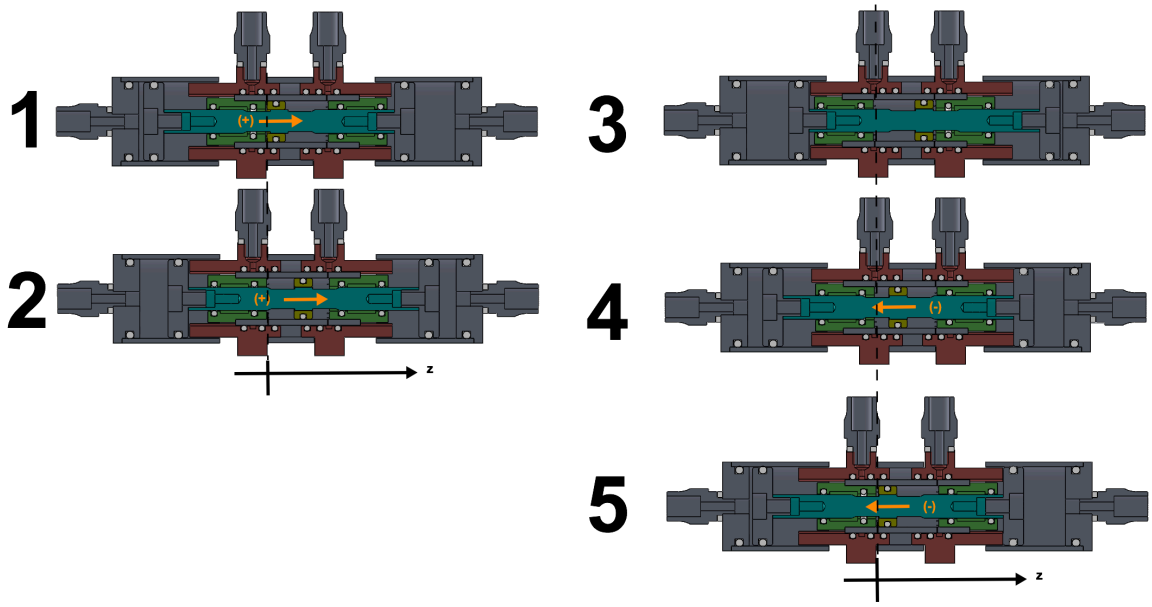


Figure C.6: Sequence of the valve behavior of prototype number 1. The sign within brackets, (+);(-) want to highlight the piston direction.

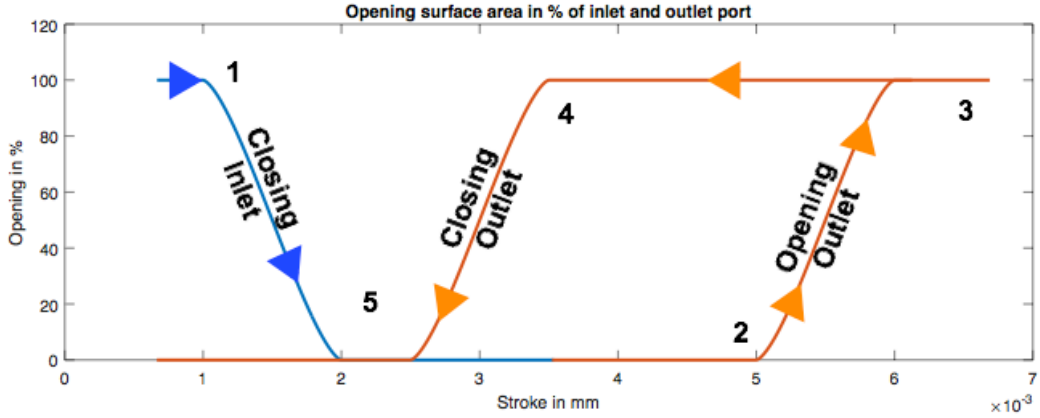


Figure C.7: Graph of the opening in % of the valve inlet/outlet as for simulation. The number represent the position illustrated in Figure C.6.

The just explained fact add an extra comparative factor in the simulation of the opening/closing law for the outlet. In Figure C.8, can be seen that the velocity $\frac{dz}{dt}$ was used to discriminate in which phase was the outlet valve.

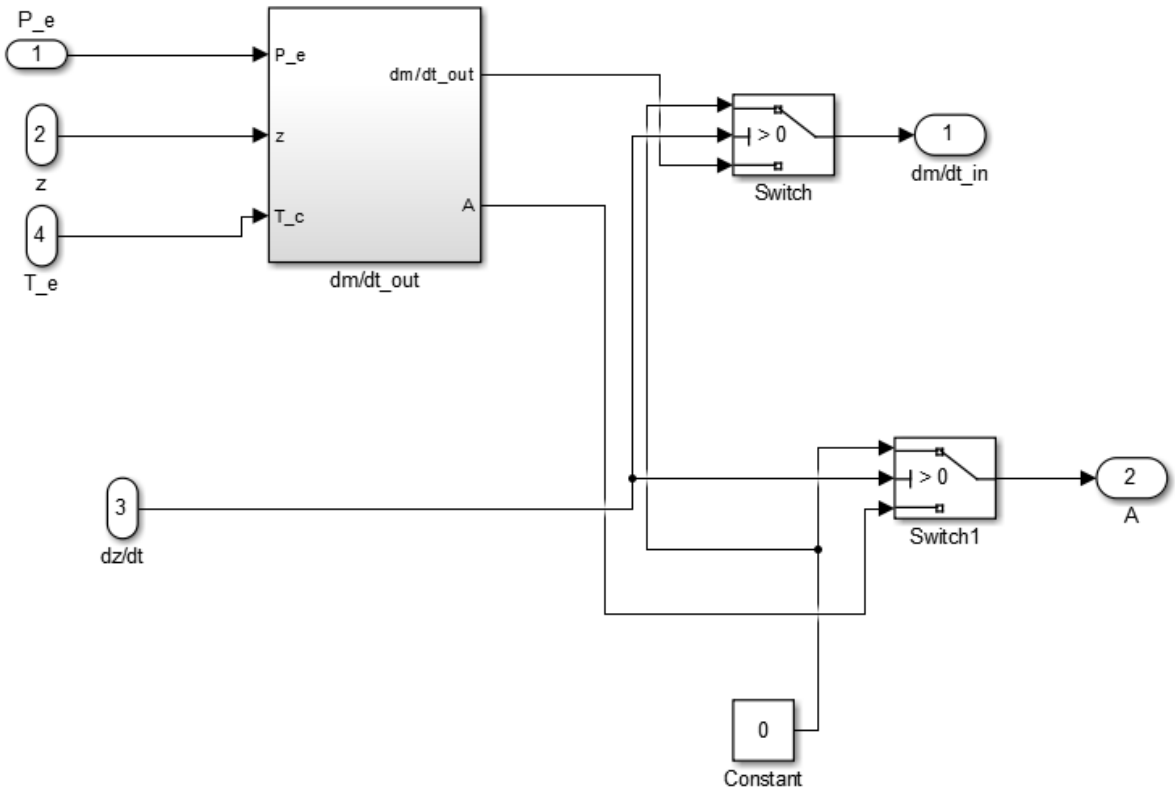


Figure C.8: Block diagram of the outlet port opening phase. The velocity is compared to zero in order to evaluate in which position the piston is as well as the state of the valve.

## C.2.5. Compressor

The compressor is simply modeled using the set of equations in Section C.1.5. The only differential equation to solve is Equation C.11 and it is straightforward. This is due to the simpler gas equation of state, the ideal gas law.The compressor block can be seen in Figure C.9 .

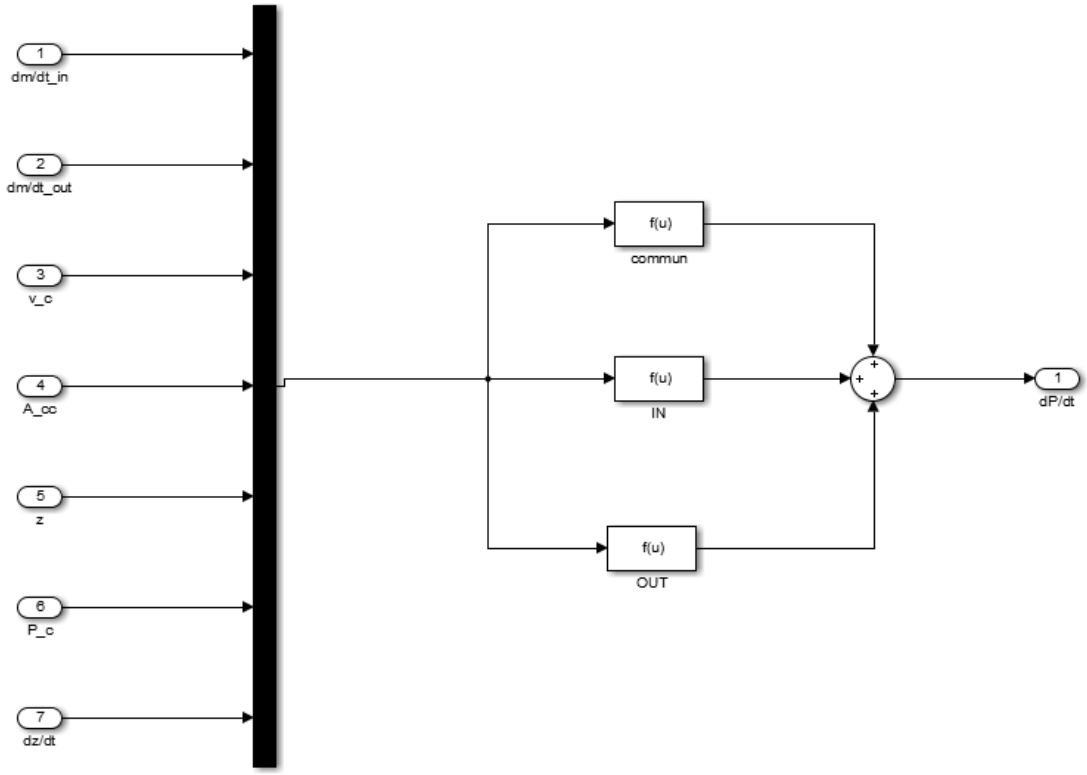


Figure C.9: Compressor block. All the input are readily available.

## C.2.6. Compressor inlet and outlet flow

The compressor inlet and outlet are modeled in similarly to the one of the expander. The main difference is the discrimination that defines when the flow is produced and in which direction it flows. This comes from the fact that the compressor has check valves that allow the flow to be established only in one direction. The comparative value was the pressure. The pressure defines if the condition to produce a flow are met. If it is the case, a flow from the higher pressure in the direction of the lower pressure is established. The block diagram for the suction phase is shown in Figure C.10. The ratio between compressor pressure and atmospheric pressure is calculated and compared to subsonic condition, sonic conditions and no flow, as for Table C.6

Table C.6: Flow state for the compressor in function of the pressure ratio.

| Formula reference | Flow State |
|---|---|
| if $\frac{P_c}{P_{atm}} \leq P_{critical}$ | sonic |
| if $P_{critical} < \frac{P_c}{P_{atm}} < 1$ | subsonic |
| if $\frac{P_c}{P_{atm}} \geq 1$ | no flow |

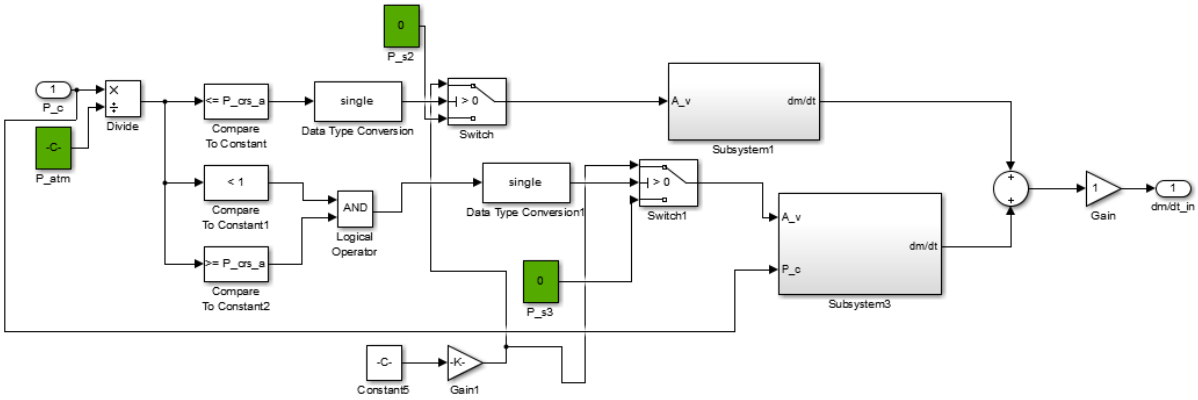


Figure C.10: Suction flow within the compressor block diagram

## C.3. Constants used for the simulation

The complexity increases with the number of values that are considered variable. To maintain a limited complexity some value where chosen as constant even if in real life are functions of the particular state of the gas. The values for the air are standard constant used to approximate the air behavior, Table C.7. For the carbon dioxide where estimated values of $c_v$, $c_p$, $\kappa$ making an average of the values found for 5.7 $Mpa$ and 1.3 $MPa$, Table C.8. These constant where found using RefpropMini [41].

Table C.7: Constants used throughout the simulation for air

| Constant | Value |
|---|---|
| $\kappa$ | 1.4 |
| $r$ | 287 $J/kgK$ |
| $P_{atm}$ | 0.1013 $MPa$ |

Table C.8: Constants used throughout the simulation for $CO_2$

| Constant | Value |
|---|---|
| $\omega$ | 0.288 |
| $T_{critical}$ | 304.19 $K$ |
| $P_{critical}$ | 7.381 $MPa$ |
| $r$ | 188 $j/kgK$ |
| $c_v$ | 657 $j/kgK$ |
| $c_p$ | 846 $j/kgK$ |
| $\kappa$ | 2.5 – |
| $u_s$ | 385 $kJ/kg$ |
| $\kappa$ | 2.5 – |

# D

# Mechanical resistance

## D.1. Aluminum 7075 properties

Table D.1: Table of the mechanical properties for aluminum 7075 T6 from Aerospace Specification Material Inc. [42]

| Physical property | Unit | Value |
|---|---|---|
| Tensile yield strength | $MPa$ | 503 |
| Shear strength | $MPa$ | 331 |
| Fatigue strength ($5 \cdot 10^8$) | $MPa$ | 159 |
| Young modulus | $GPa$ | 71.7 |
| Shear modulus | $GPa$ | 26.9 |
| Poisson ration | – | 0.33 |

## D.2. hoop stress and diametrical expansion

The hoop stress as for Hibbeler [43] reads as:

$$\sigma_h = \frac{PR}{t} \tag{D.1}$$

The cylinders will expand and retract under the effect of the pressure. The cylinders have to be sufficiently thick to withstand the cyclical force occurring during the suction phase for the motor or compression phase for the compressor.
Using Equation D.1 a minimal thickness can be found. Knowing that the fatigue strength of AL 7075 at $5 \cdot 10^8$ cycles is 159 $Mpa$ and that the worse case scenario a pressure of 5.7 $Mpa$ can be reached within the cylinder chamber. Furthermore, assume that the maximal diameter is the 13.5 $mm$ diameter found using the genetic algorithm optimization. A wall thinness of 0.25 $mm$, Equation D.2.

$$t = \frac{PR}{\sigma_h} = 0.25mm \tag{D.2}$$

Using now the constitutive equation relating stress and strain, Equation D.3, it is possible to estimate the increase in diameter due to pressure.

$$\sigma = E\epsilon = E\frac{\Delta l}{l} \tag{D.3}$$

Always assuming a diameter of 13.5 $mm$, a stress of 159 $MPa$ we can estimate the increase in circumference due to pressure will therefore be:

$$\Delta l = \frac{\sigma}{El} \tag{D.4}$$

The length $l$ is the circumference $D\pi$. We can therefore estimate that a cylinder of 0.25 thick under a pressure of 5.7 $Mpa$ made of Al 7075 has a diametrical expansion of:

$$\Delta D_{pressurized} = \frac{\sigma D}{E} = 0.03mm \tag{D.5}$$

A cylinder of a thickness 0.25 $mm$ and diameter of 13.5 $mm$ has a diametrical expansion of 0.03 $mm$ when pressurized at 5.7 $MPa$. This calculation is to assure that the cylinder does not expand over the squeeze value of the O-rings that is for a 1 $mm$ thick O-ring approximately 0.1 to 0.05 $mm$.

## D.3. Shaft buckling

Buckling is an instability failure. The thin and long shaft may very well withstand compression or tensile force while failing due to lateral instability.

Considering a 4 mm shaft made of AL 7057 were a compression force equal to 150 $N$. The force of 150 $N$ is established assuming that the shaft is at equilibrium with the maximal expander and compressor pressure, Figure D.1. The shaft diameter is 4 $mm$ whereas the piston diameter is 7 $mm$. The expander pressure is assumed to be 5.7 $MPa$.

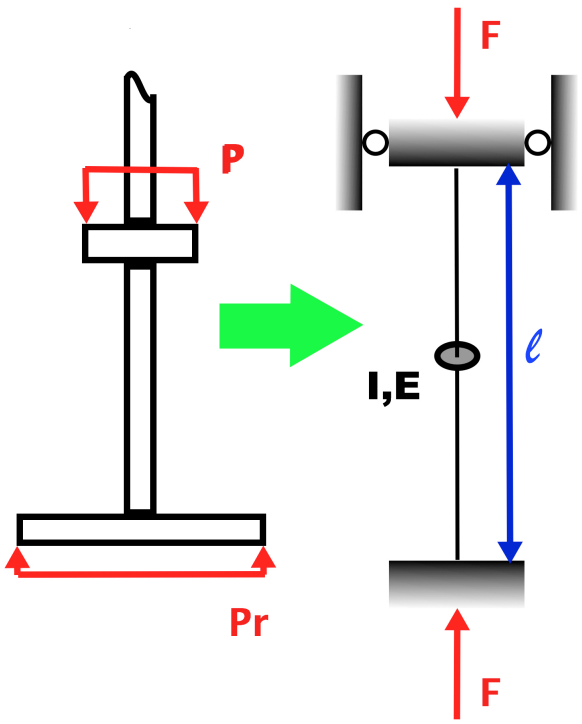


Figure D.1: Schematics of the shaft with applied force on the left. Equivalent buckling model on the right

Considering a configuration known as the fundamental case of buckling, Figure D.1, it is possible to estimate a critical length. The critical length gives the maximal length for which the shaft resist buckling. The critical length can be found using the following relationship:

$$l_{critical} = 2\pi\sqrt{\frac{EI}{F}} \tag{D.6}$$

Where $I$ is the second moment of area, that for a circle is equal to: $I = \frac{\pi * D^4}{64}$

Solving for the parameters previously defined a critical length of 490 $mm$. We can conclude that a rod clamped on both sides of a 4 $mm$ diameter in AL7075 will buckle under a load of 150 $N$ if its length exceeds 490 $mm$.

## D.4. Shoulder thickness

The shoulder prevents the O-ring to escape. When the volume enclosed by O-rings is pressurized, O-rings lay on the shoulder surface producing a certain amount of force. Shear stresses will be greater for greater diameter because the forces increase faster than the growth in the section resistance to shear. This can be understood looking at the equations. The shear stress is proportional to the force and inversely proportional to the surface area, Equation D.9. The Force increase to the square of the diameter $D$, Equation D.8 while the area increases only proportionally to $D$.
Due to this fact, it is considered only the shoulder with bigger diameter $D$. In this case, the larger diameter found in the system that needs to withstand a pressure of 5.7 $Mpa$ is 13.6 $mm$.

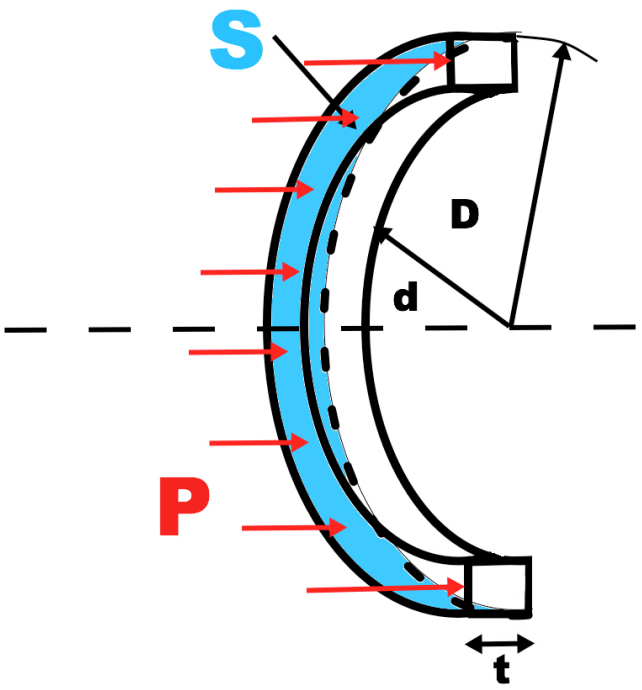


Figure D.2: Conceptual sketch of the shear resistance area of the O-ring shoulder

$$S_{shear} = \frac{D\pi}{4}t \tag{D.7}$$

$$F = \frac{(D^2 - d^2)\pi}{4}P \tag{D.8}$$

$$\tau = F/S \tag{D.9}$$

The considered area is shown in Figure D.2 and it can be calculated following Equation D.7. The value defined for endurance resistance is a data more applicable to normal stresses. Applying the Von Mises criteria we can estimate a fatigue strength for tangential stresses, Equation D.10, of 92 $MPa$.

$$\tau_{5\cdot10^8} = \frac{\sigma_{5\cdot10^8}}{\sqrt{3}} \tag{D.10}$$

Using the equations exposed before we can, therefore, define a minimal thickness $t$ of 0.3 $mm$.

# E

# Bi-stable mechanism calculation

## E.1. Spool estimated friction forces

The spool, Figure E.1, has 5 O-ring of 3x1 $mm$ 70 $Sh$. The squeeze is between 5 to 3 %. Furthermore, we can assume that only four of the five O-rings have a difference of pressure of 5.6 $Mpa$ between the boundaries of the sealing. This is because the small volume encloses within two O-rings remain pressurized if we assume the sealing to be leakage free.

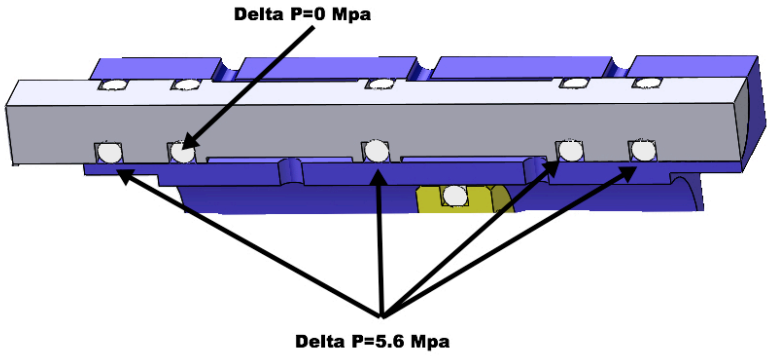


Figure E.1: model of the spool and pressure levels

Using the formula, Equation E.1, and the empirical coefficients, Figure E.2, provided by the Parker Corporation Handbook [38] we can estimate the friction forces produced by the sealing.

$$F_{friction} = f_c L + f_h A \tag{E.1}$$

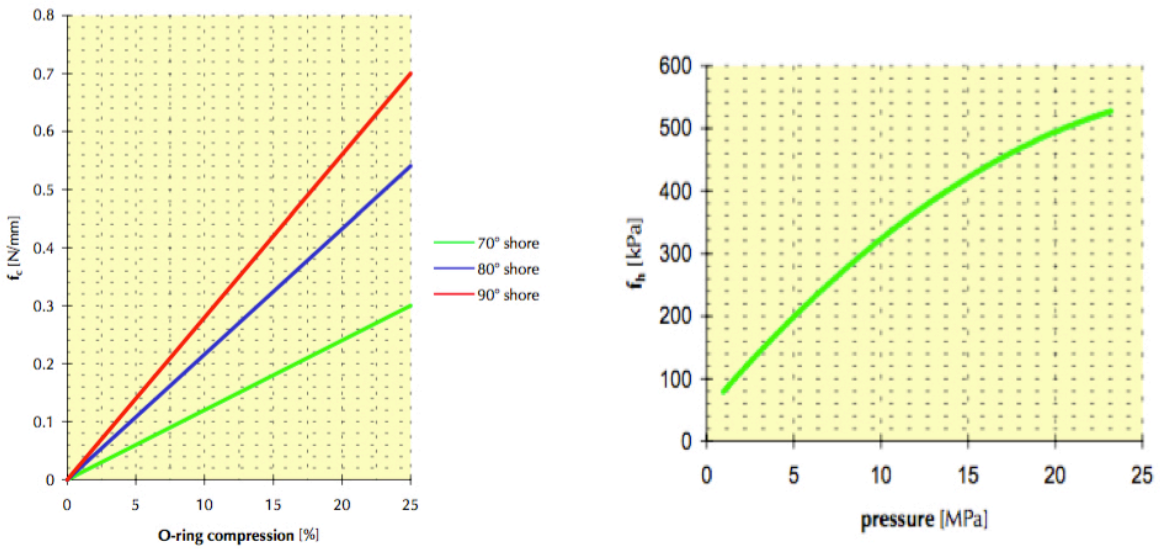


Figure E.2: Graph of empirical coefficient for the estimation of the friction force by Parker Corporate [38] converted in SI units by Plettenburg [5]

Using the a value of $f_c = 0.04N/mm$ and $f_h = 0.24MPa$, a length $L = D_{bore}\pi = 15.7mm$ and a projected area of seal $A = (D_{bore}^2 - D_{groove}^2)\pi/4$, an estimate resultant force for the 4 O-rings of $F_{friction} = 14N$ is found.

In Figure, E.3 is shown the bi-stable mechanism. This configuration was chosen because the horizontal forces compensate each other, decreasing the normal forces on the moving parts that would produce friction. We can, therefore, assume that the friction caused by the contact between the slider and its slot is negligible. Yet the resistance moment created on the connection pins is taken into account.

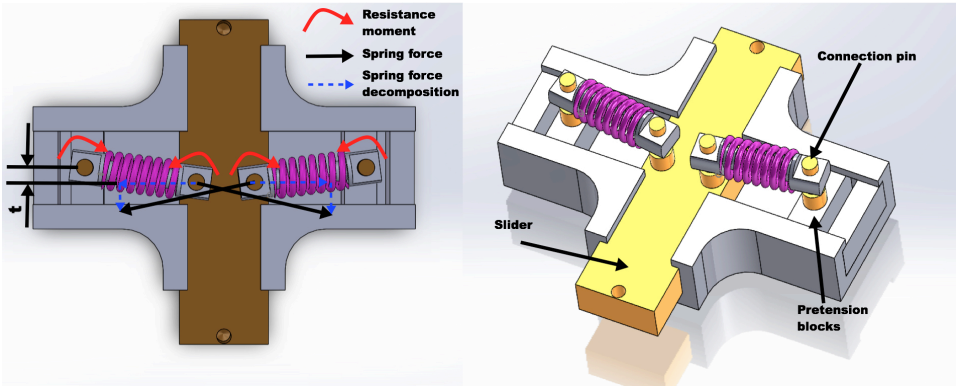


Figure E.3: Model of the spool and pressure levels

Neglecting the inertia of the slider, the springs, and the spool, we can estimate the minimal displacement out of the unstable equilibrium position of the bi-stable system. This little movement is necessary to allow the springs to move the spool.

Isolating a spring, Figure E.4, from the system and taking the sum of the moments with respect to point A we leads to:

$$\sum M_A = F_y * x_0 - 2M_{friction,pin} - \frac{F_{friction}x_0}{2} \tag{E.2}$$

The objective is to find the stiffness of the spring $k$ and the preload displacement $\Delta$ that enable the slider to drag the spool within a reasonable $y$ displacement. Let us assume

$y \in ]0; 2] mm$ and a spring stiffness $k \in [10; 20] N/mm$.

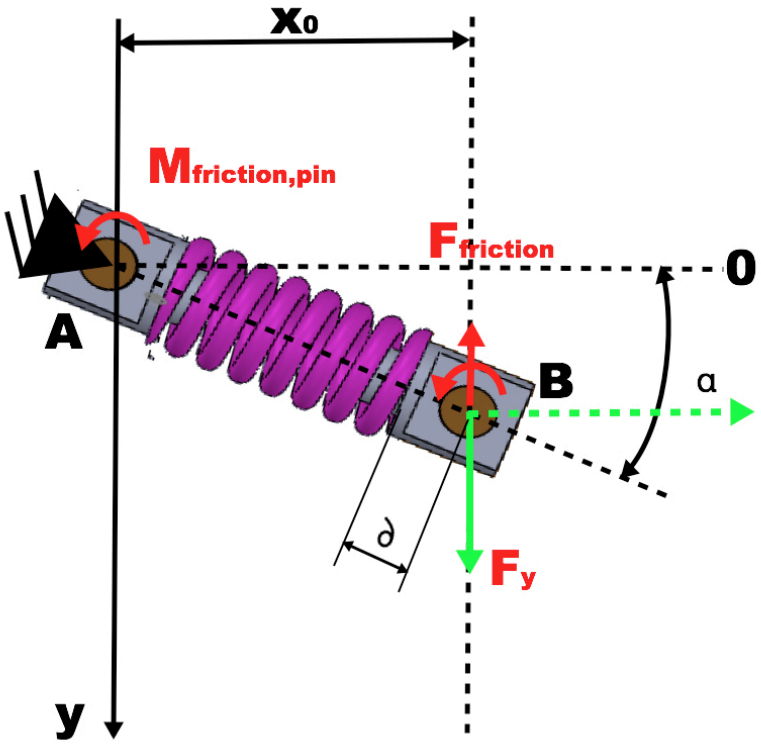


Figure E.4: Active forces applied on the spring

The characteristics length for the analysis are the distance $x_0$ expressed in term of the unloaded spring length $L$ and the distance from the center of the pin and the spring $\partial$ and the compression $\Delta$. The second dimension $L_{effective}$ describe the length of the spring with respect to the y position of point B.

$$x_0 = L + 2\partial - \Delta \tag{E.3}$$

$$L_{effective} = L + 2\partial - \sqrt{(L + 2\partial - \Delta)^2 + y^2} \tag{E.4}$$

The spring force $F_s$ is found as follow:

$$F_s = kL_{effective} \tag{E.5}$$

The projection of this force on the $y$ axis can be found using similar triangles theory as:

$$F_y = F_s \left( \frac{y}{\sqrt{(L + 2\partial - \Delta)^2 + y^2}} \right) \tag{E.6}$$

Assuming a friction coefficient $\mu = 0.30$ between brass and steel and a pin diameter of $d = 2mm$ a friction moment for the pin can be estimated as follow:

$$M_{friction,pin} = F_s \mu d/2 \tag{E.7}$$

The sum of the moment for different value of stiffness $k$ and preload displacement $\Delta$. After some iteration the values of $k = 15 N/mm$ and $\Delta = 3mm$.

Figure E.5

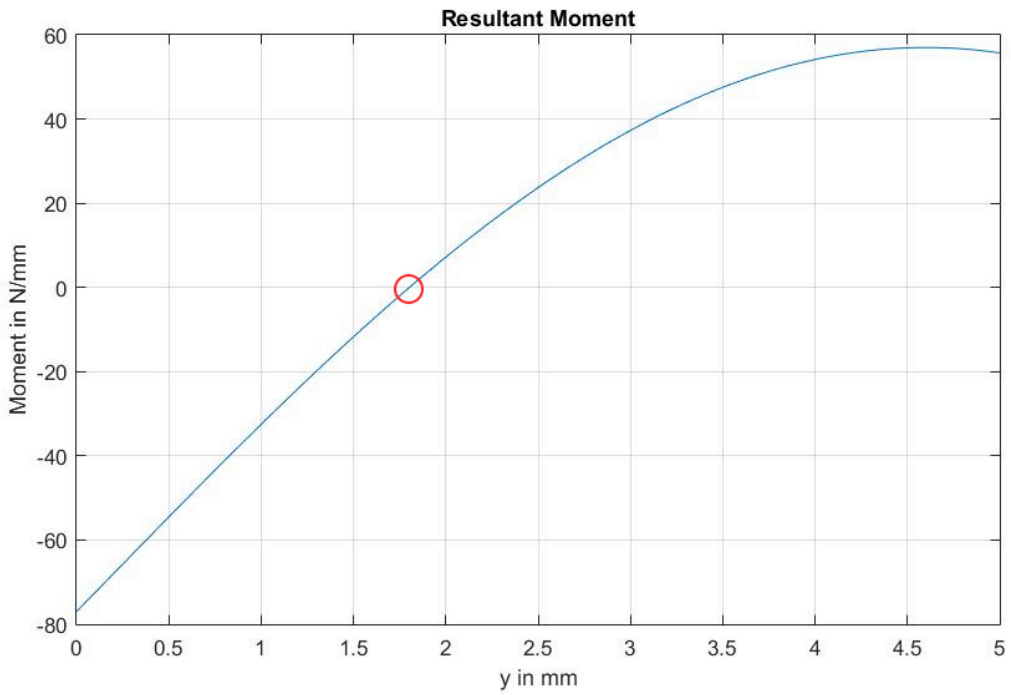


Figure E.5: Resultant moment of one spring in function to a displacement in the direction of the 4y4 positive. The spring overcome the friction moments when the moment value is greater than zero. For values smaller than zero the system would stand still.

The minimal estimate displacement is therefore 1.5 $mm$. The compressor should, therefore, move the bi-stable mechanism at least 1.5 $mm$ over the unstable equilibrium position before beginning moving the spool.

# F

# Manufacturing drawings of prototype number 3

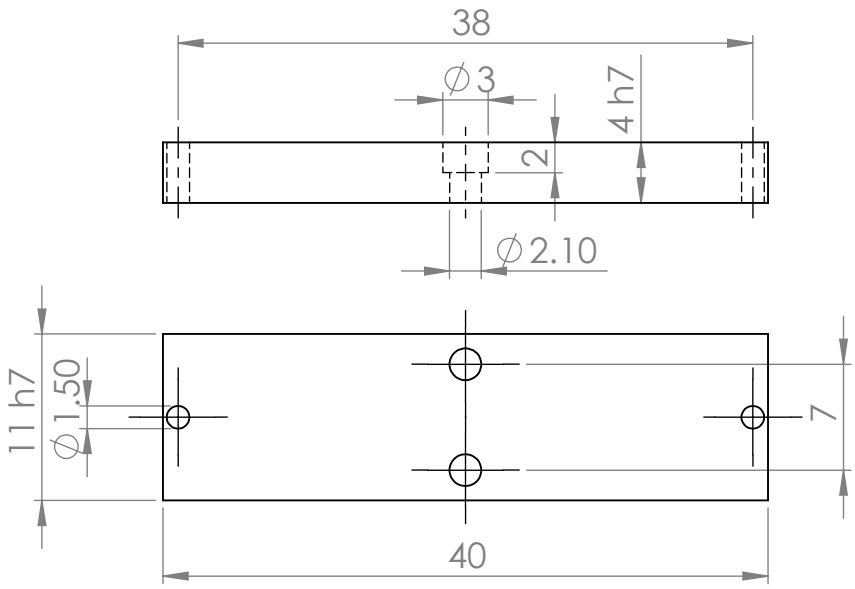


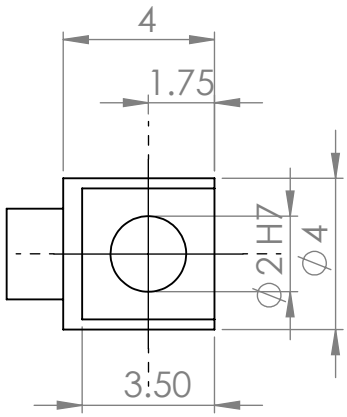


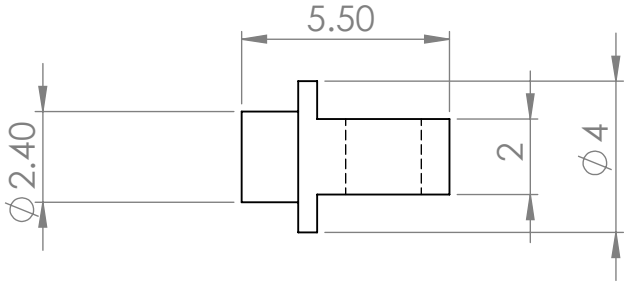


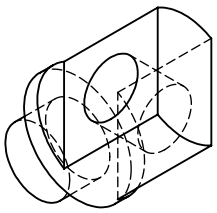

| | | | |
|---|---|---|---|
| UNLESS OTHERWISE SPECIFIED:<br>DIMENSIONS ARE IN MILLIMETERS<br>SURFACE FINISH:<br>TOLERANCES:<br>LINEAR:<br>ANGULAR: | FINISH: | DEBURR AND BREAK SHARP EDGES | DO NOT SCALE DRAWING / REVISION |

| | NAME | SIGNATURE | DATE |
|---|---|---|---|
| DRAWN | | | |
| CHK'D | | | |
| APPV'D | | | |
| MFG | | | |
| Q.A | | | |

TITLE:

# Bistable components

| | | |
|---|---|---|
| MATERIAL: | DWG NO. | A4 |
| WEIGHT: | SCALE:2:1 | SHEET 1 OF 1 |

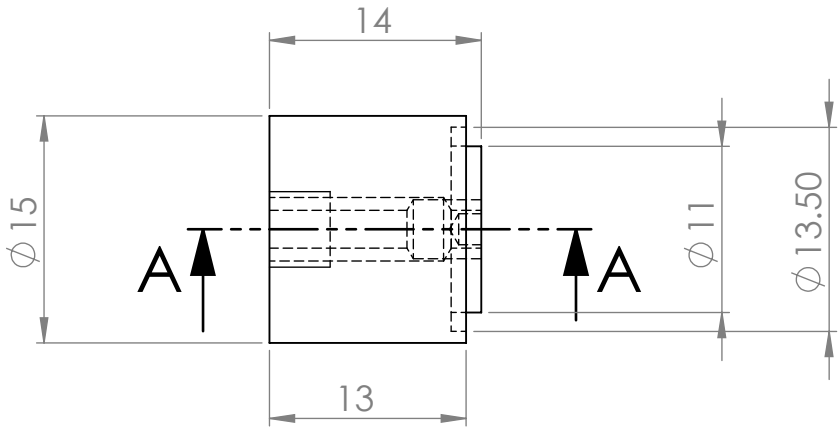


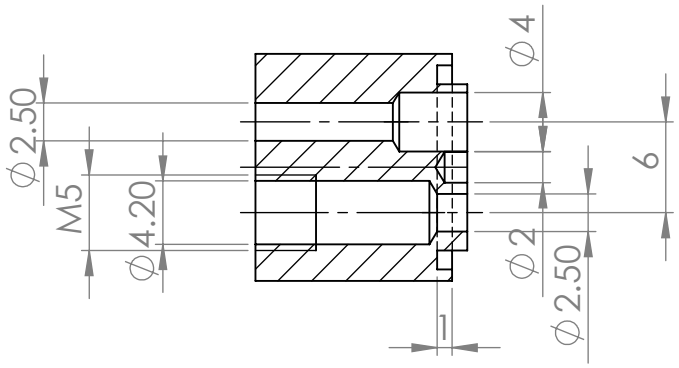


SECTION A-A

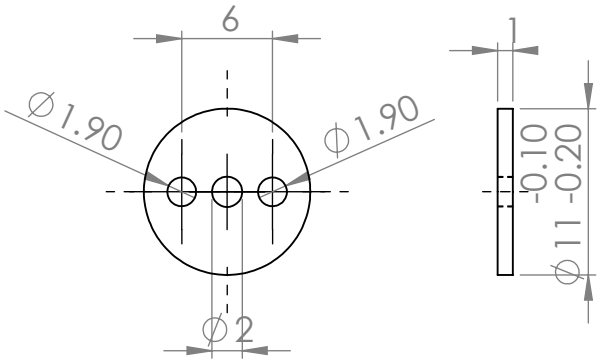


| | | | |
|---|---|---|---|
| UNLESS OTHERWISE SPECIFIED:<br>DIMENSIONS ARE IN MILLIMETERS<br>SURFACE FINISH:<br>TOLERANCES:<br>LINEAR:<br>ANGULAR: | FINISH: | DEBURR AND BREAK SHARP EDGES | DO NOT SCALE DRAWING / REVISION |

| | NAME | SIGNATURE | DATE |
|---|---|---|---|
| DRAWN | | | |
| CHK'D | | | |
| APPV'D | | | |
| MFG | | | |
| Q.A | | | |

TITLE: Compressor head

MATERIAL:

DWG NO.

A4

WEIGHT:

SCALE:2:1

SHEET 1 OF 1

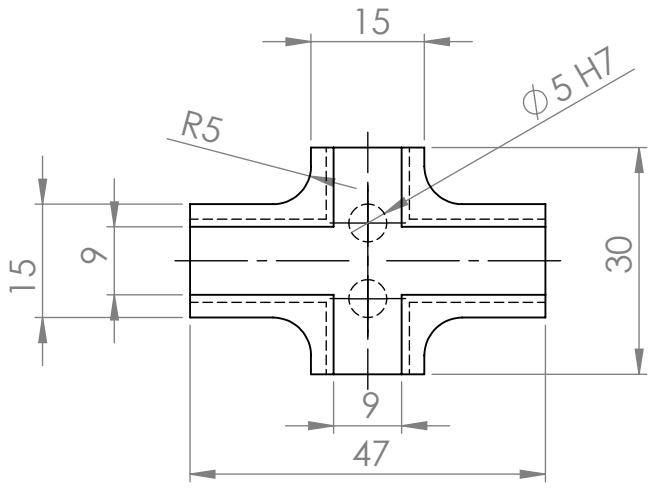


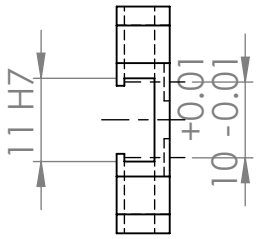


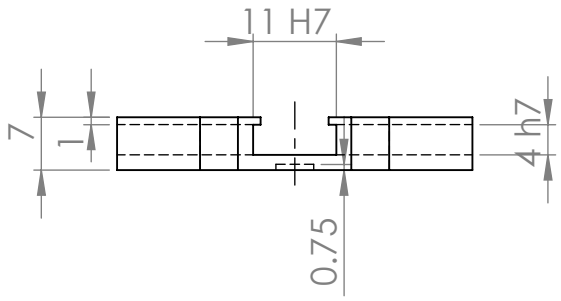


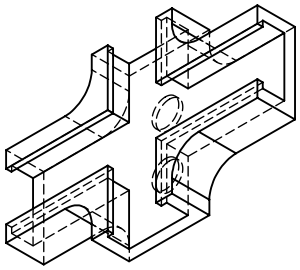

| | | | | | | | |
|---|---|---|---|---|---|---|---|
| UNLESS OTHERWISE SPECIFIED:<br>DIMENSIONS ARE IN MILLIMETERS<br>SURFACE FINISH:<br>TOLERANCES:<br>LINEAR:<br>ANGULAR: | | FINISH: | | DEBURR AND BREAK SHARP EDGES | | DO NOT SCALE DRAWING | REVISION |
| | NAME | SIGNATURE | DATE | | | TITLE: | |
| DRAWN | | | | | | Cross Bistable | |
| CHK'D | | | | | | | |
| APPV'D | | | | | | | |
| MFG | | | | | | | |
| Q.A | | | | MATERIAL: | | DWG NO. | A4 |
| | | | | | | | |
| | | | | WEIGHT: | | SCALE:1:1 | SHEET 1 OF 1 |

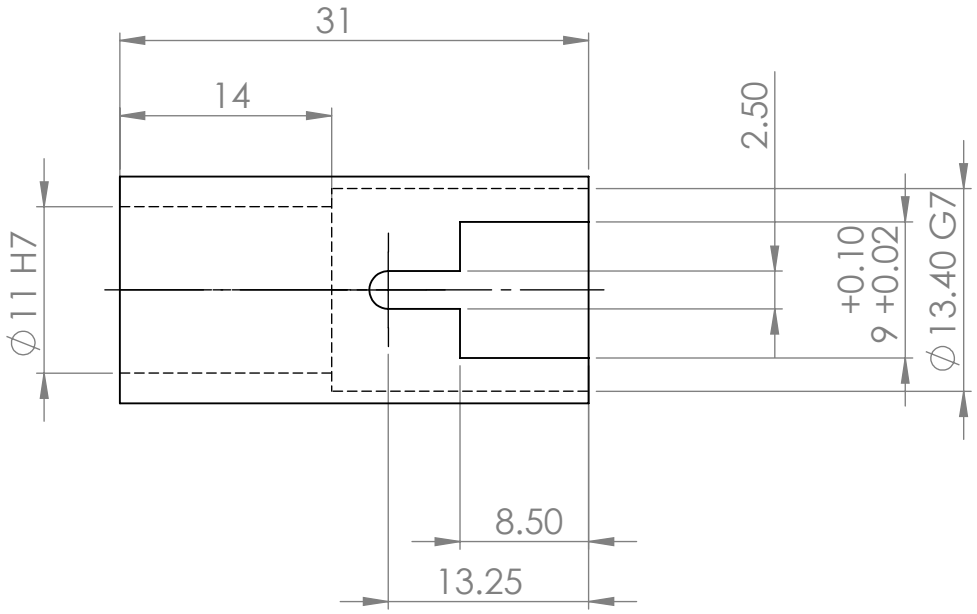


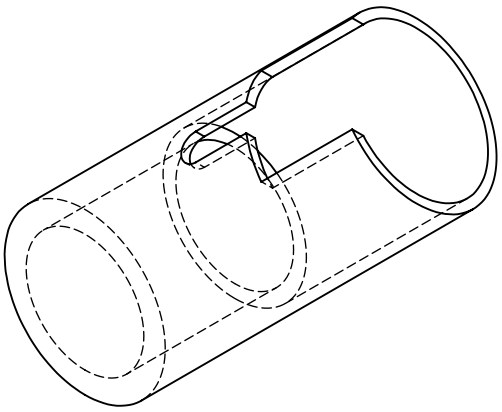

| | | |
|---|---|---|
| UNLESS OTHERWISE SPECIFIED:<br>DIMENSIONS ARE IN MILLIMETERS<br>SURFACE FINISH:<br>TOLERANCES:<br>LINEAR:<br>ANGULAR: | FINISH: | DEBURR AND BREAK SHARP EDGES |

| | DO NOT SCALE DRAWING | REVISION |
|---|---|---|
| | | |

| | NAME | SIGNATURE | DATE |
|---|---|---|---|
| DRAWN | | | |
| CHK'D | | | |
| APPV'D | | | |
| MFG | | | |
| Q.A | | | |

TITLE:

# Cylinder Compressor

| | | |
|---|---|---|
| MATERIAL: | DWG NO. | A4 |
| WEIGHT: | SCALE:2:1 | SHEET 1 OF 1 |

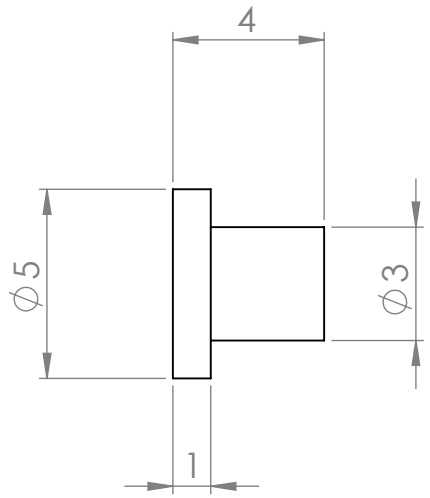


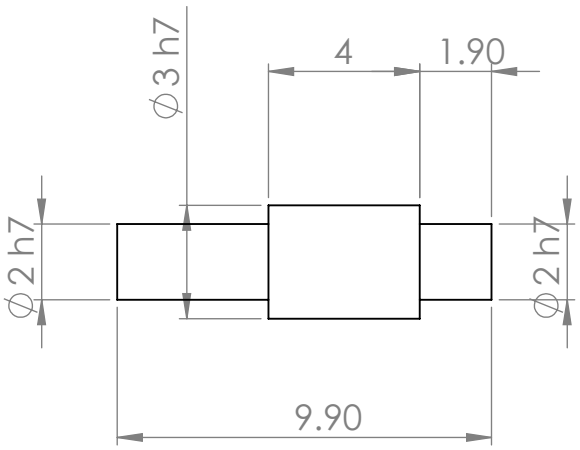


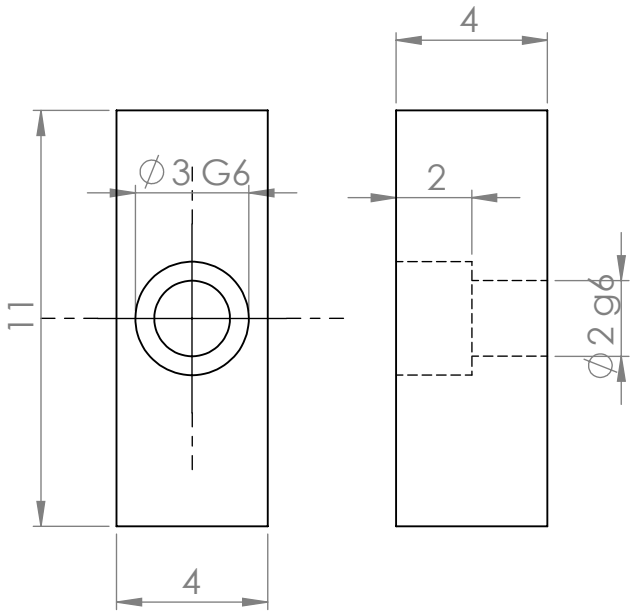


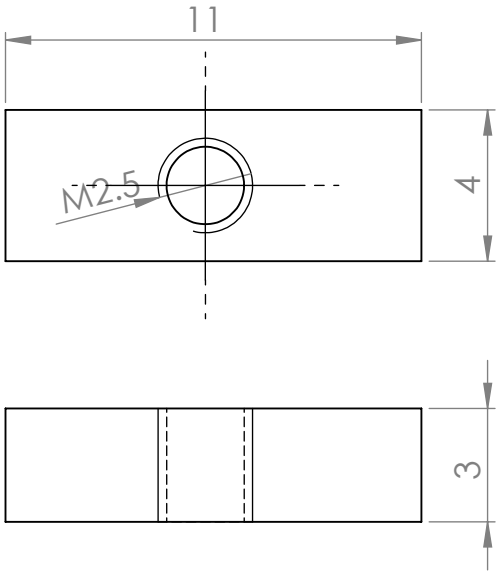


| | | | | | | | |
|---|---|---|---|---|---|---|---|
| UNLESS OTHERWISE SPECIFIED:<br>DIMENSIONS ARE IN MILLIMETERS<br>SURFACE FINISH:<br>TOLERANCES:<br>LINEAR:<br>ANGULAR: | | FINISH: | | DEBURR AND BREAK SHARP EDGES | | DO NOT SCALE DRAWING | REVISION |
| | NAME | SIGNATURE | DATE | | | TITLE: | |
| DRAWN | | | | | | Different parts | |
| CHK'D | | | | | | | |
| APPV'D | | | | | | | |
| MFG | | | | | | | |
| Q.A | | | | MATERIAL: | | DWG NO. | A4 |
| | | | | | | | |
| | | | | WEIGHT: | | SCALE:10:1 | SHEET 1 OF 1 |

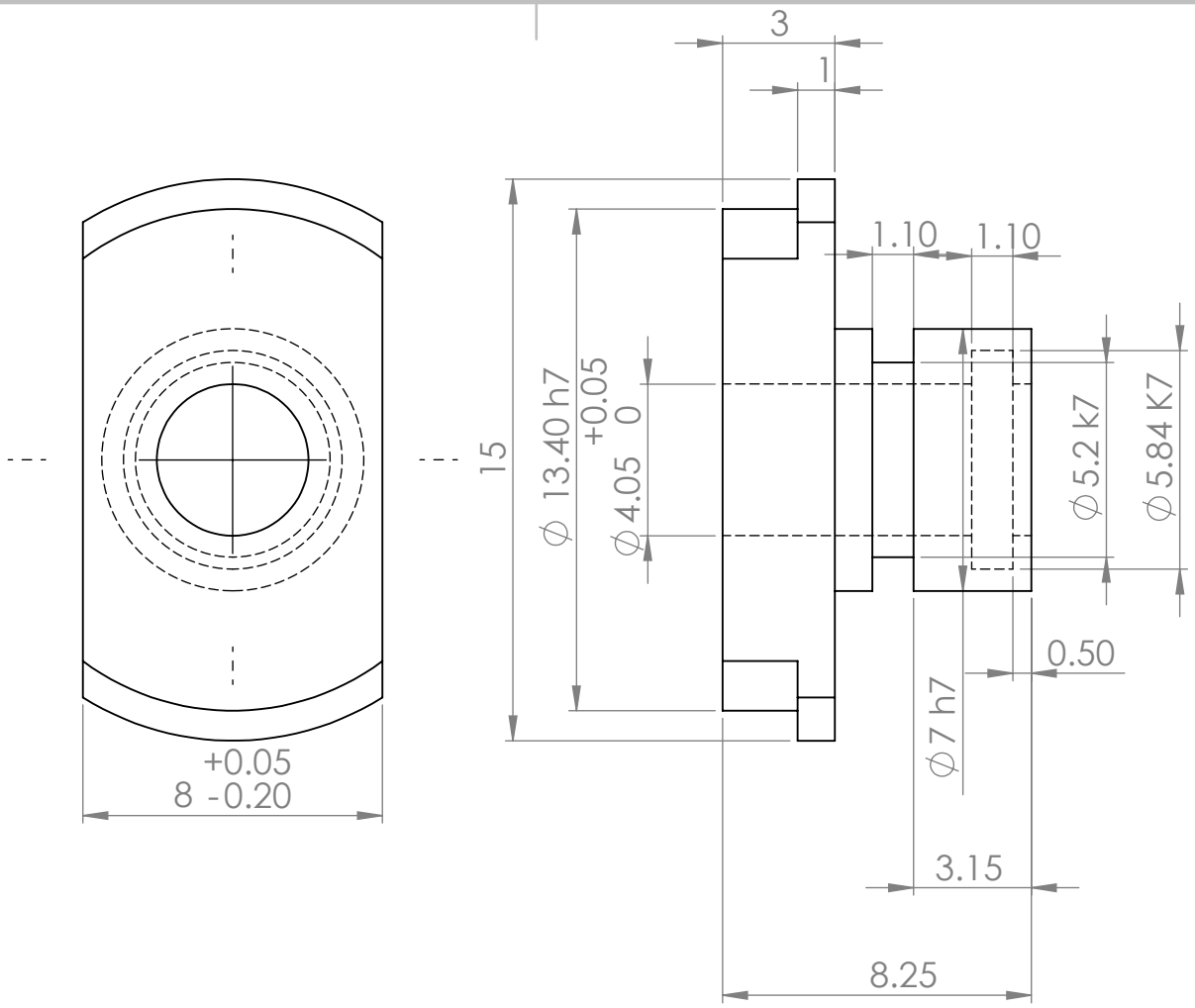


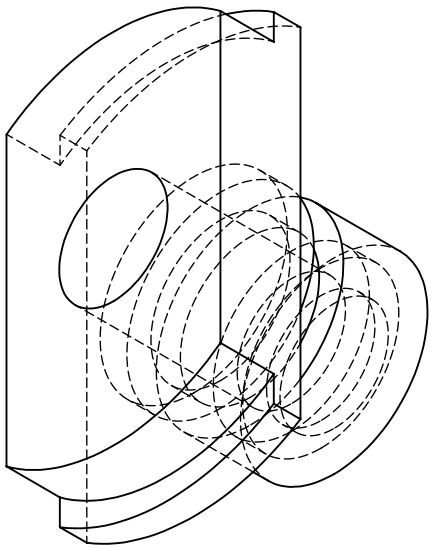

| | | | | | | | |
|---|---|---|---|---|---|---|---|
| UNLESS OTHERWISE SPECIFIED: DIMENSIONS ARE IN MILLIMETERS SURFACE FINISH: TOLERANCES: LINEAR: ANGULAR: | | FINISH: | | DEBURR AND BREAK SHARP EDGES | | DO NOT SCALE DRAWING | REVISION |
| | NAME | SIGNATURE | DATE | | | TITLE: | |
| DRAWN | | | | | | Expander Plug | |
| CHK'D | | | | | | | |
| APPV'D | | | | | | | |
| MFG | | | | | | | |
| Q.A | 2 | | | MATERIAL: | | DWG NO. | A4 |
| | | | | | | | |
| | | | | WEIGHT: | | SCALE:2:1 | SHEET 1 OF 1 |

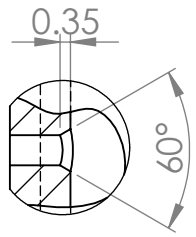


DETAIL A

SCALE 4 : 1

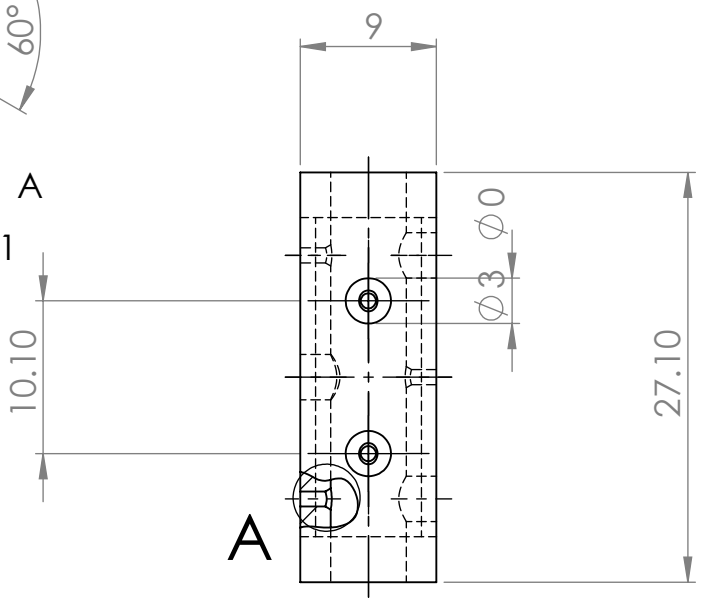


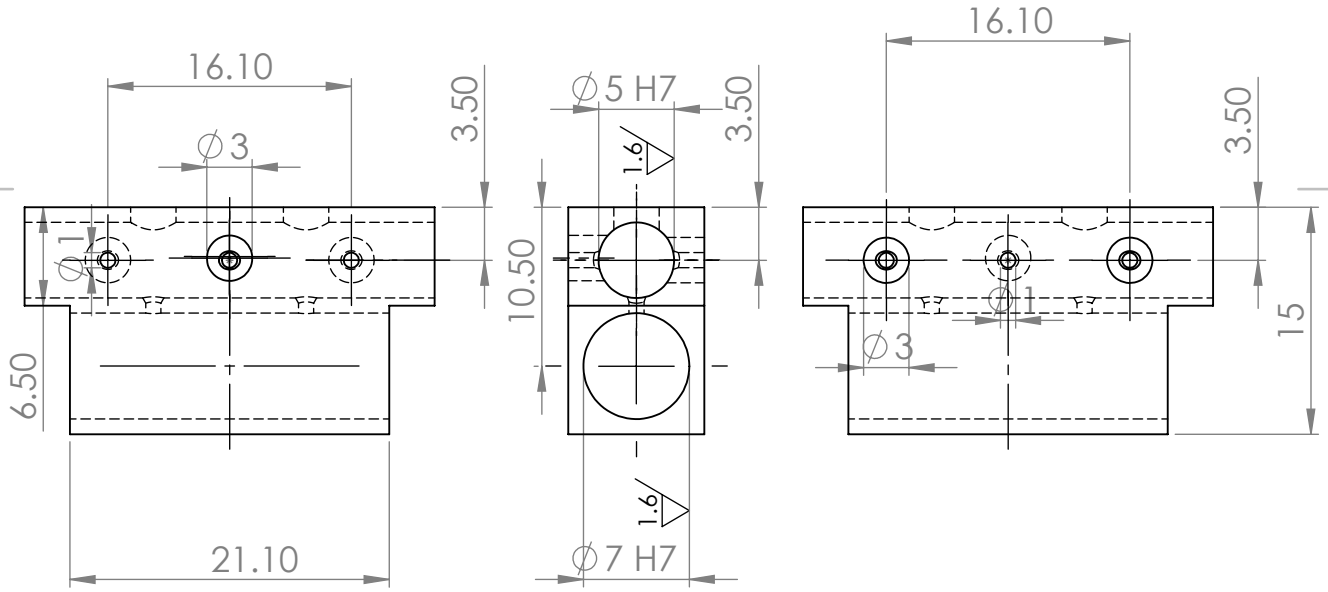


| | | | | | | | |
|---|---|---|---|---|---|---|---|
| UNLESS OTHERWISE SPECIFIED: DIMENSIONS ARE IN MILLIMETERS SURFACE FINISH: TOLERANCES: LINEAR: ANGULAR: | | FINISH: | | DEBURR AND BREAK SHARP EDGES | | DO NOT SCALE DRAWING | REVISION |
| | NAME | SIGNATURE | DATE | | | TITLE: | |
| DRAWN | | | | | | Housing | |
| CHK'D | | | | | | | |
| APPV'D | | | | | | | |
| MFG | | | | | | | |
| Q.A | | | | MATERIAL: | | DWG NO. | A4 |
| | | | | | | | |
| | | | | WEIGHT: | | SCALE:2:1 | SHEET 1 OF 1 |

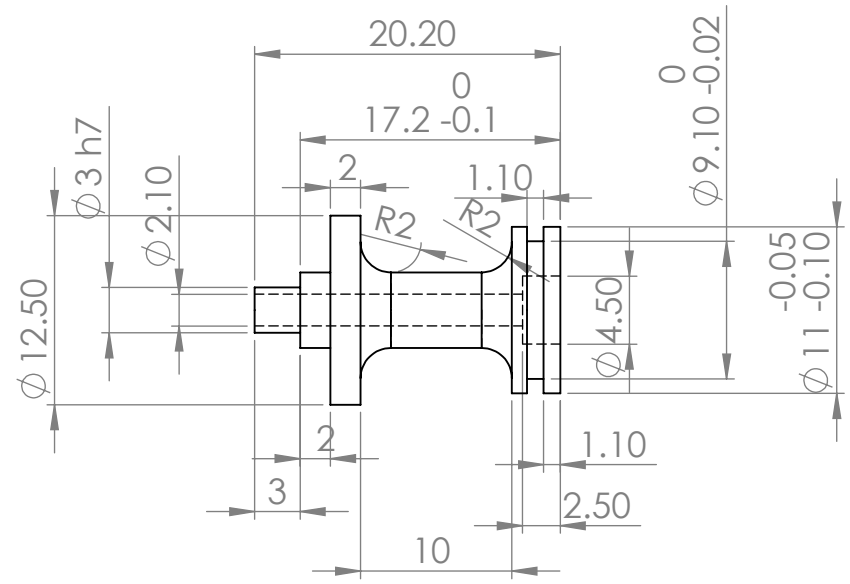


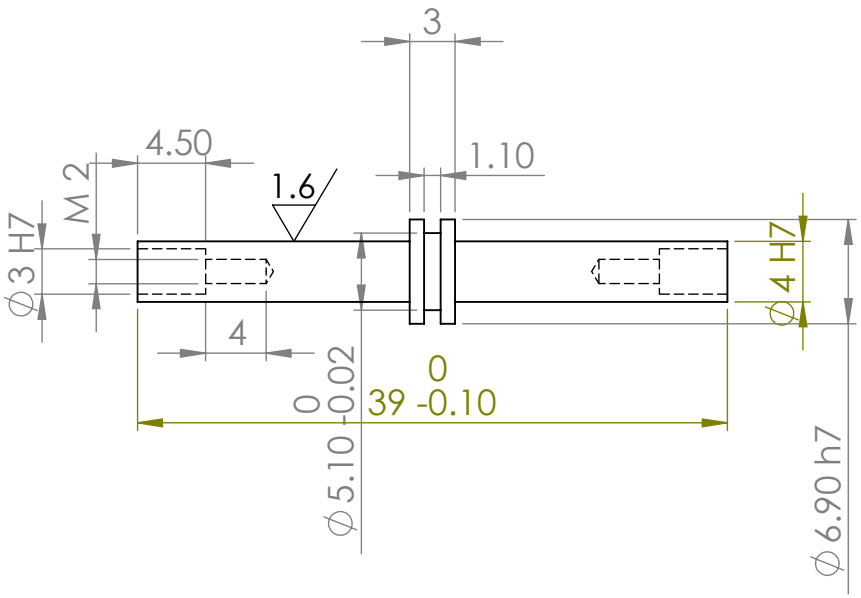


| | | | | | | | |
|---|---|---|---|---|---|---|---|
| UNLESS OTHERWISE SPECIFIED:<br>DIMENSIONS ARE IN MILLIMETERS<br>SURFACE FINISH:<br>TOLERANCES:<br>LINEAR:<br>ANGULAR: | | FINISH: | | DEBURR AND BREAK SHARP EDGES | | DO NOT SCALE DRAWING | REVISION |
| | NAME | SIGNATURE | DATE | | | TITLE: | |
| DRAWN | | | | | | Compressor piston and shaft | |
| CHK'D | | | | | | | |
| APPV'D | | | | | | | |
| MFG | | | | | | | |
| Q.A | | | | MATERIAL: | | DWG NO. | A4 |
| | | | | | | | |
| | | | | WEIGHT: | | SCALE:2:1 | SHEET 1 OF 1 |

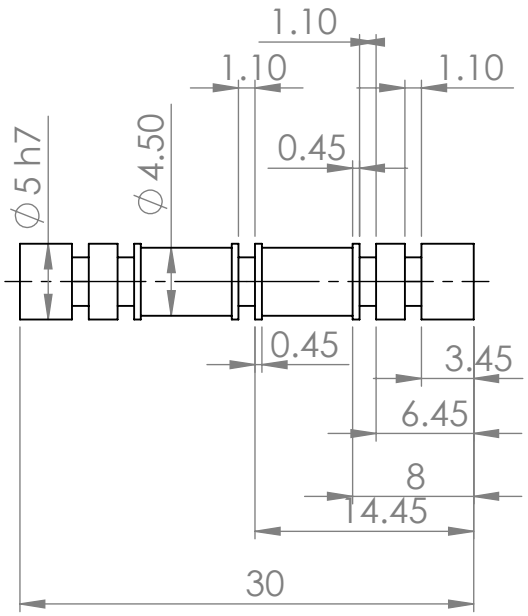


| | | | |
|---|---|---|---|
| UNLESS OTHERWISE SPECIFIED:<br>DIMENSIONS ARE IN MILLIMETERS<br>SURFACE FINISH:<br>TOLERANCES:<br>LINEAR:<br>ANGULAR: | FINISH: | DEBURR AND BREAK SHARP EDGES | DO NOT SCALE DRAWING / REVISION |

| | NAME | SIGNATURE | DATE |
|---|---|---|---|
| DRAWN | | | |
| CHK'D | | | |
| APPV'D | | | |
| MFG | | | |
| Q.A | | | |

TITLE:

# Spool

| | | |
|---|---|---|
| MATERIAL: | DWG NO. | A4 |
| WEIGHT: | SCALE:2:1 | SHEET 1 OF 1 |

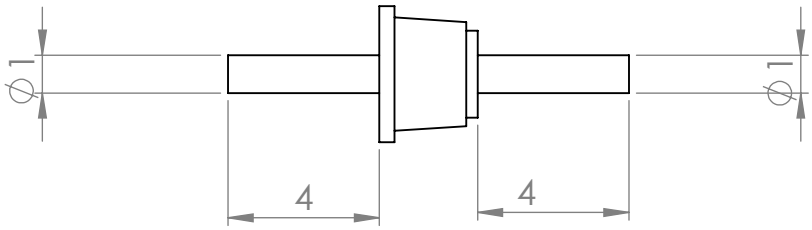


| | | | |
|---|---|---|---|
| UNLESS OTHERWISE SPECIFIED:<br>DIMENSIONS ARE IN MILLIMETERS<br>SURFACE FINISH:<br>TOLERANCES:<br>LINEAR:<br>ANGULAR: | FINISH: | DEBURR AND BREAK SHARP EDGES | DO NOT SCALE DRAWING / REVISION |

| | NAME | SIGNATURE | DATE |
|---|---|---|---|
| DRAWN | | | |
| CHK'D | | | |
| APPV'D | | | |
| MFG | | | |
| Q.A | | | |

TITLE:

# Compressor Valve

| | | |
|---|---|---|
| MATERIAL: | DWG NO. | A4 |
| WEIGHT: | SCALE:5:1 | SHEET 1 OF 1 |

# Bibliography


[1] Michael Wehner, Michael T Tolley, Yiğit Mengüç, Yong-Lae Park, Annan Mozeika, Ye Ding, Cagdas Onal, Robert F Shepherd, George M. Whitesides, and Robert J. Wood. Pneumatic Energy Sources for Autonomous and Wearable Soft Robotics. Soft Robotics, 2(00):1–12, 2014.

[2] Andrew D. Marchese, Robert K. Katzschmann, and Daniela Rus. A Recipe for Soft Fluidic Elastomer Robots. Soft Robotics, 2(1):7–25, 2015.

[3] Homayoon Kazerooni. Design and analysis of pneumatic force generators for mobile robotic systems. IEEE/ASME Transactions on Mechatronics, 10(4):411–418, 2005.

[4] Michael Goldfarb, Eric J. Barth, Mike Gogola, and J Wehrmeyer. Design and energetic characterization of a liquid-propellant-powered actuator for self-powered robots. IEEE/ASME Transactions on Mechatronics, 8(2):254–262, 2003.

[5] Dick H Plettenburg. A Sizzling Hand Prosthesis. PhD thesis, TU Delft, 2002.

[6] Grzegorz Granosik and Johann Borenstein. Minimizing air consumption of pneumatic actuators in mobile robots. IEEE International Conference on Robotics and Automation, 2004. Proceedings. ICRA '04. 2004, 4:3634–3639, 2004.

[7] Kevin B. Fite, Thomas J. Withrow, Keith W. Wait, and Michael Goldfarb. A Gas-Actuated Anthropomorphic Transhumeral Prosthesis. Proceedings 2007 IEEE International Conference on Robotics and Automation, (April):3748–3754, 2007.

[8] Cagdas D. Onal, Xin Chen, George M. Whitesides, and Daniela Rus. Soft mobile robots with on-board chemical pressure generation. International Symposium on Robotics Research (ISRR), pages 1–16, 2011.

[9] Michael Wehner, Yong Lae Park, Conor Walsh, Radhika Nagpal, Robert J. Wood, Talia Moore, and Eugene Goldfield. Experimental characterization of components for active soft orthotics. Proceedings of the IEEE RAS and EMBS International Conference on Biomedical Robotics and Biomechatronics, pages 1586–1592, 2012.

[10] Xiangrong Shen and Michael Goldfarb. Energy Saving in Pneumatic Servo Control Utilizing Interchamber Cross-Flow. Journal of Dynamic Systems, Measurement, and Control, 129(3):303, 2007.

[11] Morgan K Boes, Mazharul Islam, Yifan David Li, and Elizabeth T Hsiao-Wecksler. Fuel Efficiency of a Portable Powered Ankle-Foot Orthosis. Rehabilitation Robotics (ICORR), 2013 IEEE International Conference on, pages 1–6, 2013.

[12] Kalid Al-Dakkan. Energy saving control for pneumatic servo systems. Aim 2003, 2003.

[13] Yong Mao, Jiaxin Wang, Shi Li, and Zhuo Han. Energy-Efficient Control of Pneumatic Muscle Actuated Biped Robot Joints. 2006 6th World Congress on Intelligent Control and Automation, pages 8881–8885, 2006.

[14] Flavia Vitale, Dino Accoto, Luca Turchetti, Stefano Indini, Maria Cristina Annesini, and E Guglielmelli. Low-temperature H2O2-powered actuators for biorobotics: Thermodynamic and kinetic analysis. Robotics and Automation (ICRA), 2010 IEEE International Conference on, pages 2197–2202, 2010.

[15] Charles Thorpe and Hugh Durrant-Whyte. Springer Tracts in Advanced Robotics: Field robots. 2001.

[16] Cagdas D. Onal and Daniela Rus. A modular approach to soft robots. Proceedings of the IEEE RAS and EMBS International Conference on Biomedical Robotics and Biomechatronics, pages 1038–1045, 2012.

[17] Andrew D Marchese, Cagdas D Onal, and Daniela Rus. Experimental Robotics. 88:41–54, 2013.

[18] Dirk C. Doedens. Optimal CO 2 pressure for a pneumatic system. Master's thesis, TU Delft, 2015.

[19] Cutler J Cleveland and Christopher G Morris. Dictionary of energy. Elsevier, 2005.

[20] Lucien Borel and Daniel Favrat. Thermodynamique et énergétique, volume 1. PPUR presses polytechniques, 2005.

[21] Marc A. Rosen and Cornelia Aida Bulucea. Using Exergy to Understand and Improve the Efficiency of Electrical Power Technologies. Entropy, 11(4):820–835, 2009.

[22] Yu-xi Luo, Xuan-yin Wang, and Jun-bo Lei. Enthalpy and exergy transfers of high pressure switching expansion reduction. Journal of Shanghai Jiaotong University (Science), 17(1):45–52, 2012.

[23] Daniel Favrat, Francois Marechal, and Olivier Epelly. The challenge of introducing an exergy indicator in a local law on energy. Energy, 33(2):130–136, 2008.

[24] Giorgio Soave. Equilibrium constants from a modified Redlich-Kwong equation of state. Chemical Engineering Science, 27(6):1197–1203, 1972.

[25] Johan Rob. Ultralight Pressure Regulator for Application in Pneumatic Prostheses. Master's thesis, TU Delft.

[26] Qiyue Xu, Junpeng Sun, Maolin Cai, Yan Shi, and Xiangheng Fu. A power recovery type pressure reducer in the high pressure pneumatic system. pages 1–6, 2014.

[27] V. Lemort and A. Legros. Positive displacement expanders for Organic Rankine Cycle systems. Elsevier Ltd, 2016.

[28] Junjiang Bao and Li Zhao. A review of working fluid and expander selections for organic Rankine cycle. Renewable and Sustainable Energy Reviews, 24:325–342, 2013.

[29] Horst Kruse, Hans Rüssmann, Eduardo Martin, and Rainer Jakobs. Positive Displacement Carbon Dioxide Expansion Machines - Chances and Limitations -. Engineering Conference, pages 1–10, 2006.

[30] O E Balje. Turbomachines : a guide to design selection and theory. Wiley, New York, 1981.

[31] Mitsuhiro Fukuta, Tadashi Yanagisawa, Masashi Higashiyama, and Yasuhiro Ogi. Performance of Vane-Type CO2 Expander and Characteristics of Transcritical Expansion Process. HVAC&R Research, 15(4):711–727, 2009.

[32] Peter Beater. Pneumatic Drives. 2007.

[33] Jose A. Riofrio and Eric J. Barth. Design of a free piston pneumatic compressor as a mobile robot power supply. Proceedings - IEEE International Conference on Robotics and Automation, (April), 2005.

[34] Justin W Raade, Homayoon Kazerooni, and Timothy G McGee. Analysis and design of a novel power supply for mobile robots. IEEE International Conference on Robotics and Automation, 2004. Proceedings. ICRA '04. 2004, (April):4911–4917, 2004.

[35] De-yuan Meng, Guo-liang Tao, and Xiao-cong Zhu. Adaptive robust motion trajectory tracking control of pneumatic cylinders. Journal of Central South University, 20(12):3445–3460, 2013.

[36] Yang Song, Leisheng Huang, Tao Wang, and Wei Fan. Research on the Friction of the Pneumatic Servo System. pages 27–30, 2015.

[37] X. Tran, H. Dao, and K. Tran. A new mathematical model of friction for pneumatic cylinders. Proceedings of the Institution of Mechanical Engineers, Part C: Journal of Mechanical Engineering Science, 230(14):2399–2412, 2016.

[38] Parker Corporation. Parker O-Ring Handbook.

[39] Y.M. Kim and D. Favrat. Energy and exergy analysis of a micro-compressed air energy storage and air cycle heating and cooling system. Energy, 35(1):213–220, 2010.

[40] E. Richer and Y. Hurmuzulu. A High Performance Pneumatic Force Actuator System Part 1 - Nonlinear Mathematical Model. ASME Journal of Dynamic Systems, Measurement, and Control, 122(3):416–425, 2001.

[41] National Institute of Standard and Technology. RefpropMini.

[42] Aerospace Specification Metal Inc. Aluminum 7075 T6.

[43] R C Hibbeler. Mechanics of materials TT -. Prentice Hall„ Boston :, 8th ed. edition.